Preparation and characterization of vapour deposited films based on substituted 2,5-diphenyl-1,3,4-oxadiazole derivatives

Dissertation

Zur Erlangung des akademischen Grades
Doktor der Naturwissenschaften
(Dr. rer. nat.)
in der Wissenschaftsdisziplin Weiche Materie

Eingereicht an der
Mathematisch-Naturwissenschaftlichen Fakultät
der Universität Potsdam

Von
Magister Chem. Chenggang Xü

Geboren am 06. 03. 1969 in Xi'an

Potsdam, im März 2004

Nomenclature

The general molecular structure of the substances studied in this work is shown in Fig.1, the substituents and their abbreviations used in this work are listed in Tab. 1.1.

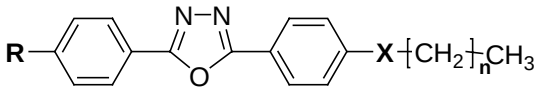

Fig.1.1 1,3,4-oxadiazole derivatives studied in this work.

Tab. 1.1 The substituents and their abbreviations

R / Abbreviation		**X** / Abbreviation	
CN- (para)	*p*C	Ether, —O—	Et
CN- (meta)	*m*C	Ester, —C(=O)—O—	Es
CH_3O-	MO	Amide, —NH—C(=O)—	A
CH_3OCO-	ME		
NO_2-	NI		
H-	H		

Please note that all substances studied in this work are derivatives of 2,5-diphenyl-1,3,4-oxadiazole (DPO), so this part of the molecule is omitted in the nomenclature to keep the name concise. The basic nomenclature used in this work is illustrated with the following examples:

Example 1:

2,4-Bis(4-nitrophenyl)-1,3,4-oxadiazole

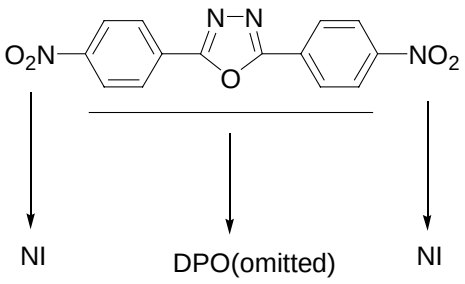

This substance is referred to NINI in this work.

Example 2:

2-(4-Cyanophenyl)-5-(4-hexadecyloxyphenyl)-1,3,4-oxadiazole

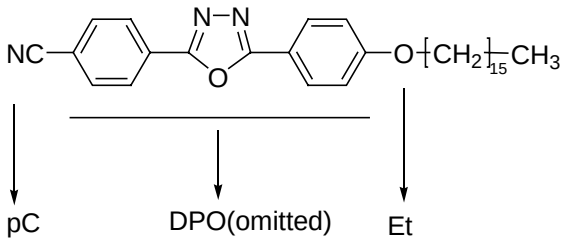

So this substance is named as *p*CEt16 in this work, while 16 represents the number of carbon atoms in the aliphatic chain.

Example 3:

2,5-Di(4-dodecanoylaminophenyl)-1,3,4-oxadiazole

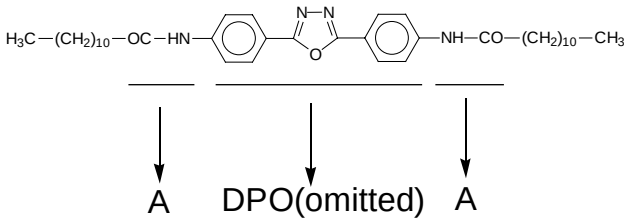

This substance is named as 11AA11 in this work, the number 11 at the beginning and the end represents the number of carbon atoms in each of the two aliphatic chains.

The chemical structure of all the investigated oxadiazole derivatives and their abbreviations used in this work are listed alphabetically in Tab. 1.2.

Tab. 1.2 Chemical structure of all the investigated oxadiazole derivatives and their abbreviations

Name	Structure	Note
CDMO	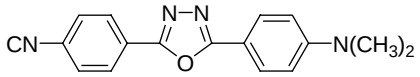	
12EsEs12	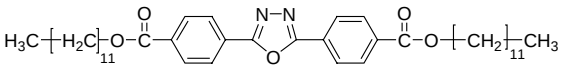	
HA11	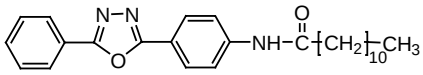	
HEt16	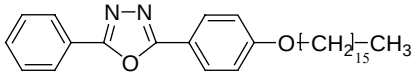	
*m*CEt16	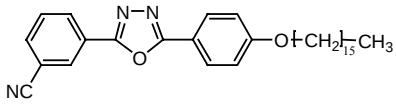	
MEEt16	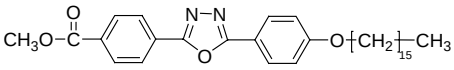	
MEME	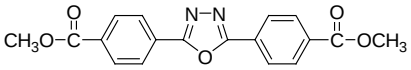	
MOEt16	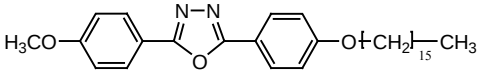	
*n*AA*n*	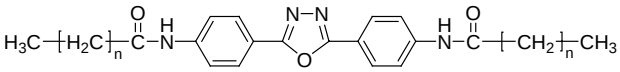	*n* = 6, 10, 16
NIA11	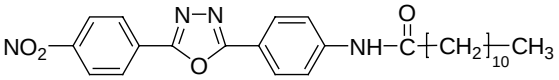	
NIEt12	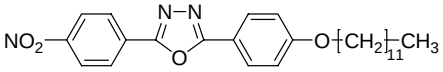	
NINI	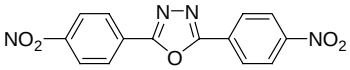	
*p*CA11	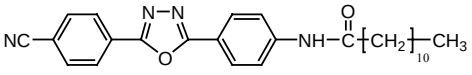	
*p*CE*t*n	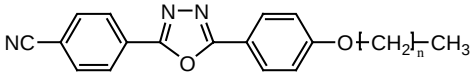	*n* = 0, 4, 9, 11, 15

1 Introduction

The research in the area of new materials in recent years arise more interest in organic materials. The physical and chemical properties of organic materials can be easily tuned by variation of their chemical structures and by control of the supramolecular architecture to meet the requirements of a particular application area [1, 2]. One such example is 1,3,4-oxadiazole, which is a hetero-aromatic ring containing two nitrogen atoms, two carbon atoms and one oxygen atom. 1,3,4-oxadiazole compounds are highly thermal stable [3-7]. They possess promising emission in UV and blue region and are widely used as scintillator compounds [8, 9]. They are also interesting candidates for application areas like thin-film-transistors (TFT) and light emitting devices (LEDs) [10-13].

The development of electronic devices show clearly tendency of miniaturisation. In the nanometer range the inter- and intramolecular structures of materials have a large impact on the physical properties of the device. It is necessary to combine the functional parts which possess special physical properties and the support part which facilitate the formation of ordered film structures.

Thin film based on 1,3,4-oxadiazole compounds can be prepared via methods like Langmuir-Blodgett technique (LB), Vapour Deposition method (VD) or Spin Coating process [3, 14-17]. Freydank et al. [18] have investigated systematically LB films of 2,5-diphenyl-1,3,4-oxadiazole compounds. The results show that an apliphatic chain attached to the phenyl ring helps to stabilize the monolayer at the water-air interface. For some molecules, the intermolecular hydrogen bonds also contribute to the stabilization of LB multilayers after the film is transferred onto the substrates.

Vapour Deposition (VD) is a widely used film preparation method. Several advantages such as freedom from impurities and high productivity make it widely applied in the electronics industry [19]. The use of 1,3,4-oxadiazole in LEDs is also realized through VD. Although the application of 1,3,4-oxadiazole compounds as electron transport layers in LEDs are quite often reported in the literature [20-22], the structure of the layers are rarely investigated, in spite of the fact that the physical properties are deeply influenced by the intermolecular structures of the layers [23-26].

The aim of this work is the investigation of the correlation between the chemical structure of a substance and its corresponding VD film structure. The influence of film preparation conditions on the film structure is also investigated in this work.

The first step to achieve this aim is the synthesis of different 1,3,4-oxadiazole compounds, which are likely to form ordered VD films. The synthesis is concentrated on derivatives of 2,5-diphenyl-1,3,4-oxadiazoles because the LB films made from these materials have already been systematically investigated. The chemical structures and the purities of the synthesized substances will be investigated using Infrared Spectroscopy (IR) and High Pressure Liquid Chromatography (HPLC).

The next step is the preparation of VD films using the available as well as the new synthesized 1,3,4-oxadiazole compounds. The films will be characterized by means of X-ray specular reflection (XSR), Atom Force Microscopy (AFM) and Reflection Absorption Infrared Spectroscopy (RAIRS).

Systematic experiments will be carried out to investigate the influence of the chemical

structure on the film structure. The main points are the influence of the head group of the molecule, the length of the aliphatic chain and the bridge group which connects the aliphatic chain and 2,5-diphenyl-1,3,4-oxadiazole unit.

Physical deposition parameters such as substrate temperature and film growth rate can influence the film growth and therefore change the structure of the resulting film. For a given substance the film structure can be more or less controlled by changing these physical deposition parameters. For this reason the study of the influence of physical deposition parameters on film growth is also a part of this work.

The change in film structure will result in a change of the physical properties. For 1,3,4-oxadiazoles, the absorption in UV region and luminescence properties may be influenced. The last step of this work is the study of such effects using UV and PL spectroscopy.

2 Literature review

VD as well as LB films of compounds, which have structures analogous to the oxadiazole compounds investigated in this work (see page 1, Fig.1.1), have been widely studied. Among them are 4-alkoxy-4'-cyanobiphenyls and 4-alkyl-4'-cyanobiphenyls (*n*OCB and *n*CB, *n* donates the number of methylenes in the substituents), thiophene derivatives and oligophenylenes. On the other hand, only few paper are published dealing with the morphology study of VD or LB films based on aromatically substituted 1,3,4-oxadiazoles.

The *n*OCB and *n*CB differ with our oxadiazole compounds mainly in that they do not possess an oxadiazole ring between two phenylene rings. Therefore the two phenylene rings in *n*OCB molecules form a linear rod while the aromatic part of oxadiazoles is banana-shaped. Like oxadiazoles, thiophenes are also molecules with a heterocyclic aromatic five numbered ring. Moreover, some thiophene derivatives also tends to have banana-shaped molecules.

2.1 Oxadiazole compounds

2.1.1 Crystal structure of 1,3,4-oxadiazoles

A knowledge of the molecular conformation and arrangement in a crystal is a very important information for the VD film investigation. In recent years the crystal structures of several oxadiazole compounds without substituted aliphatic chain were studied [27-44], most of them in our research group. This information is very useful in the analysis of the film structure, especially for the aliphatic chain substituted oxadiazoles, whose crystal structure is up to now unavailable due to the difficulty in obtaining crystals big enough for structural analysis. Franco [45] has summarized the results of these studies and found that the molecular arrangement in most of the crystals is determined by the presence of π-complexes, the complex which results from the interaction between the electron rich ring system (π-donor, phenyl ring) and electron poor ring system (π-acceptor, oxadiazole ring) of two molecules [46], outlined in Fig. 2.1. The inter-planar distances between the molecules which build the π-complexes are in the range of 0.333 to 0.371 nm.

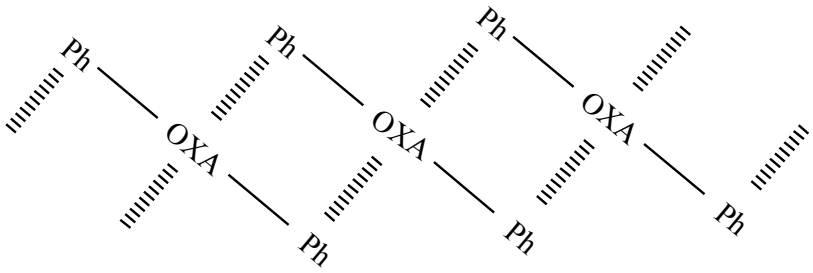

Fig. 2.1 Schematic illustration of π-complexes in oxadiazole crystals. Ph and OXA represent phenyl and oxadiazole ring, respectively. Solid line is the chemical bond connecting phenyl and oxadiazole ring. π-π interactions are denoted by dashed bonds.

In a crystalline form the 1,3,4-oxadiazole ring is always perfectly planar. The phenyl and oxadiazole ring derivate slightly from coplanar. The dihedral angles between the oxadiazole and phenyl rings are lower than 10° for most compounds.

2.1.2 Vacuum deposited and LB-films of oxadiazole derivatives

Low molecular weight oxadiazole derivatives (Fig. 2.2) [47-52] as well as polymers containing oxadiazole structures [53, 54] are often employed in LED development. Spin-coating is the most widely applied method for polymer film preparation and vapour deposition for low molecular weight oxadiazoles. PBD is the most commonly used low molecular weight oxadiazole as electron transport material [21, 22, 55-61], but it crystallizes quickly as a pure VD film [62]. An et al. have avoided the crystallization by employing the multiple Alq_3/PBD quantum well structure [61].

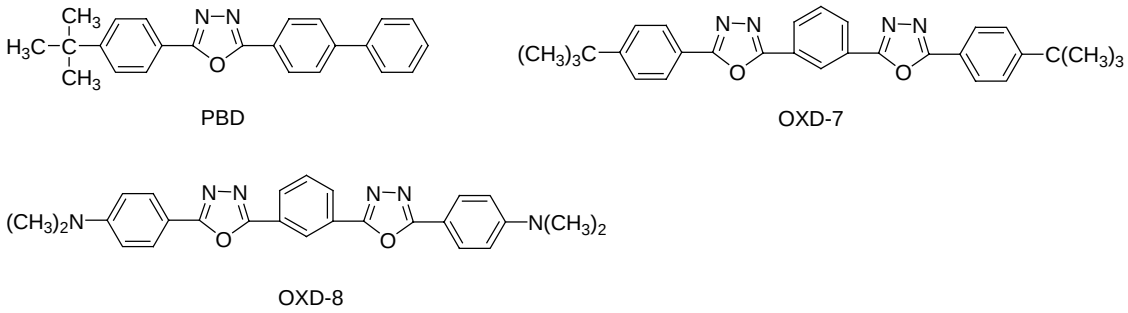

Fig. 2.2 Molecular structure of some oxadiazole derivatives used for VD film [47-52].

Hamada et al. [51] have prevented the degradation of LED due to the crystallization in organic layer by using OXA-7 and OXA-8. The life time of the cell was extended to 40 days, 20 times that of a PBD cell.

Although some authors [25, 26] have mentioned correlation between the film morphology and the electrical properties of the organic films, no work has been invested in morphology studies of VD oxadiazole films except in our group [14, 15, 63].

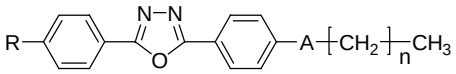

Fig. 2.3 General structure of oxadiazole compounds studied in [18]. R(head group): H, NO_2, $COOCH_3$, NH_2, $N(CH_3)_2$, CN, CH_3, CH_3O; A(bridge group): -O-, -NHCO-, -COO-, -N=CH-.

Freydank [18] and Reiche et al. [16, 64] have systematically investigated the influence of the molecular structure of oxadiazole compounds (general structure see Fig. 2.3) on their LB film structure. The results show that for the LB film at the water-air interface has the highest stability as the alkyl chain has an optimal length of 10 methylene units. The head group strongly influences the stability of a monolayer, when the brigde group is ether and ester, but such an influence is not observed when the bridge group is an amide structure. The interaction between the phenyl ring, which is an electron donor, and the oxadiazole ring, which is an electron acceptor, leads to the shift of molecules by the length of one phenyl ring along the direction perpendicular to the water surface during the compression of the monolayer at the water-air interface [18].

Reiche et al. [63] have studied the VD film of 2-(4-Nitrophenyl)-5-(4-dodecanoylaminophenyl)-1,3,4-oxadiazole (Fig. 2.3 with R = NO_2, A = -NHCO- and *n* = 10) and compared the structure with its LB film. The film periodicity of VD film (3.3 nm) in direction normal to the substrate surface is much smaller than for LB film (5.7 nm). Molecular modelling gives a film structure which is in good agreement with experimental

data and consists of layers built up by molecules with alternating orientation with respect to the normal direction of the film (Fig. 5.63, page 90). Intermolecular hydrogen bonds between amide groups are regarded to stabilize the film.

It worth noting that some of the oxadiazole compounds (*p*CEt16, NIEt12, MEEt16 and MOEt16) studied in this work could form thermotropic mesophase. 2,5-diphenyl substituted 1,3,4-oxadiazole compounds were regarded as non mesomorph due to the banana shape of the 2,5-diphenyl-1,3,4-oxadiazole part [65]. In the last twenty years, however, different shapes of molecules containing oxadiazole ring were found to have mesophases [66-72]. The formation of mesophases implies that the intermolecular interactions reach such a balance, that the molecules self-organize and form a certain degree of order. Although the films studied in this work were all prepared at the substrate temperature below the mesophase temperature, nevertheless the substances were evaporated above the mesophase, in some cases even above the isotropic temperature, the self-organization of the molecules could still have an influence on the film formation.

2.2 Vacuum deposited films of other organic compounds

2.2.1 Oligophenylenes

Alkoxy-cyanobiphenyls (*n*OCB) are widely known as liquid crystals [73]. Itaya et al. have investigated the vacuum-deposited films of 8OCB, 9OCB, 10OCB and 12OCB by means of AFM, UV and in situ PL [74-76].

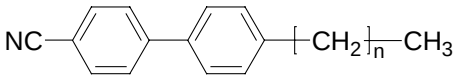

Fig. 2.4 Chemical structure of *n*OCB.

They have used two types of substrates: hydrophilic quartz plates and hydrophobic quartz plates, which were covered by a layer of closely packed long alkane chains normal to the substrate surface.

The 8-, 9- and 10OCB-deposited films on hydrophilic substrates at elevated temperature (round 20°C) were in a needle type crystalline state and emitted monomer-like fluorescence, while films on hydrophobic substrates were amorphous and emitted excimer fluorescence. It was suggested that 8-, 9- and 10-OCB deposited on low-temperature hydrophilic substrates contain H-aggregate structures of cyanobiphenylyloxy groups. A discontinuous spectral change was found in the in situ PL spectra for the deposition on hydrophilic substrates. This change was ascribed to the structural transformation from an amorphous to crystalline state during film growth [76]. Such a spectral change, however, does not appears for films deposited on hydrophobic substrates.

The influence of hydrophilicity of the substrates on the deposition behaviour of 8-, 9- and 10OCB was interpreted on the basis of the molecular arrangement in the monolayer just on substrate surfaces. In case of hydrophobic substrates, the first layer consists of only one layer of down-pointing molecules (Fig. 2.5 a). On hydrophilic substrate the first layer is composed of anti-parallel pairs arranged in such a way that alkyl chains in the layer are likely to interpenetrate into long alkyl chains normal to the substrate surface (Fig. 2.5 b) [74]. The first layer arrangement on the hydrophilic substrate (Fig. 2.5 a) seems to be

unstable compared with that on the hydrophobic substrate (Fig. 2.5 b), because interaction among 8OCB molecules in the first layer in arrangement (a) is repulsive. As a result the structural transformation from amorphous to crystalline state occurs.

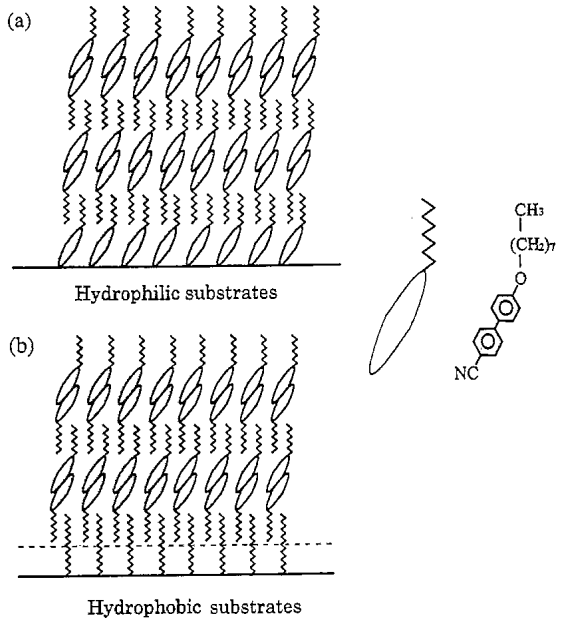

Fig. 2.5 Illustration of model representing the orientation of 8OCB molecules deposited on (a) hydrophilic and (b) hydrophobic substrate (before the structural transformation during deposition). Figure from [74].

In contrast, the UV and PL spectra of 12OCB-based films were almost independent of the deposition conditions, the films consist of a number of small plate crystals with smectic-like structure [75]. The structural transformation from amorphous to crystalline state did not occur in the growth of 12OCB films. H-aggregate structures of the cyanobiphenylyloxy groups were also found in the film. The difference of film deposition behaviour between 12OCB and others (8-, 9- and 10OCB) were ascribed to large van der Waals attraction among long alkyl chains of 12OCB compared with other OCBs. So for 12OCB, molecule-molecule interactions rather than molecule-substrate interactions are likely to be predominant in the molecular aggregation process during film growth.

The 12OCB film has a bilayer structure in which molecules form the H-aggregate structure, the films of 8-, 9- and 10OCB deposited at low substrate temperatures (≈ 5°C) also have similar film structures. The long axes of the cyanobiphenylyloxy groups of 8-, 9-, 10- and 12OCB molecules orient relatively perpendicularly to the substrate surface. As a result of large van der Waals intermolecular attraction, the degree of orientation of 12OCB films is the largest among *n*OCB films.

4-*n*-pentyl-4'-cyano-*p*-terphenyl (5CT) is also a mesogen (Fig. 2.6). It differs to our oxadiazole in that the middle ring is a phenylene instead of oxadiazole ring. It is worth noting that the three phenylenes are not coplanar, although they have a straight shape, while the three rings in 2,5-diphenyl-1,3,4-oxadiazole are almost coplanar and have a banana shape.

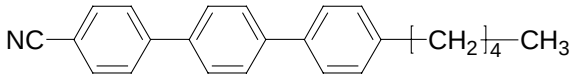

Fig. 2.6 Chemical structure of 5CT.

Sumiyoshi et al. [77] deposited 5CT on quartz glass plate. A UV and PL investigation demonstrated that 5CT films form H-aggregate-like structures with their long axes parallel to each other and relatively perpendicular to the substrate surface. Similar to *n*OCB, the 5CT films have a bilayer structure almost independent of deposition conditions.

All the aforementioned results show that alkyl chain substituted oligophenylenes prefer to stand in the VD films, which is an important difference to the VD film of p-sexiphenyl (6P). 6P molecules are mainly oriented in crystalline thin films normal to the substrate surface at a high substrate temperature and a very low growth rate, but parallel to the substrate surface when deposited at low substrate temperature (50°C) [78].

2.2.2 Oligothiophenes

The series of oligothiophenes (Fig. 2.7), quarter-(4T) and sexi-thiophene (6T) in particular, have attracted great interest due to their potential application in field effect transistors (FETs) or light emitting diodes (LEDs).

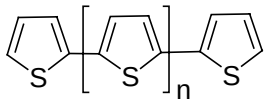

Fig. 2.7 Chemical structure of oligothiophene.

The most widely used technique for oligothiophene thin film preparation is vacuum deposition. The molecules prefer to have an all-trans configuration in bulk crystals [79-83] as well as in thin films [84, 85]. Here only the efforts devoted to the film preparation on Si(SiO_2 or SiH) or glass is summarized.

Horowitz et al. have deposited 6T on Si/SiO_2 and found that increasing the substrate temperature close to the melting point of 6T could improve the field-effect mobility by an order of magnitude [86]. The end-on orientation of 6T molecules in films has been confirmed by means of UV spectroscopy [84, 87, 88] and IR [89, 90]. IR investigations reveal that a large proportion (70~80%) of the 6T molecules have their axis oriented nearly normal to the substrate when deposited at room temperature. This proportion can be further increased up to 90% by elevating the substrate temperature during deposition or annealing after deposition. Lovinger et al. [91] confirmed that in evaporated polycrystalline 6T films the molecules are oriented preferentially nearly normal to the Si/SiO_2 substrate. On the Si(SiH) substrate, however, the 6T molecules orientated preferentially with their axis parallel to the substrate [89, 90].

Mena-Osteritz has investigated the alkyl substituted 4T and 10T (Fig. 2.8) films, which self-assembled on the surface of highly oriented pyrolytic graphite (HOPG) from solution, by means of STM. The results shows that the 4T and 10T backbones of the molecules lay parallel to HOPG surface. An all trans conformations for the thiophene rings and alkyl chains are preferred in the film. The side chains longer than propyl, e.g., hexyl, are essential to immobilize the backbones onto the surface [92].

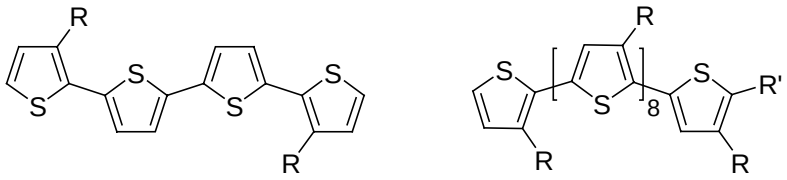

Fig. 2.8 Alkyl substituted 4T (left) and 10T (right) investigated in [92]. R=$C_{12}H_{25}$, R'=$COOCH_2C_6H_6$

Mushrush et al. [93] have investigated the VD films of alkyl substituted phenylene-thiophene oligomers (Fig. 2.9). The results show that vertical molecular alignment is predominant for all films, but the longer oligomers exhibit smaller apparent tilt angles of the molecular long axes with respect to the substrate normal, contrary to what was observed for the unsubstituted analogues [94].

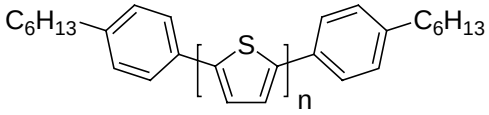

Fig. 2.9 Alkyl substituted phenylene-thiophene oligomers investigated in [93]. *n* = 1,2,3,4

Sassella et al. have investigated OMBD films of 4H6T molecules on (001)-oriented potassium acid phthalate (KAP) single crystals and silica. They have found that the 6T backbone stand at a tile angle of 55° with respect to the substrate normal in the film.

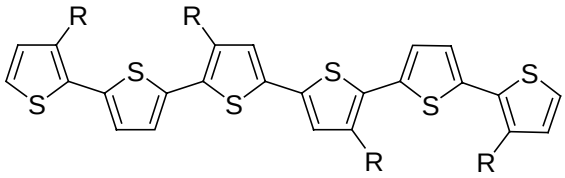

Fig. 2.10 Alkyl substituted 6T investigated in [95]. R=C_6H_{13}

In this part only the organic compounds with calamitic shape are reviewed. The study of substances with discotic shape like perylenetetracarboxylic dianhydride (PTCDA) and phthalocyanines are not reviewed here because they have few similarity to 1,3,4-oxadiazole compounds.

3 Experimental

3.1 Synthesis of aromatic 1,3,4-oxadiazoles

One aim of this work is to investigate the influence of the chemical structure on film formation with general structures illustrated in Fig.1.1 (page 1). The main points of interest are the influence of the head group (R in Fig.1.1), aliphatic chain (*n* in Fig.1.1) and the bridge group (X in Fig.1.1) which connect the aliphatic chain and 2,5-diphenyl-1,3,4-oxadiazole. Oxadiazoles with amide, ether and ester bridge groups are synthesised for the purpose of investigating the influence of bridge groups. Several oxadiazoles with different head groups such as cyano, methyl ester and nitro were prepared to the aim of head group influence investigation. Oxadiazoles with different lengths of substituted alkyl chain are also synthesised, so that the influence of alkyl chain length can be studied.

Numerous methods of 1,3,4-oxadiazole synthesis have been developed due to the important role of this category of compounds. Hetzheim [96, 97] and Hill [98, 99] provides very extensive reviews of the synthesis and the characterisation of 1,3,4-oxadiazoles. In this work several substituted 2,5-diphenyl-1,3,4-oxadiazole compounds were synthesised according to existing literature and the former work of our research group [18]. The synthesis is summarized in this section.

The building of the 2,5-diphenyl-1,3,4-oxadiazole unit is always the most important step of synthesis, except in cases where the 2,5-diphenyl-1,3,4-oxadiazole unit is commercially available. In this work, the 2,5-diphenyl-1,3,4-oxadiazole structure is mainly achieved through elimination of water from dibenzoyl hydrazine compounds. This step is schematically illustrated in Scheme 3.1. For the elimination of water $POCl_3$ or $SOCl_2$ can be used. The dibenzoyl hydrazine is stirred in $POCl_3$ or in $SOCl_2$ at reflux. The resulted oxadiazoles are usually soluble in $POCl_3$ or $SOCl_2$, thus the system become a clear solution at the end of the reaction.

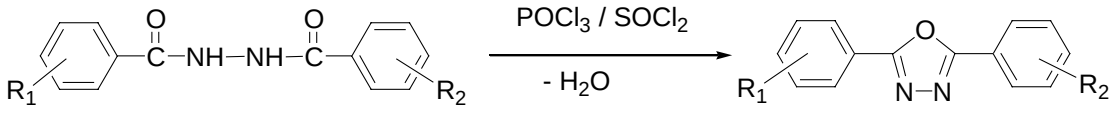

Scheme 3.1 The synthesis of 2,5-diphenyl-1,3,4-oxadiazole derivatives.

3.1.1 2,5-Diphenyl-1,3,4-oxadiazoles with an alkoxy substituent

This series of oxadiazoles is synthesised in roughly two steps. In the first step a diabenzoyl hydrazine with substituent is synthesised. Then the dibenzoyl hydrazine is cyclized to oxadiazole in the second step. The reaction route for synthesis of oxadiazoles

with an ether bridge is shown in Scheme 3.2. The phenyl ring of one of two raw materials is already substituted with an alkoxy group. However the synthesis routes for different alkyl chain lengths are somewhat different due to the availability of the raw materials.

For alkyl chain lengths n = 8 or 15 (n is the number of $–CH_2–$ unit in the chain), the dibenzoyl hydrazine is obtained from the reaction of substituted benzoyl chloride with alkoxy benzoic acid hydrazide. The latter is synthesised by stirring alkoxy benzoic methyl ester in hydrazinhydrate.

For alkyl chain lengths n = 9 or 11, the dibenzyol hydrazine is synthesised in the reaction of substituted benzoic acid hydrazide with alkoxy benzoyl chloride, which is available by heating the corresponding alkoxy bezoic acid under reflux in $SOCl_2$. For alkyl chain length n = 4, the commercially available 4-pentyloxybenzoyl chloride can be directly used for synthesis.

The dibenzoylhydrazines were then cyclized by eliminating a molecule of water. Phosphoroxyl chloride ($POCl_3$) serves as a water eliminating agent.

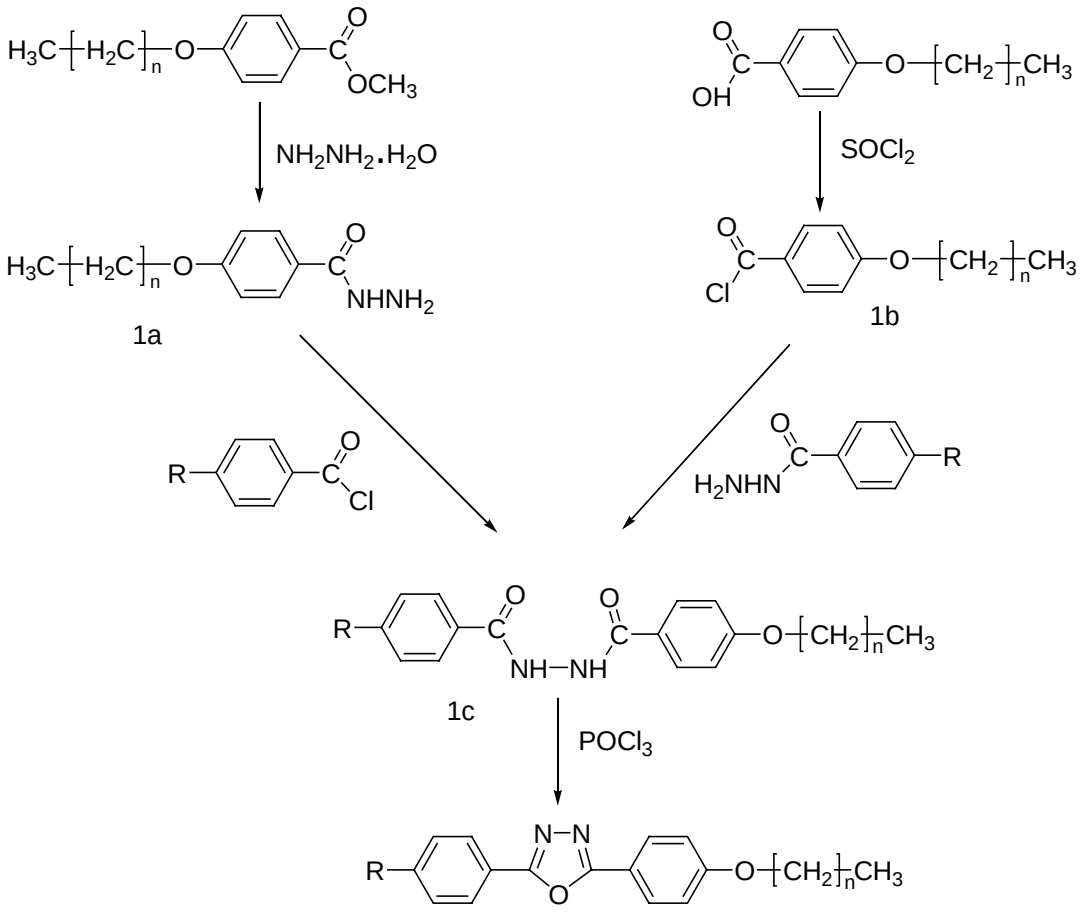

Scheme 3.2 The preparation of 2,5-diphenyl-1,3,4-oxadiazoles with ether bridge

Tab. 3.1 1,3,4-oxadiazole derivatives with ether bridge group

R	*n*	Name
p-CN-	15, 11, 9, 4, 0	*p*CEt16,12,10,5,1
m-CN-	15	*m*CEt16
NO_2-	15, 11	NIEt16,12
CH_3O-	15	MOEt16
CH_3OOC-	15	MEEt16
H-	15	HEt16

3.1.2 2,5-Diphenyl-1,3,4-oxadiazole derivatives with an amide bridge group

Unlike the synthesis of oxadiazoles with ether bridges, which are obtained in the cyclization of alkoxy substituent dibenzoyl hydrazine, oxadiazoles with an amide bridge group are prepared by joining an alkyl acid chloride with an amino substituted 2,5-diphenyl-1,3,4-oxadizole. The preparation can also be roughly divided into two steps, in the first step an amino substituted 2,5-diphenyl-1,3,4-oxadiazole is synthesised and afterwards the alkyl chain is connected to it over the amino group via an acylation reaction.

In the first step the dibenzoyl hydrazine is obtained by dropping the substituent benzoic acid chloride solution (in THF) into the pyridine solution of 4-nitro benzoic acid hydrazide. Depending on the availability of the raw materials, substituent benzoic acid hydrazide and 4-nitro benzoic acid chloride can also be used. The resulting dibenzoyl hydrazine is then cyclized with $POCl_3$, thus an oxadiazole with nitro end group is synthesised. Afterwards the nitro group is reduced to an amino group by $HCOONH_4$ with Palladium/Carbon as catalyst in methanol.

In the second step the connection of alkyl chain over an amide bridge to phenyl ring in the 2,5-diphenyl-1,3,4-oxadiazole is realized in the reaction of amino substituted 2,5-diphenyl-1,3,4-oxadiazole with alkyl acid chloride.

The preparations of this series of oxadiazoles are shown in Scheme 3.3, Scheme 3.4 and Scheme 3.5. The prepared substances are listed in Tab. 3.2:

Tab. 3.2 1,3,4-oxadiazole derivatives with amide bridge group.

R	*n*	Name
NO_2-	10	NIA11
p-CN-	10, 15	*p*CA11,16
H-	10	HA11

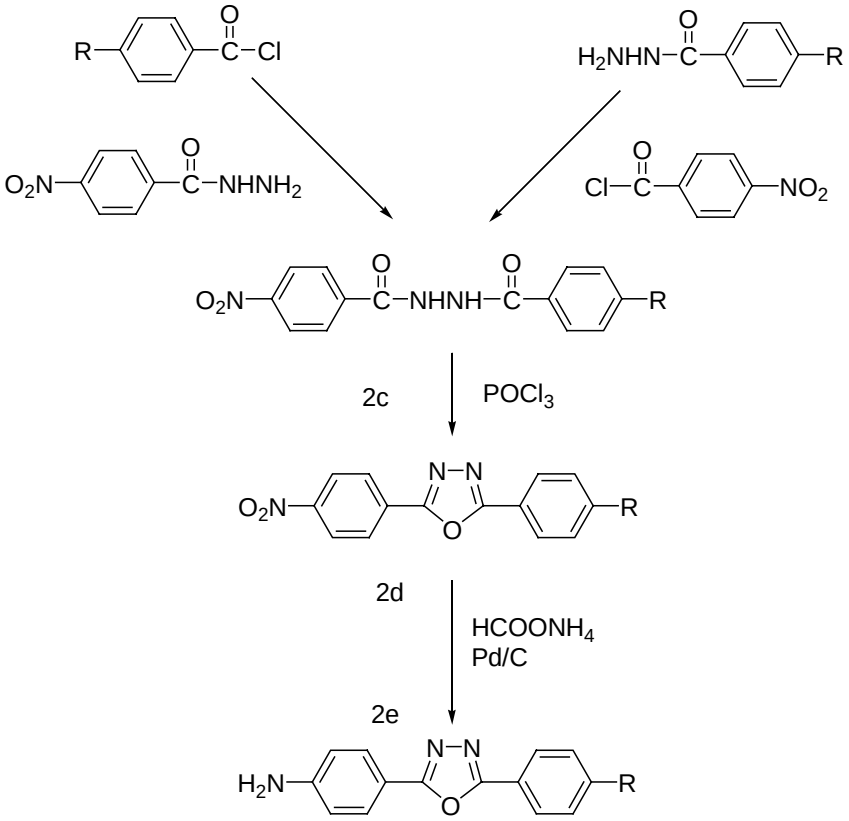

Scheme 3.3 The preparation of amino substutuent 2,5-diphenyl-1,3,4-oxdiazole

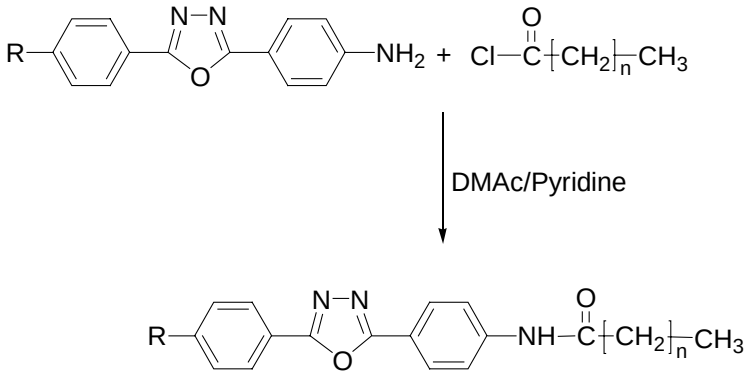

Scheme 3.4 Synthesis of 2,5-diphenyl-1,3,4-oxadiazoles with an amide bridge group

In the Scheme 3.3, when R is an amino group, the hydrazine can only be obtained with low yield using 4-amino benzoic acid hydrazide and 4-nitro benzoic acid chloride. The reason for this is that the amino group of the phenyl ring can also react with benzoic acid chloride resulting in byproducts, which are difficult to separate. Therefore the mixture is treated with $POCl_3$ in the cyclization reaction and the subsequent reaction. The end product is purified by recrystallization.

When R is a nitro group, a symmetrical nitro substituted 2,5-diphenyl -1,3,4-oxadiazole is synthesised. This substance will be reduced into 2,5-di(4-aminophenyl)-1,3,4-oxadiazole. After connecting the alkyl chains at both amino groups, symmetrical 2,5-diphenyl-1,3,4-oxadizole with two amide bridge groups can be obtained. This process is shown in Scheme 3.5:

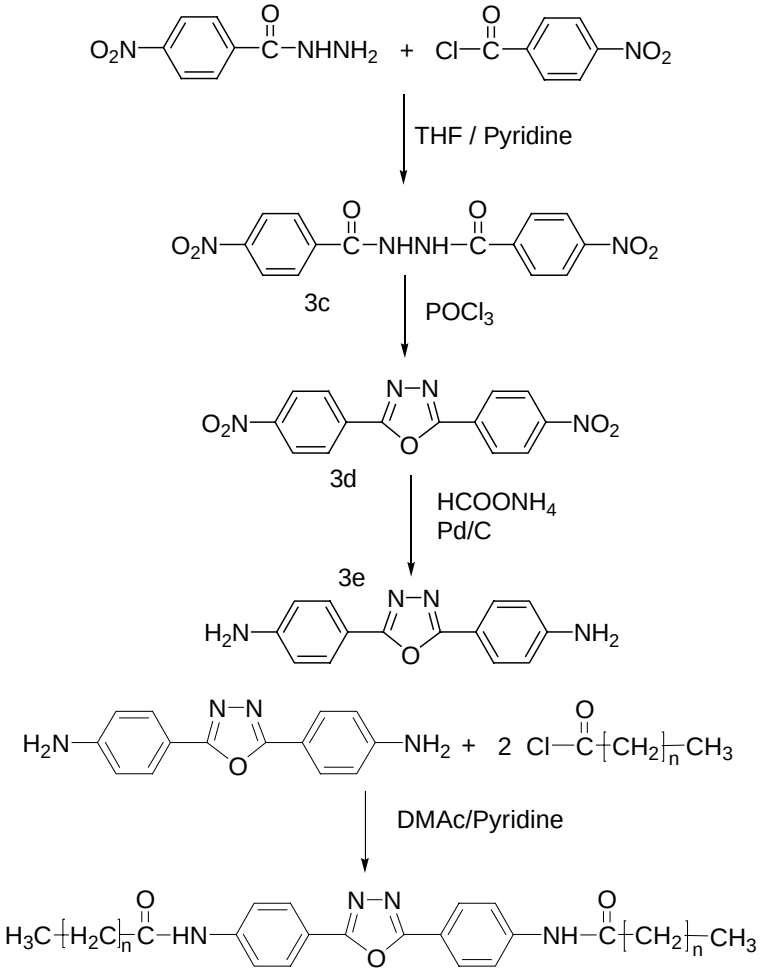

Scheme 3.5 Synthesis of symmetrical substituted 2,5-diphenyl-1,3,4-oxadiazoles with amide bridge groups.

Tab. 3.3 Symmetrical substituted 1,3,4-oxadaizole derivatives with amide bridge groups.

n	Name
16, 10, 6	17AA17, 11AA11, 7AA7

3.1.3 Symmetrical substituted 2,5-diphenyl-1,3,4-oxadiazoles with ester bridges

To synthesize this kind of oxadiazole, a short alkyl chain substituted symmetrical 2,5-diphenyl-1,3,4-oxadiazole with ester bridges is first prepared. The alkyl chain is then extended in an ester exchange reaction with a long chain alkyl alcohol in tetraisopropylorthotitanat. The synthesis is shown in Scheme 3.6:

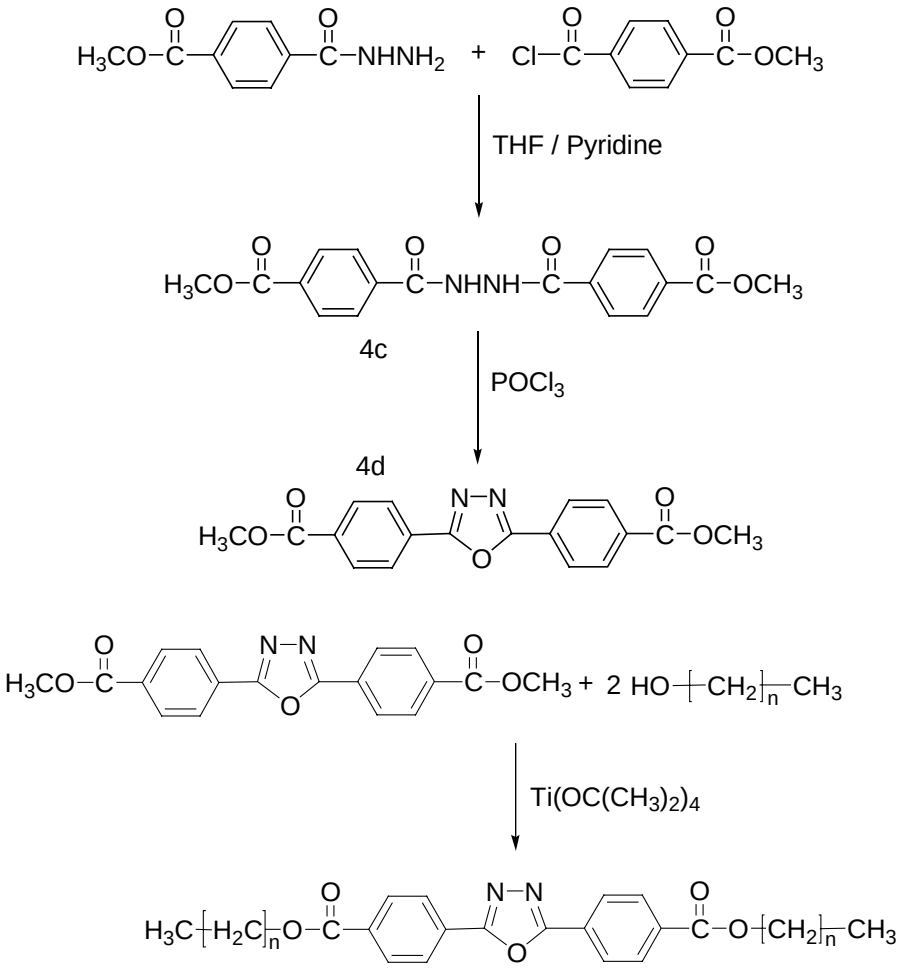

Scheme 3.6 Synthesis of symmetrical 2,5-diphenyl-1,3,4-oxadiazoles with ester bridges, n = 11.

Tab. 3.4 Symmetrical 1,3,4-oxadiazole derivative with ester bridges.

n	Name
11	12EsEs12

3.2 Vapour deposition film preparation

Vapour **d**eposition (VD) is an important method for preparing thin films. There are two procedures in VD, namely the film deposition in **H**igh **V**acuum (HV) and in **U**ltra **H**igh **V**acuum (UHV), sometimes referred to as **O**rganic **M**olecular **B**eam **D**eposition (OMBD). The difference between these two procedures is that in HV the residual gas can still influence the film growth, while in UHV this influence is so small that film can growth without disturbance. Compared with other well known methods for monolayer preparation such as Langmuir-Blodgett film deposition from, in most cases, water-air interface and self-assembled film deposition from solution, Vapour deposition in HV or UHV has the advantage of providing both a clean environment and substrate. Moreover, the OMBD technique allows in-situ film diagnostic methods such as **R**eflection **H**igh-**E**nergy **E**lectron **D**iffraction (RHEED), **L**ow **E**nergy **E**lectron **D**iffraction (LEED) to be used [19].

3.2.1 High vacuum deposition setup

Polished silicon wafers with a thin, native oxide layer, characterized by a **r**oot **m**ean **s**quare **r**oughness **(rms**, definition see 3.3.2, page 22**)** of 5 Å are used as substrates. According to Kern [100], they are carefully cleaned by sonication in acetone, ethanol and chloroform (for 10 minutes in each solvent) and subsequently in piranha (a 1:2 mixture of H_2O_2 and H_2SO_4) under reflux just before the deposition. The oxadiazole powder is evaporated from a Knudsen cell (Fig. 3.1) with a shutter in front of the orifice at a vacuum of 10^{-6} mbar. The distance between the effusion cell and the substrate is 150 mm and next to the substrate a quartz micro-balance FTM 5 (Edwards) is fixed for monitoring the film thickness and deposition rate (see Fig. 3.2). The temperature of the substrate holder can be controlled in a range from –20 to 200°C by resistive heating elements and water cooling.

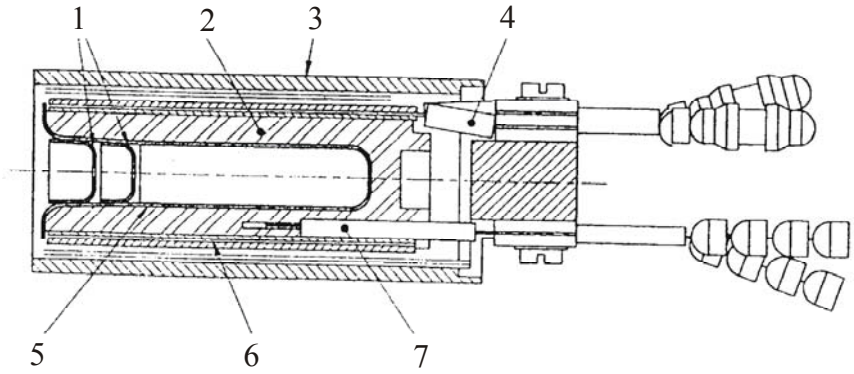

Fig. 3.1 Cross section of the effusion cell. 1. PBN end caps with apertures; 2. graphite crucible; 3. furnace housing; 4. heater connections; 5. PBN furnace liner; 6. heater; 7. thermocouple assembly

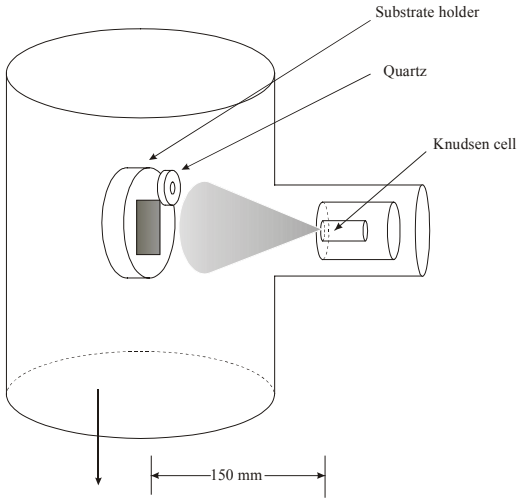

Fig. 3.2. Experimental setup of High Vacuum deposition

3.2.2 Film growth

The process starts by the evaporation in the Knudsen cell (Fig. 3.1) at a background vacuum about 10^{-7} to 10^{-9} mbar. The evaporation rate of the substance is controlled by adjusting the temperature in the Knudsen cell, so the film growth speed is consequently controllable. A simple mechanical shutter in front of the orifice of the Knudsen cell can interrupt the beam fluxes, i.e., to control the film thickness exactly.

The molecules rush out of the Knudsen cell through the orifice and form a molecule beam pointed towards the substrate. After the molecules are absorbed on the surface of the substrate, the film growth began. Several surface processes are involved in the film growth, the most important are: [101]

1. adsorption of the molecules on the substrate surface,

2. migration of the molecules or dissociation of the adsorbed molecules,

3. incorporation of the molecules into the crystal lattice of the substrate or the layer already grown,

4. thermal desorption of the molecules not incorporated into the crystal lattice.

There are two types of absorption, physical adsorption and chemical adsorption. Chemical bonds are created between molecule and substrate in the case of chemical adsorption, i.e. electron exchange between molecule and substrate, while for physical adsorption there is no electron transfer between the adsorbed molecule and substrate, and the attractive forces are van der Waals type [101]. A simple criteria to distinguish between the two is given by Henzler [102]. The adsorption with an adsorption energy below 50 $KJ \cdot mol^{-1}$ is referred to physical adsorption, otherwise it is chemical adsorption.

The organic molecules are generally large and the usually employed substrate temperatures are maintained well below the desorption temperature of the molecules, as a result the sticking coefficient can be assumed equal to unity, i.e. all of the molecules striking the substrate surface adhere to that surface [19].

The mobility of the molecules on the substrate depends strongly on the substrate temperature. The interaction between substrate and molecule determines the type of film growth. Three types of film growth are generally observed and accepted, they are illustrated schematically in Fig. 3.3.

When the interactions between molecules and substrate are more strong than that among molecules, the first layer of molecules tend to form a complete monolayer on the substrate. The second layer is somewhat less tight than the first layer, and finally the binding towards that of the crystal of the substance. This is the layer-by-layer model of film growth.

In the opposite case, the molecules are more strongly bund to each other than to the substrate, small clusters are nucleated directly on the substrate surface and then grow into islands of the condensed phase. This model of film growth is named as island or Volmer-Weber model.

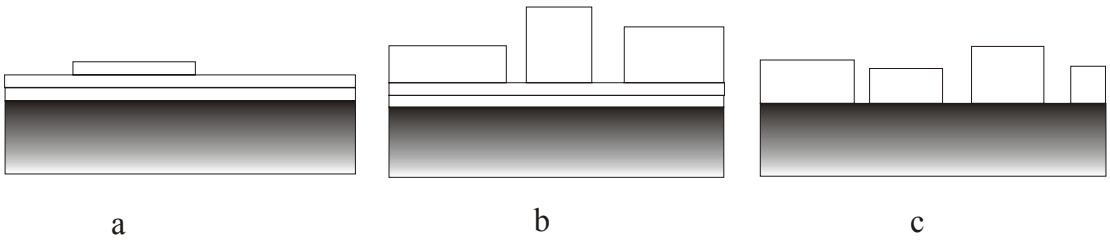

Fig. 3.3 Schematic illustration of the three film growth type a) layer-by-layer or Frank-van der Merwe; b) layer plus island or Stranski-Krastanov; c) island or Volmer-Weber mode [19] [103].

The layer plus island model, or Stranski-Krastanov model, is an intermediate case. After the first or several monolayers islands are formed on top of the intermediate layer [101].

The two methods of vapour deposition, HV and OMBD, differ in the vacuum in which the deposition occurs. The vacuum must meet the following requirements:

The mean free path, defined as the average distance traversed by the molecules between successive collisions, of the evaporated molecules must be longer than the distance from Knudsen cell to substrate.

For growing a sufficient clean epilayer, the monolayer deposition times of the background gas must be much longer, usually 5 orders of magnitude, than that of the deposited substance.

In a background vacuum of 10^{-5} mbar the average free path is much larger than the distance between the orifice of the Knudsen cell and the substrate (about 0.2 m). So the collision between molecules and gas is neglectable, the beam form depends mainly on the geometry of the Knudsen cell.

A vacuum of 10^{-5} mbar, i.e. HV, does meet the first requirement, while the second requirement can only be fulfilled in UHV [101].

The main aim of this work is the investigation of correlation between chemical structures of the oxadiazoles and its corresponding VD film structures. Although in the literature the influence of vacuum on film quality of some substance is reported, the experimental results shows that the film quality of oxadiazole is not strongly influenced. So most films in this work are prepared in HV.

In this work, the films were firstly prepared in vacuum at certain substrate temperature (T_s), then taken out and the film characterization such as X-ray specular reflectivity (XSR), Atom Force Microscopy (AFM) were carried out at room temperature. Some measurements were done in-situ by annealing the sample, the concrete conditions will be given by the corresponding discussion.

3.3 Bulk material and film characterization

3.3.1 X-ray

X-ray diffraction is a method of investigating the fine structure of a material. Diffraction is essentially due to the existence of certain phase relations. Two rays of the same wavelength are completely in phase whenever their path lengths are the same or differ by a whole number of wavelengths. This condition for efficient specular reflection is called Bragg's law:

$$2d \sin\theta_B = n\lambda \qquad 3\text{-}1$$

where d is the distance between the lattice planes, θ_B the Bragg angle, which is defined as the angle between the direction of the incident beam and the lattice plane and n is an integer.

X-ray diffraction can also provide information on the film thickness by analysis of a given peak using the so-called Scherrer formula:

$$\beta_{1/2} = \frac{0.9\lambda}{D \cdot \cos\theta_B} \qquad 3\text{-}2$$

where $\beta_{1/2}$ is the peak width at an intensity to half of the maximum intensity (FWHM), D is the film thickness, λ and θ_B are the same as in equation 3-1. It can be seen from this equation that the width of the diffraction curve increases as the thickness of the film decreases, providing that the film structure is not affected by the thickness.

3.3.2 Atom force microscopy (AFM)

Atom **F**orce **M**icroscopy (AFM) is a method of investigating nanometer- and atomic-scale structures and processes.

In AFM a tip is built on a cantilever, which is a flexible beam and is used as a force sensor. Driven by piezoelectric driver the cantilever moves over the surface of a sample in a raster scan. The cantilever bends in response to the force between the tip and the sample. A photodetector detects the bending and sends the data to a computer. Unlike STM a tunnelling current between tip and sample surface is not necessary for AFM, so the sample must not be electro conductive. AFM measures the force caused by, for example, electrostatic, van der Waals, frictional, capillary and magnetic interactions.

AFM images reflect the height information of the film topography. To quantitatively compare different films, the **r**oot **m**ean **s**quare **r**oughness **(rms)** can be calculated based on the height profile of the films obtained by AFM. The RMS r_{RMS} is defined as:

$$r_{RMS} = \sqrt{\frac{1}{n}\sum_{i=1}^{n}\left(r_i - \bar{r}\right)^2} \qquad 3\text{-}3$$

where $\bar{r}$ is the average height of the calculated region, r_i is the height of single scanned point. The rms roughness describes the fluctuations of surface heights around an average surface height. It should be taken into account that r_{RMS} depends on the size of the region where r_{RMS} is calculated. So the comparison of r_{RMS} is only meaningful when they are come form the region of same size.

In this work the films were measured with an AFM PSI SA1/BD2 from Park Scientific in contact mode with feedback on.

3.3.3 Reflection absorption infrared spectroscopy (RAIRS)

While AFM delivers information about the film topography, RAIRS provides information not only about the chemical structure of the film, but also about the structure and orientation of the film. The chemical and structural analysis of the RAIRS spectra always relies on the comparison with the spectra of bulk materials. Certain band positions as well as intensities are influenced by the interaction between molecules, thus by comparison the band positions and intensities of difference condensed states a deep understanding of the interaction between molecules can be obtained.

The IR spectra of bulk *n*-alkanes [104], LB monolayer of alkyl acid [105] and self assembling films of alkanethiols [106-108] have been studied in detail, and the relationship between band position and mesoscopic structure is well understood. The methylene symmetrical and asymmetrical stretching vibrations, which are located between 3000-2800 cm^{-1}, provide insights into the environment and conformation of the alkyl chain. These two bands shift to a higher wavenumber region when the freedom of the alkyl chain is increased. The band positions of methylene stretching vibrations are essentially higher in solution than in bulk, while that of the films are similar to the bulk, indicating a similar intermolecular environments for CH_2 groups in bulk and film.

Hydrogen bond (H-bond) is another kind of intermolecular interaction which can be best detected by means of IR spectroscopy. H-bond has been recognized as an interaction between the hydrogen in an X-H group of a molecule with a Y atom, usually in another molecule. So a hydrogen atom is associated with two atoms. X and Y can be same or different type of atoms, usually atoms with high electronegativities such as F, O, N are involved in the formation of strong H-bond. Typical H-bonds form between molecules with –OH, -COOH, -CONH groups. The hydrogen stretching band shifts to lower wavernumbers and becomes broader as result of formation of H-bond $X-H\cdots Y$. In contrast to the stretching band, the bending band, if visible in the spectra, usually increases in wavenumber due to the formation of H-bond. Vibrations involving the Y atom may be changed because the formation of H···Y bonds change the force field around Y. A good example is the blue shift of the C=O band of amide group from its solid state to solution.

The main problem in RAIRS measurements is the low signal-noise ratio for the thin films, which are usually 20 nm to 50 nm thick. In this work the films for RAIRS are deposited on a both side polished silica substrate which is transparent to infrared light. The RAIRS spectra were measured in a Perkin-Elmer FTIR 2000 spectrometer with a reflection setup, which is shown schematically in Fig. 3.4.

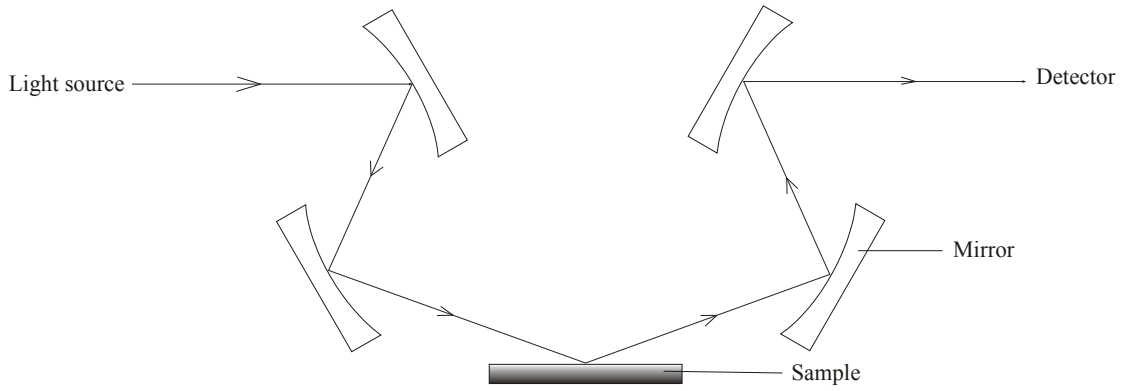

Fig. 3.4 The reflection setup for RAIRS

To increase the signal-noise ratio films are deposited on both sides of the substrate and

spectra are recorded with at least 300 scans. Because the silica substrate can reflect only less than 10% of the incident light, a metal mirror is put under the sample so that the reflection can be enhanced (Fig. 3.5). The sample and mirror are fixed on a heating plate, so the temperature influence on the film structure can also be studied.

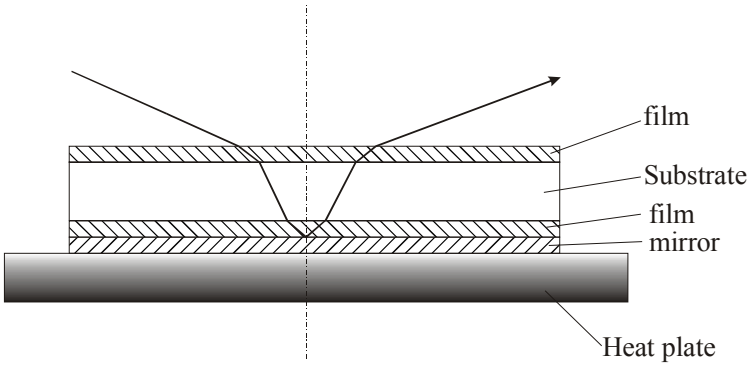

Fig. 3.5 Sample setup. A mirror is build under the sample to enhance the reflection.

3.3.4 Thermal gravimetric analysis and differential scanning calorimetry (TGA and DSC)

The thermal stability of the evaporated substance is of critical importance in vapour deposition. The **T**hermal **G**ravimetric **A**nalysis (TGA) is a simple but practical method for determining the thermal stability of the substance. The bulk substance, about 5 mg, was measured under nitrogen flow using a TGA 7 Perkin-Elmer device. The 5% weight loss temperature was adopted as the thermal degradation temperature of the substance. All evaporations were carried out far below this temperature to ensure that the molecules are not destroyed during film deposition. After deposition the chemical structure of the substance is checked again with IR spectroscopy.

The phase transitions of the substance is studied by means of **D**ifferential **S**canning **C**alorimetry (DSC). About 5 mg of substance was tested with a DSC 7 device of Perkin-Elmer with a heating rate of 10 K/min. For some runs 5 or 20 K/min were used. The precision of the temperature control of both equipment is 0.5 K.

3.3.5 Ultraviolet and Visible absorption and Photo Luminescence spectroscopy

Ultra**v**iolet and **Vis**ible absorption spectroscopy (UV-Vis) is the measurement of the absorption of ultraviolet (wavelength 200-400 nm) and visible light (wavelength 400-800 nm) after it passes through a sample or after reflection from a sample surface. The energy

of UV-Vis light corresponds to the energy needed to excite eletrons between energy levels of the molecular orbitals, in particular, transitions involving π orbitals and lone pairs. UV-Vis spectroscopy is of most use for identifying conjugated systems which tend to have stronger absorptions.

Photo **L**uminescence (PL) is the emission of photons when an electron moves form the **l**owest **u**noccupied **m**olecular **o**rbital (LUMO) of an excited state to the **h**ighest **o**ccupied **m**olecular **o**rbital (HOMO).

The UV-Vis and PL properties are of great interest in the study of thin films. They reflect the change of energy levels of the molecules caused by intramolecular interaction or/and intermolecular interaction. Although the molecular conformation and consequently the electron distribution may be influenced by the intramolecular arrangement, information about intermolecular interaction can still be obtained by studying the optical properties of a substance in thin films, solution and solid states.

3.3.6 Computer simulation

Simple computer simulation was carried out in this work to obtain the length of molecules in vacuum. The energy minimization was done using closed shelled wave function in AM1 method of MOPAC, which is a component of Chemoffice 5.0 software package.

3.4 Thermal stability of the studied oxadiazoles

The thermal stability of the substances is of critical importance in vapour deposition and device applications. The thermal stability of the oxadiazoles were studied by means of TGA and DSC. The oxadiazoles were sublimated at least once before they are employed in film preparation. IR spectra and HPLC were used to test the stability of a substance in the process of sublimation or evaporation. If the HPLC shows that the substance still has a high degree of purity after evaporation and IR demonstrates that the chemical structure remains unchanged, it can be concluded that the thermal stability of the substance is high enough for vapour deposition.

Here we take *p*CEt16 as an example to illustrate the analysis. The TGA and DSC analysis show that the degradation of this substance begins when the temperature reaches 250°C and the weight lost reaches 8% at 350°C in nitrogen. The melting of *p*CEt16 occurs between 123~127°C. The highest temperature applied to evaporate this substance is 160°C, far below the thermal degradation temperature. This is also the case for all other oxadiazoles studied in this work.

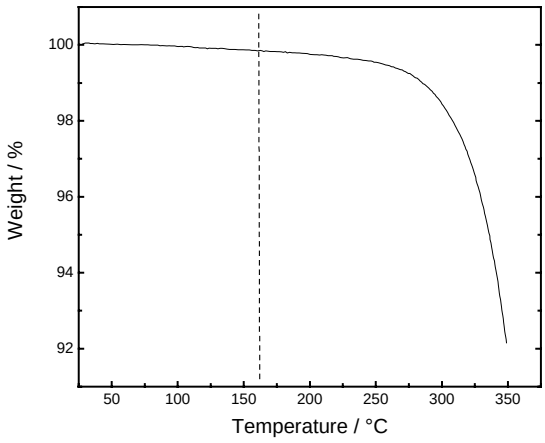

Fig. 3.6 TGA investigation of thermal stability of *p*CEt16. The dash line is the highest temperature applied in the vacuum evaporation.

The TGA gives information about thermal stability over a short period of time. A typical film preparation process could last as long as 10 hours. The long term thermal stability was tested with IR and HPLC. The HPLC shows that no other structure appears after evaporation and the IR spectra before and after evaporation are identical (Fig. 3.7). Combining the IR and HPLC results, we can conclude that the chemical structure of *p*CEt16 was not destroyed during deposition.

Freydank [18] has investigated the thermal stability of NIA11 by means of **g**as **c**hromatography (GC) and **m**ass **s**pectrometry (MS). The results showed that the NIA11 was not degraded in the evaporation process. The substance possesses a thermal stability high enough for VD film preparation.

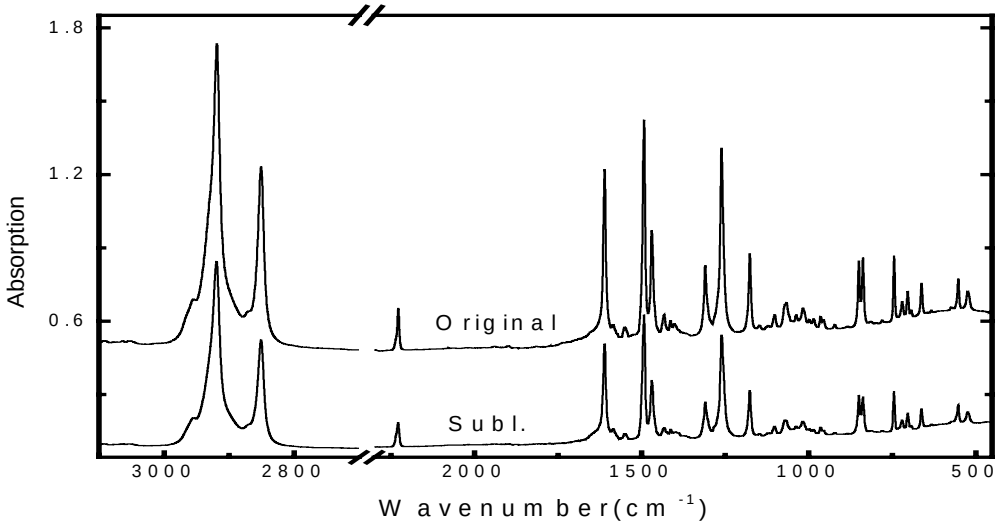

Fig. 3.7 IR investigation of original (up) and sublimated (down) *p*CEt16 in KBr. The curves are shifted along Y axis for clarity.

4 Influence of the deposition condition on the film formation

4.1 Introduction

The packing of organic molecules in a film is an equilibrium of several intermolecular interactions within a narrow energy range of less than 1 eV, including π-π overlap, electrostatic, van der Waals interaction and, for some molecules, hydrogen bonding [25, 109-114]. Physical film deposition conditions such as vacuum, substrate temperature (T_s) and growth rate can also influence this equilibrium and subsequently the film morphology [19]. The influence of those factors were also investigated in this work. The result show that, however, they are correlated to each other, i.e. the effect of a given physical deposition factor is influenced by other factors. For this reason during the investigation of the effect of a physical deposition parameter, the other parameters were kept constant as well as possible.

In this chapter the effect of the film growth conditions on its morphology will be discussed and experimental results presented to clarify aspects of the processes involved.

4.2 Influence of the vacuum

In the literature the typical growth of film were carried out in a background vacuum ranging from 10^{-7} to 10^{-11} mbar[1] [87, 95, 115-122]. According to Herman, the deposition is a concurrence process between contaminants, usually the residual gas molecules, and substance. For growing a sufficiently clean film, the background vacuum must be high enough, so that time needed to grow one monolayer of contaminants is 10^5 times longer that needed for the substance [101]. According to Herman's calculation, the vacuum required for growing film at typical film growth rate (1 monolayer/s) is 10^{-12} mbar.

Tanigaki et al. [123] have compared the crystalline structure of films of GaPcCl grown at a rate of 0.5 Å/min on (001) KBr under base vacuums of 5×10^{-6} and 3×10^{-9} mbar. Electron diffraction investigation showed that films prepared at higher vacuum have a higher degree of orientational order. Forrest [19] has compared films of PTCDA on HOPG prepared in a bell jar metal deposition system with a base pressure of 10^{-7} mbar and UHV-OMBD system. The high resolution STM image of the films prepared with UHV-OMBD system could always be obtained, while no clear images can be obtained for similar films deposited in the bell-jar system, which provides vacuum in the HV range. Böhler et al. [124] has reported that by growing organic light-emitting diodes (OLEDs) at a base pressure ranged form 10^{-4} to 10^{-9} mbar, the device performance increased when the vacuum is increased.

[1] It is customary to quote pressures in HV/UHV environments using units of Torr or mbar, where 1 Torr = 1.3332 mbar = 133.32 Pa.

In this work films prepared in HV and UHV were also compared. *p*CEt16 was chosen for this investigation, because within our labs there is considerable expertise built up from many experimental studies in its use and properties. Films with a thickness of 20 nm were deposited on Si/SiO_2 in a background vacuum of 10^{-6} mbar (HV) and 10^{-9} mbar (UHV) with T_s = 80°C. Due to the difficulty in controlling the film growth rate, the growth rate for UHV is double that used in HV. According to the result of our study, the effect of this growth rate difference is negligible (See §4.3, page 29). After the deposition the films are taken out of the chamber and measured with AFM at ambient condition. The AFM images are illustrated in Fig. 4.1.

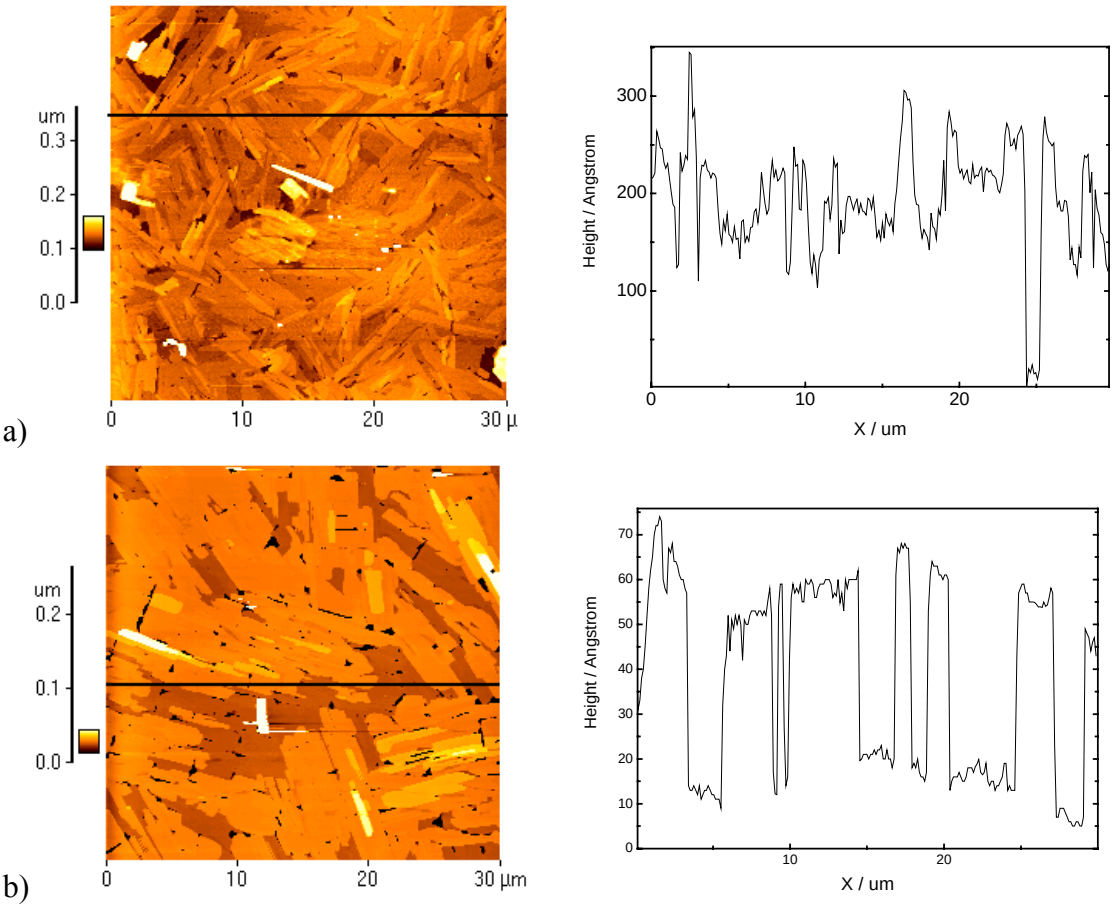

Fig. 4.1 AFM images of *p*CEt16 film deposited in background vacuum of 10^{-6} mbar (a) and 10^{-9} (b). The film thicknesses for both films are 20 nm. The film growth rates for 10^{-9} and 10^{-6} mbar are 1.2 and 0.5 nm/min, respectively.

The AFM images show similar topography for films deposited in HV and UHV. The surfaces of both films are characterized with slice-form domains. For films deposited in HV, the boundaries of the domains fuse together and form a large domain expanded over the whole scope of the image. Such fusion of small domains is not obvious for film deposited in UHV. The RMS roughness for films grown in HV and UHV are 4.7 nm and 6.5 nm, respectively. The film periodicities for both films obtain by XSR are 4.7±0.1 nm.

This comparison shows that, at least for our HV and UHV facility and for film

morphology study, the vacuum is not a critical deposition parameter. The main part of this work deals with the influence of the chemical structure of oxadiazole compounds on their VD film structure. The HV setup has the advantage of simplicity which means that the materials, the substrates, the evaporators and the chamber can be cleaned and changed quickly which enables a wide range of experiments to be conducted quickly and efficiently. For this reason the majority of the investigated films are prepared in HV equipment.

4.3 Influence of the film growth rate

The film growth rate, defined as the film thickness grown in a certain time, is a parameter describing the speed of film growth. In our deposition facility, the film thickness can only be measured indirectly using a quartz micro-balance (SQ) during deposition, so the growth rate deduced may bear an error to the real growth rate on substrate. However by comparing the film thickness measured by SQ and other method like XSR, this error is found to be below 20 % in most cases. Therefore the growth rate obtained by SQ is adopted in this work unless otherwise mentioned.

The film growth is a process in which the molecules diffuse along substrate or sublayer and order themselves into the glitter structure. The more molecules arrive at the substrate in a certain time, the less time for molecules to diffuse on the substrate. Together with another factor, the substrate temperature, the film structure can be controlled.

Typical growth rates for organics range from 10^{-3} to 10^{2} Å/s [19]. Since the monolayer (ML) thickness ranges from 3 to 50 Å, these rates correspond to 0.7 ML/h to 6 ML/s. The low end of this range has a danger of adsorbing contaminants onto the surface faster than the deposited molecules, while at the high rates the growth is difficult to control. Generally, at the sufficiently high rate and/or low substrate temperatures the film growth becomes a kinetically controlled, nonequilibrium process, resulting in structures which can be significantly distorted from the bulk crystal [19]. For example, Botta et al. [125] have found that, under certain conditions, the growth type of films based on a sexithiophene derivative is determined by the growth rate.

In this work the influence of growth rate on the topography of several oxadiazoles is investigated. Due to the fact that in-situ film characterisation is not possible, the substrate-substance lattice mismatch is neglected in this work. The focus of the work is on the structure of thick films, i.e. the film is thick enough that the influence of the substrate on the film structure is negligible. Reiche et al. [14, 63] have found that the molecules of oxadiazole compounds stand with a tilt angle on the Si/SiO_2 substrate. The monolayer thickness ranges from 2 to 5 nm, moreover the surface of Si/SiO_2 substrate is amorphous, so in this case the influence of substrate on the film growth over two or more monolayers could be neglected.

4.3.1 2-(4-Cyanophenyl)-5-(4-hexadecyloxyphenyl)-1,3,4-oxadiazole (*p*CEt16)

The influence of growth rate on film morphology is studied in HV. Films were prepared at growth rates of 0.04, 0.17 and 0.48 nm/min and measured with AFM after deposition. The results are shown in Fig. 4.2.

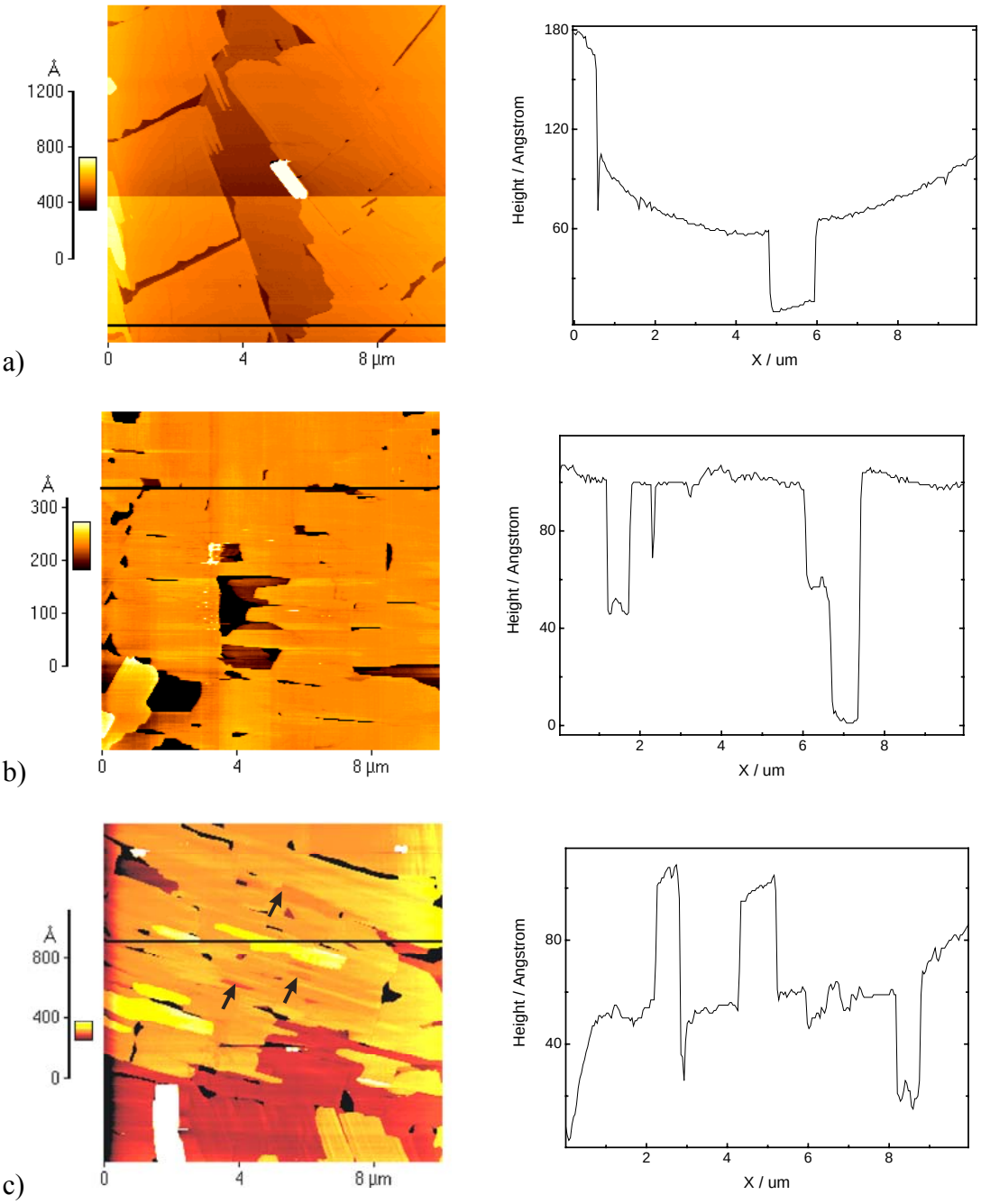

Fig. 4.2 AFM images of *p*CEt16 films with T_s = 85°C. The growth rate for films in a),b) and c) are 0.04, 0.17 and 0.48 nm/min. The thickness of the films obtained by XSR are 12, 19 and 24 nm for a) b) and c), respectively. The abruptly change of brightness in a) is caused by the measurement, not by the film itself.

The surfaces of all three films are characterized by the domain structures. Careful examination of the images revealed that each domain consists of many small sub-domains. The small and dark points or gaps in the images are a result of the incomplete fusion of sub-domains. The density of such dark points in Fig. 4.2 (a) are lower than in the other two images. The terrace is clear to recognize in all three images and their heights were determined to be 4.8 ± 0.5 nm, in good agreement with the value obtained by XSR. But in Fig. 4.2 (c) exist many spots with relative low brightness, some of them are denoted with arrows. The depth of such spots amounts 1 - 2 nm, much smaller than the terrace height. These low spots may come from the fast film growth.

The investigation of the effect of growth rates in the range from 0.04 to 0.48 nm/min shows that in this region the growth rate has no influence on the film periodicity, however, lower rates result in smoother domains.

4.3.2 4,4'-Bis(4-dodecanoylamino)-2,5-diphenyl-1,3,4-oxadiazole (11AA11)

The influence of growth rate on the VD film building behaviour is also studied with 11AA11, which is a symmetrical substituted oxadiazole compounds.

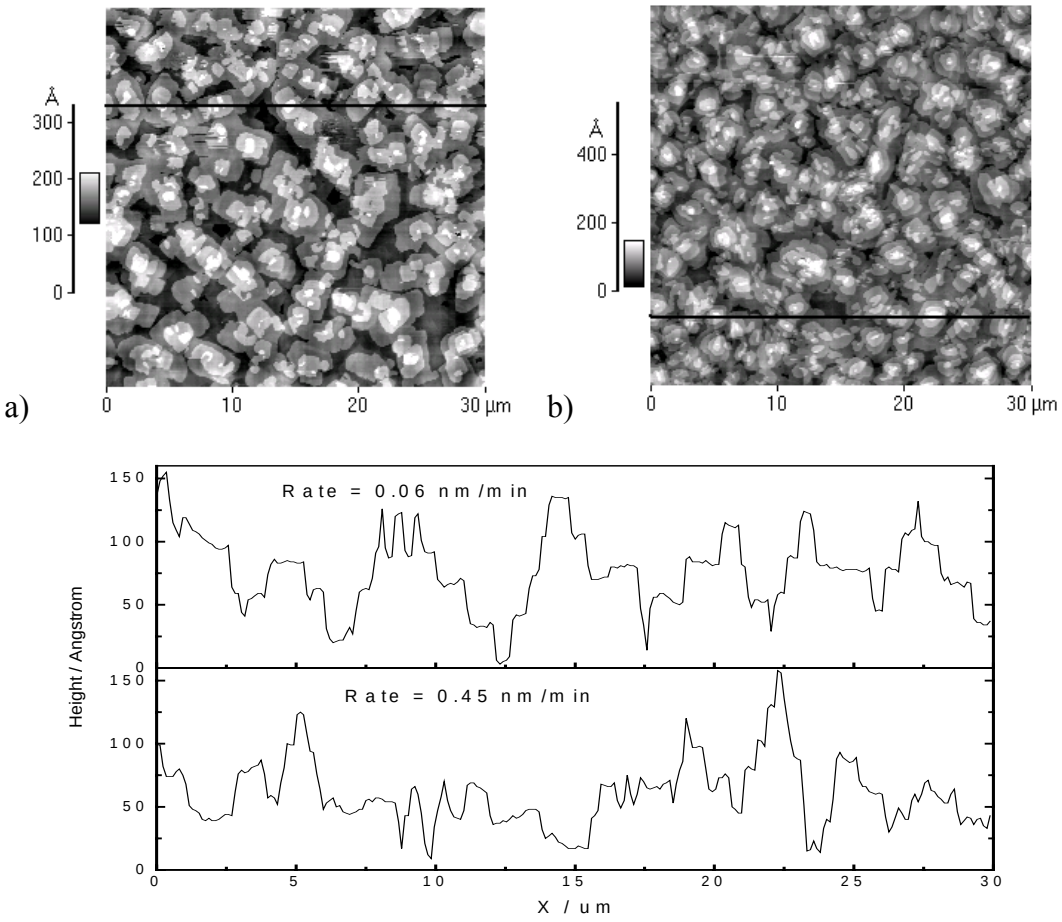

Fig. 4.3 AFM images of 11AA11 films with T_s = 155°C. The growth rates is 0.05 nm/min for a) and 0.5 nm/min for b).

Only when the T_s is higher than 85°C, can 11AA11 form layered films on Si/SiO_2 (See §5.3.4, page 94). Films of 11AA11 were prepared at $T_s > 85$°C at low (about 0.05 nm/min) and high (about 0.5 nm/min) growth rates, as the monolayer (ML) thickness is 3.2 ± 0.1 nm, these rates correspond to 0.016 ML/min and 0.16 ML/min, respectively.

AFM investigations revealed that the growth rates influence the film topology. $T_s = 155$°C as an example, both the films grown at high and low rate have domain structure and clear terrace, the AFM images show clear layer plus island (Stranski-Krastanov) growth mode. But the film with growth rate of 0.05 nm/min (Fig. 4.3 a) has averagely bigger domains than the film grown at higher rate (0.5 nm/min) (Fig. 4.3 b). Grown at low rate and high T_s, the slowly arriving molecules have sufficient thermal energy and time to diffuse on the substrate or film surface and order themselves into a minimum energy site. This results in domains with relative bigger size.

When the substrate temperature is equal to or slightly higher than 85°C, where the film structure changes from an amorphous to a layered structure, the influence of growth rate is more obvious. At this T_s the growth is just at an equilibrium state and increasing the growth rate can turn it into a nonequilibrium, kinetically controlled process which results in films just like grown at $T_s < 85$°C. Fig. 4.4 illustrates this effect. The film grown at T_s = 95°C at a growth rate of 0.5 nm/min has a layered film structure, one peak appears in its XSR curve. In contrast to that, the film grown at T_s = 105°C at a growth rate of 20 nm/min has amorphous film structure with no peaks appearing in its XSR curve.

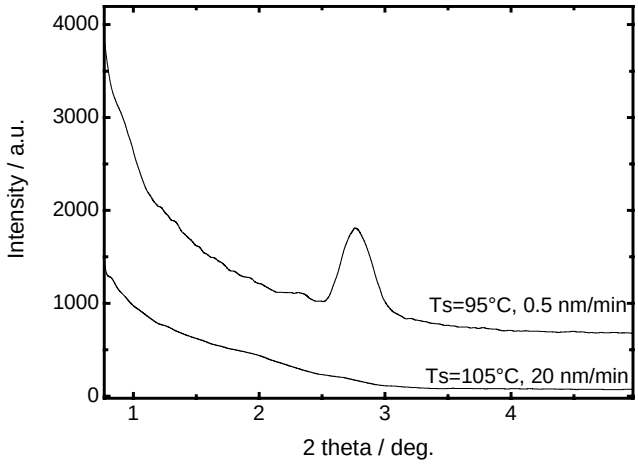

Fig. 4.4 The influence of growth rate on the film structure based on 11AA11. The films were prepared with growth rates of 0.5 and 20 nm/min at T_s = 95°C and 105°C, respectively. The peak in the XSR curve corresponds to film periodicity of 3.2 ± 0.1 nm. Film thickness for both films are 40 nm.

In the literature, the most important argument of applying high rate for film growth is to assure that a minimal density of impurities and defects will be incorporated into the film. Estimated using a simple kinetic theory, even in a background vacuum of 5×10^{-9} mbar, the time needed for the rest gas to form a monolayer on the substrate is only 3 minutes [19]. According to this theory it is impossible to deposit a film without incorporating

impurities even at a background vacuum of 10^{-9} mbar, because the preparation of substrate etc. needs much longer than 3 minutes. The AFM results of this study have shown that lower growth rates result in larger and smoother domains. The reason may be that the impurities like molecules of rest gas have very limited influence on the film growth due to their small size compared with organic molecules. On the other hand, impurities are always expelled out in the slow growth of crystals. The latter factor has always been neglected in the theory of film growth.

4.4 Influence of the substrate temperature (T_s)

The substrate temperature (T_s) is a very important physical parameter which influences the structure of vapor deposited films [19, 24, 126-128]. In the literature the applied T_s ranged from 80 to 400 K. Similar to the situation of growth rate, low T_s has also the risk of absorbing impurities faster than substance on the substrate. For organic molecules the sticking coefficient is assumed equals to unity, i.e. all molecules striking the substrate adhere to its surface. This situation results since the organic molecules are large and the substrate temperature is maintained well below the evaporation temperature [19].

In this work the influence of T_s on the film morphology is investigated for many oxadiazole compounds. The investigation of the influence of T_s shows that the effect of T_s varies with the molecular structure, especially the amide group in the molecule. So the influence of T_s will be discussed in detail in §5, where the influence of chemical structure on the film formation behaviour of oxadiazole compounds are discussed. Here just *p*CEt16 and 11AA11 are taken as two examples to illustrate the general effect of T_s on the film formation.

4.4.1 2-(4-Cyanophenyl)-5-(4-hexadecyloxyphenyl)-1,3,4-oxadiazole (*p*CEt16)

The films of *p*CEt16 were prepared at T_s ranges from –15°C to 85°C. Since the investigation of growth rate on the film topography shows that low rate result in smooth domain surface, the growth rate was maintained between 0.01 and 0.02 nm/min. After deposition the films were measured with AFM and XSR.

The AFM images demonstrate the strong correlation between film topology and T_s. The film prepared at –15°C has a surface characterized with random distributed thread-like structure. Increasing the T_s up to 25°C and 60°C, the film topology is significantly changed. These films are characterized by smooth terraces of several micrometers in lateral dimension with a height of the terraces of 5.0 ± 0.5 nm.

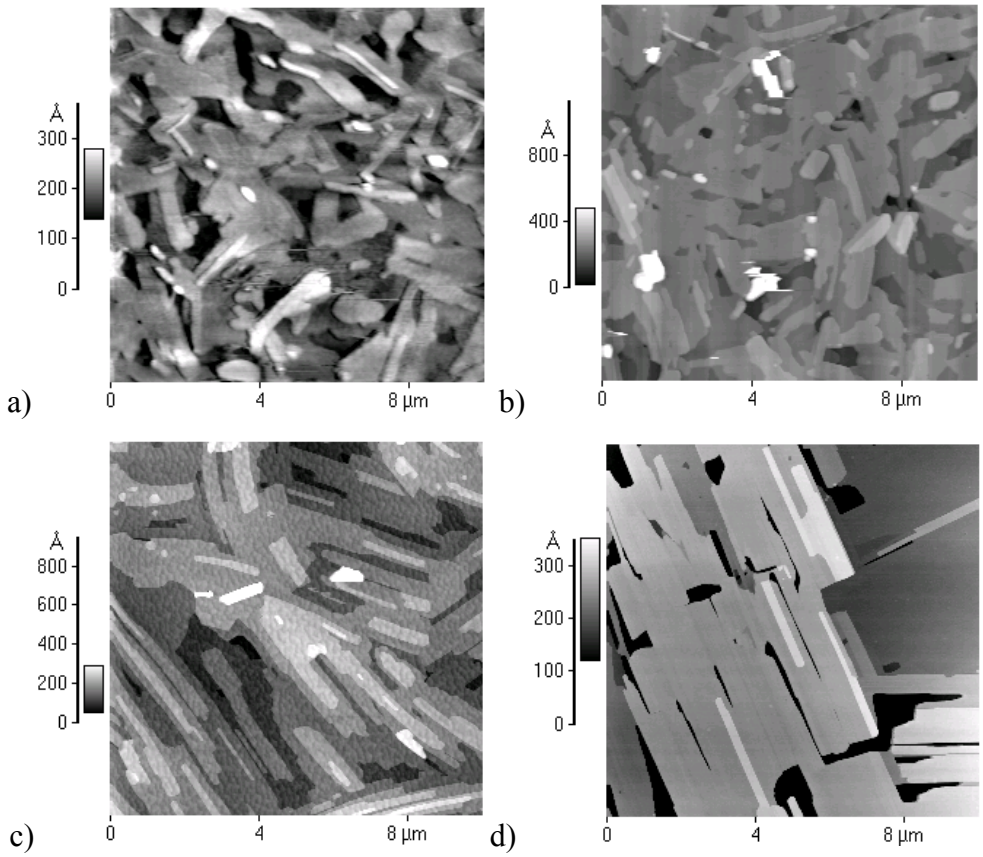

Fig. 4.5 AFM images of *p*CEt16 films deposited on Si/SiO_2 at T_s = (a) –10°C, (b) 25°C, (c) 60°C and (d) 85°C. The growth rates are maintained between 0.01 and 0.02 nm/min. The film thickness for all films measured with quartz micro-balance is 15 nm.

Further increasing the T_s to 85°C, the size of domains in the lateral dimension became very long (up to 20 µm). The XSR investigation revealed that *p*CEt16 always forms films with layered structures in the investigated T_s range, but the film periodicity is different for T_s < 60°C and T_s > 85°C. The film periodicity for T_s < 60°C is 4.8 ± 0.1 nm, but 4.5 ± 0.1 nm for T_s > 85°C (Fig. 4.6). The reason for this difference is discussed in §5.2.2 (page 54).

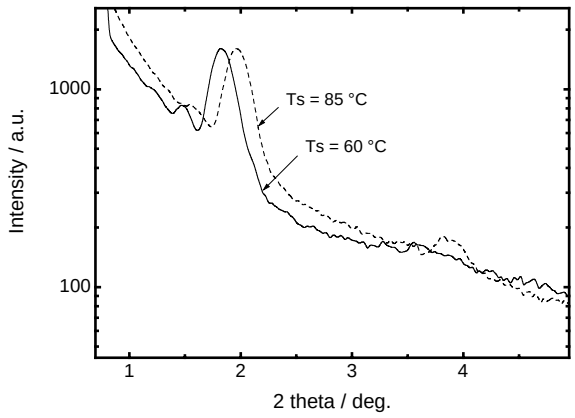

Fig. 4.6 The influence of T_s on the film structure of *p*CEt16 film. The films were prepared at T_s = 60°C and 85°C. The film periodicity for T_s = 60°C and 85°C are 4.8 ± 0.1 nm and 4.5 ± 0.1 nm, respectively.

4.4.2 4,4'-Bis(4-dodecanoylamino)-2,5-diphenyl-1,3,4-oxadiazole (11AA11)

11AA11 has the ability to build intermolecular H-bonds due to the amide unit in its structure. In addition to π-π, dipole-dipole and Van der Waals interactions, H-bonds contributes also to the balance between different interactions in the process of film formation. Furthermore, the temperature influences the strength of H-bonds and subsequently the film structure.

An XSR investigation of film grown at T_s = 30°C und T_s = 155°C was carried out to get an insight into the film structure (Fig. 4.7). For T_s = 30°C, a very weak peak in the XSR curve corresponding to a film periodicity of 3.9 nm was found, the film is nearly amorphous. In contrast to 30°C, the film with T_s = 155°C has a strong peak in its XSR curve corresponding to film periodicity of 3.2 ± 0.1 nm, indicating that the film has layered structure.

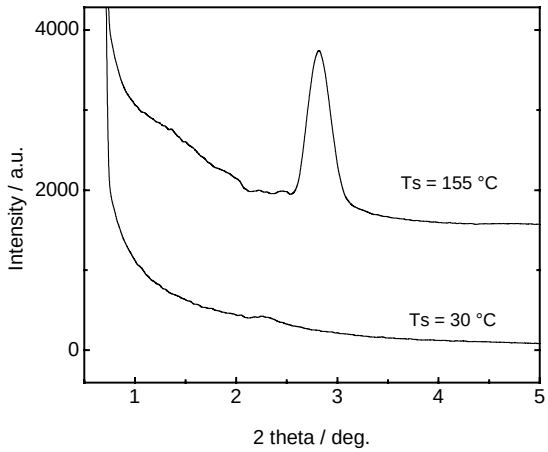

Fig. 4.7 The XSR results of 11AA11 films deposited on Si/SiO_2 with T_s = 30 and 155°C. The peak in the curve for T_s = 155°C corresponds to film periodicity of 3.2 ± 0.1 nm.

Fig. 4.8 shows the AFM images of 11AA11 films deposited on Si/SiO_2 at T_s from 30 to 175°C. The surface of films prepared at 30, 80 and 95°C are characterized with cloud-like structures, whose size increase with the increase of T_s (Fig. 4.8 a, b and c). Terrace structure could not be found in the AFM images for these films until the T_s was elevated to 135°C. Very unclear terrace could be recognized in the AFM images of films grown with T_s of 135°C. The film deposited at T_s = 155°C has already very clear terrace structure, revealing the layer-by-layer growth mechanism for the film. The average terrace height was measure by height profile scanning to be 3.1 ± 0.5 nm. This value is smaller than the calculated molecule length in extended conformation (3.83 nm).

The size of domains in images e) and f) of Fig. 4.8 show the strong dependence on T_s. By increasing T_s by 20°C (from 155°C to 175°C), the average diameter of domains increased from about 5 µm to more than 10 µm. At higher T_s the molecules arriving at the substrate

have a higher energy and can therefore spend a longer time finding a minimum energy site at the edge of the already grown crystals, which results in larger domains.

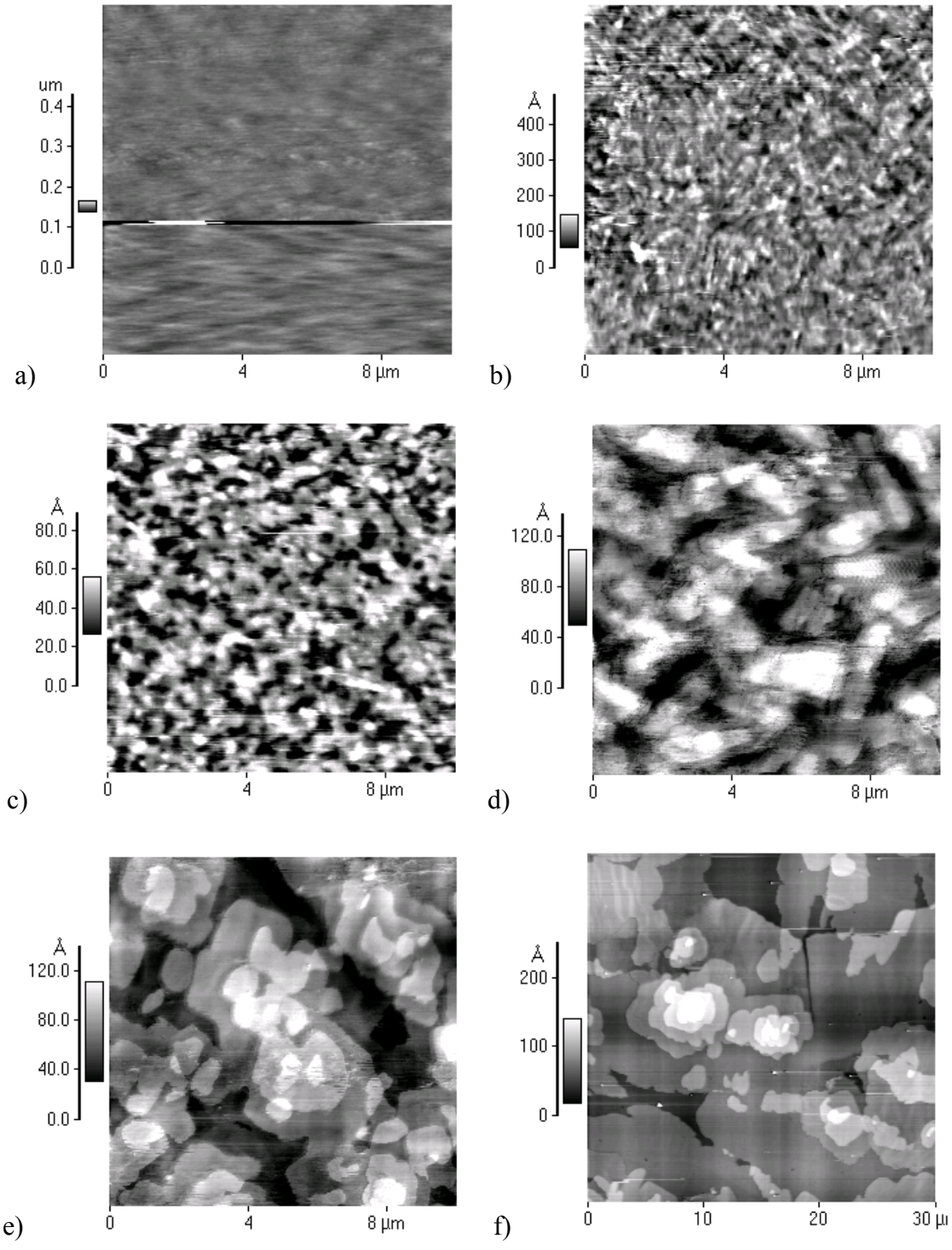

Fig. 4.8 AFM images of 11AA11 films deposited on Si/SiO_2 at T_s = (a) 30°C, (b) 85°C, (c) 95°C, (d) 135°C, (e) 155°C and (f) 175°C. The growth rates are maintained between 0.04 and 0.3 nm/min. The film thickness for all films measured with quartz micro-balance are 30 nm. The terrace height in e) and f) is measured to be 3.1 ± 0.5 nm. Please note that the scale of f) is 30 × 30 µm.

The presence of amide groups in the molecules provides the possibility of intermolecular hydrogen bonding. The effect of T_s on film morphology is therefore also different. The oxadiazole *p*CEt16 has no amide group in molecules. In all the investigated T_s range, *p*CEt16 can form films with layered structure. The T_s influences only the topology of the deposited film. The films deposited at low T_s show granular surface, while those prepared at high T_s have smooth domains and clear terrace structure. Similar effect on film topography can also be found for 11AA11 film. In contrast to *p*CEt16, 11AA11 could not form layered film at low T_s, layered film structure could only be found for film deposited at relative high T_s. The amorphous film deposited at low T_s can be converted to layered film by annealing over certain temperature. For detailed discussion about H-bond and thermal induced structural transition please see §5.3.4 (page 94).

4.5 Summary

The study of the influence of the physical deposition conditions on the film formation of aliphatic substituted oxadiazoles can be summarized as follows.

1. The vacuum in the range from 10^{-6} mbar to 10^{-9} mbar has a small influence on the film topology, but does not influence the film structure significantly. A vacuum of 10^{-6} mbar is high enough for film morphology studies.

2. Within the range of growth rates from 0.05 nm/min to 0.5 nm/min, lower rate results in smoother and bigger domains.

3. The substrate temperature (T_s) has a significant influence on the film topology. High T_s results in large smooth domains with clear terrace structures. For different substances the T_s has different effects on the film structure. In the case of *p*CEt16, the films are always layered within the investigated T_s range. But 11AA11 can only form layered films at high T_s.

5 Chemical structure and film formation of substituted oxadiazoles

As outlined earlier in chapter 1, the main aim of this work is the investigation of the correlation between the chemical structure of a substance and its corresponding VD film structure. In chapter 4 the general studies about the influence of physical deposition conditions on the film formation have been discussed. In this chapter results of growth studies performed using oxadiazoles with general structures shown in Fig.1.1 are described and discussed. These molecules differ by chain length, head groups and bridge groups.

5.1 Influence of the aliphatic chain length

The aromatic and the aliphatic part of the molecules prefer different periodic in-plane structures when they are separately packed in a crystalline arrangement [129]. The Van der Waals interaction between the aliphatic chains, the electrostatic interaction, π-π overlap and, for some molecules, the hydrogen bond contributes to the total energy of the system. The formation of layered films is a results of the balance between those interactions. A study of LB films based on 2,5-diphenyl-1,3,4-oxadiazoles shows that the aliphatic chain can help to form stable layers at the air-water interface as well as on substrate [18]. In VD films of oxadiazole compounds, the aliphatic chain may also has this effect and serve as the supporting part.

Itaya et al. [74-76] studied the structures of VD films based on *n*OCBs with alkyl chain length of 8, 9, 10 and 12 carbon atoms by means of UV and PL spectroscopy. They found that, on the quartz substrate, the film structure of 12OCB is independent of substrate property (hydrophilic or hydrophobic) or temperature due to the strong Van der Waals interaction induced by the long alkyl chain. Leadbetter et al. [130] and Hori et al. [131, 132] investigated the influence of aliphatic chain length on the mesophase (Smetic A) structure of 4-cyano-4'-alkoxybiphenyls (*n*OCB) and found that, when $n > 6$, the crystal structure is independent on n. The layer periodicities increase almost linearly with n. The relation between the film periodicity and n can be described with following equation:

$$D = an + b \qquad 5\text{-}1$$

D represents layer periodicity while a and b are the contributions of a methylene unit and the core region (biphenyl part), respectively, to the layer periodicity. Here a = 0.213 nm and b = 1.14 nm.

In this section results of growth studies performed using oxadiazoles substituted with aliphatic chains with different lengths are described.

5.1.1 2-(4-Cyanophenyl)-5-(4-alkoxyphenyl)-1,3,4-oxadiazole (*p*CEt*n*)

To investigate the influence of aliphatic chain length on the VD film structure, cyano substituted 2,5-diphenyl-1,3,4-oxadiazoles with different length of aliphatic chains were synthesised. Their names are abbreviated here as *p*CEt*n* (*n* denoted the number of carbon atom in the chain).

From the chemical point of view, no typical intermolecular hydrogen bond can be formed for this series of oxadiazoles, instead, intermolecular interactions between cyano groups can influence the film building.

The layer periodicity of films of *p*CEt*n* were investigated with XSR. For *p*CEt16, the layer periodicity is slightly influenced by the substrate temperature. For the purpose of comparison substrate temperature of 25°C was used for all films. This temperature is still below the phase transition temperature of *p*CEt16 and all other substance form layered films at this temperature.

The lengths of the *p*CEt*n* molecules (L) in the extended chain conformation were determined by AM1 calculations using CS Chem3D Pro 5. The film periodicities were derived from XSR investigations. All those data are listed in Tab. 5.1.

Due to the banana shape of aromatic part and the nonlinear shape of ether bonding, two possible conformations exist for *p*CEt*n* (Fig. 5.1). They are named as cis- (Fig. 5.1 a) and trans- (Fig. 5.1 b) conformation in this work for the convenience of discussion.

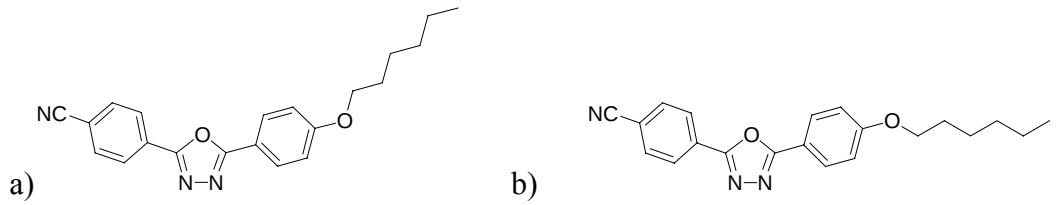

Fig. 5.1 Possible conformations for *p*CEt*n*, a) cis; b) trans.

Tab. 5.1 Calculated length of the *p*CEt*n* molecules in the extended chain conformation L(*n*) and layer periodicities D(*n*) derived from XSR measurements.

n		5	10	12	16
L(*n*) [nm]	cis	1.8	2.4	2.7	3.3
	trans	2.0	2.6	2.9	3.5
D(*n*) [nm]		2.4 ± 0.1	3.4 ± 0.1	3.7 ± 0.1	4.8 ± 0.1

The film periodicities of *p*CEt*n* are obviously bigger than the corresponding molecule lengths. The film topographies were measured with AFM, the images are shown in Fig. 5.2.

The images clearly show layered film structure. Further research revealed that the film topologies of each oxadiazole are greatly correlated with substrate temperature (See §4.4, page 33). Generally the higher substrate temperature results in bigger domain and lower roughness . The heights of the terraces in Fig. 5.2 were obtained from the height profile of the images. They correspond to the internal layer periodicities in Tab. 5.1. The results of AFM and XSR show clearly a bilayer-by-bilayer film growth mechanism of *p*CEt*n* on Si/SiO_2.

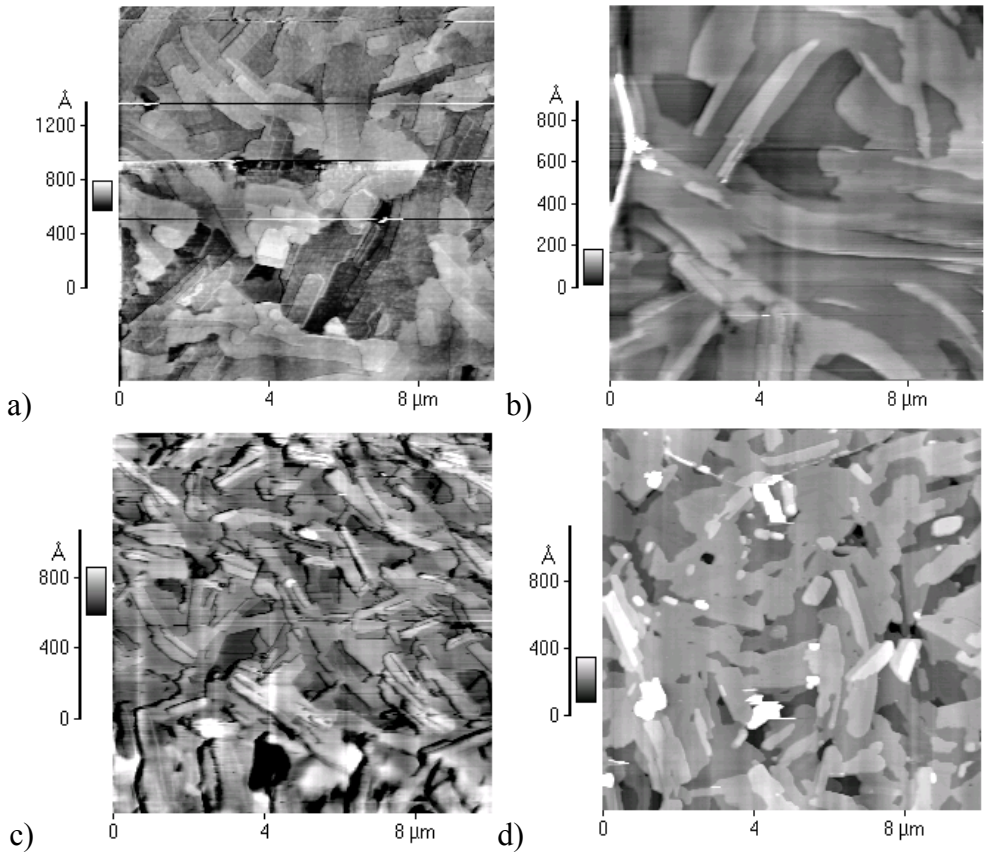

Fig. 5.2 AFM images of *p*CEt*n* films deposited at T_s = 25°C. a) *p*CEt5; b) *p*CEt10; c) *p*CEt12; d) *p*CEt16. The sizes of all images are 10 × 10µm. The film thickness for all films are 30 nm (measured with quartz micro-balance)

The *p*CEt1, i.e. the molecule has the shortest aliphatic chain (only $–OCH_3$), was also deposited on Si/SiO_2. The AFM image of the film is shown in Fig. 5.3.

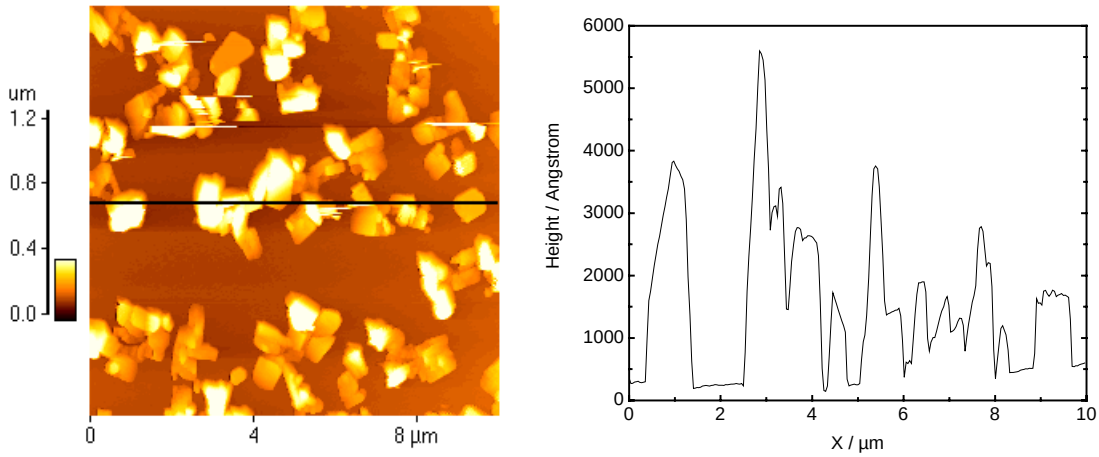

Fig. 5.3 The AFM image (left) of *p*CEt1 film deposited at T_s = 30°C. The height profile along the black line in AFM image is also shown (right).

The AFM investigation reveals that the *p*CEt1 can not form layered films on the Si/SiO_2. The image is characterized with many islands with size of micrometer in lateral and the normal direction of the substrate. No layered film structure could be found in the image.

The comparison of film formation behaviour of *p*CEt*n* show the effect of aliphatic chain.

Even a short chain of 5 carbon atoms can contribute greatly to the layered growth of films.

The film periodicities are plotted against *n* with the exception of *n* = 1. Linear dependence of film periodicity on *n* can be clearly seen from Fig. 5.4. This linearly dependence reveals that, in spite of their different length, the alkyl chains in the different films are standing at the same tilt angle to the substrate. The aromatic part of the molecules of different films have the same arrangement, i.e. the film structures are determined by the aromatic part of the molecules.

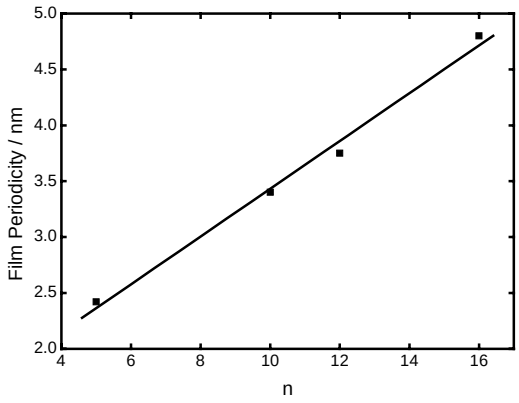

Fig. 5.4 Dependence of film periodicity (D) on the number of carbon atoms in the backbone of the chain.

Finally, for *p*CE*tn* with 16 ≥ *n* ≥ 5 the dependence of bilayer thickness D on the alkoxy chain length can also be described with the equation 5-1. For *p*CE*tn*, the a and b in equation 5-1 are 0.214 and 1.29 nm, respectively.

$$D = an + b = 0.214n + 1.29 \qquad 5\text{-}2$$

Similar to OCBs, here a and b are the contributions of a methylene unit and the core region to the layer periodicity, respectively. This linear dependence indicates that the molecules in the films of *p*CE*tn* with *n* ≥ 5 are ordered in the same manner. The aliphatic chain of *p*CE*tn* films are tilted at the same angle to the substrate. The variation of film periodicities are caused mainly by the change in chain length.

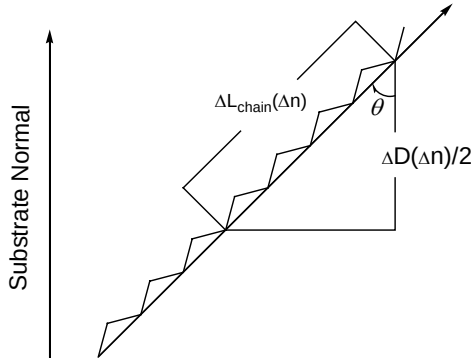

Fig. 5.5. Schematic illustration of tilt angle calculation of aliphatic chain.

As shown in Fig. 5.5, the tilt angle of the alkoxy chains θ can be calculated according to the following equation:

$$\cos\theta = \frac{\Delta D(\Delta n)}{2 \cdot \Delta L_{chain}(\Delta n)} = \frac{0.214 \cdot \Delta n}{0.128 \cdot \Delta n \cdot 2} \qquad 5\text{-}3$$

In this equation, D is the film periodicity, L_{chain} is the length of the aliphatic chain, which was obtained by AM1 calculation of MOPAC. Because of the bilayer structure of the film, the L_{chain} in the equation is multiplied by 2. The tilt angle of the aliphatic part is determined according to this equation to be about 33°.

5.1.2 4,4'-Bis(4-acylamino)-2,5-diphenyl-1,3,4-oxadiazole (*n*AA*n*)

Besides *p*CEt*n*, the chain length dependence of *n*AA*n* were also investigated by means of XSR and AFM. All the films are prepared at T_s above 120°C, above which the film periodicities of *n*AA*n* are almost temperature-independent (See Fig. 5.67 at page 94).

The film topologies were investigated with AFM (Fig. 5.6). Film surfaces of 17AA17 and 11AA11 are characterized by smooth terraces several micrometers wide with a height of 3.8 ± 0.5 nm and 3.2 ± 0.5 nm, respectively. The corresponding film periodicities obtained by XSR are 3.9 ± 0.1 nm and 3.2 ± 0.1 nm, in agreement with the values obtained by AFM. The film of 7AA7 has a granular surface, terraces can hardly be recognized (Fig. 5.6 c), although XSR results revealed a layered film structure.

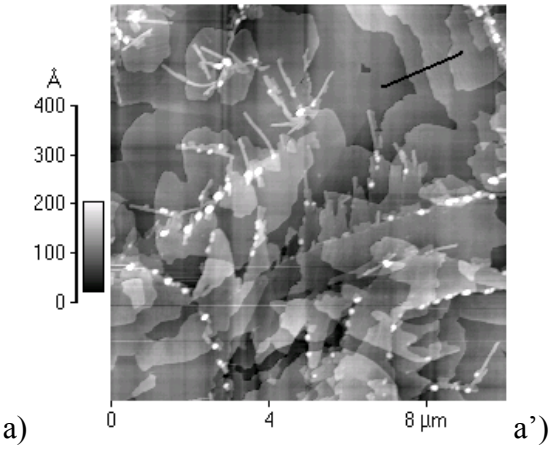

a)

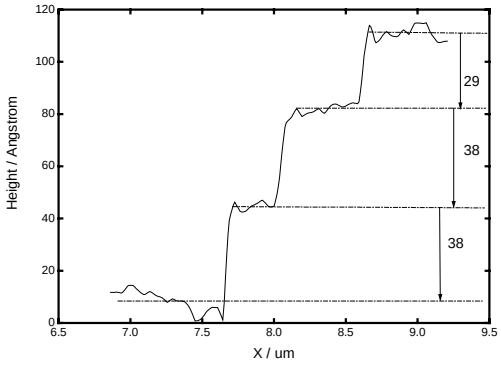

a')

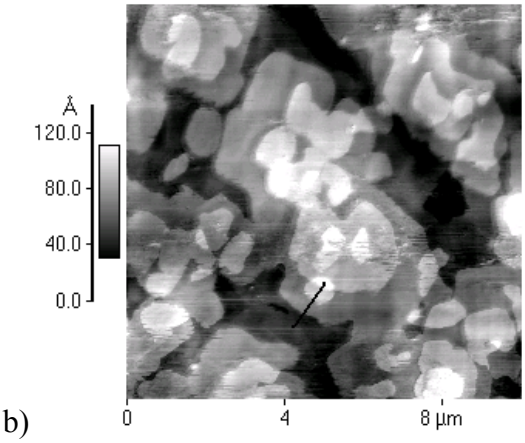

b)

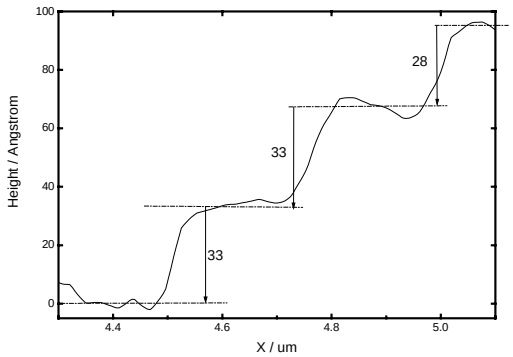

b')

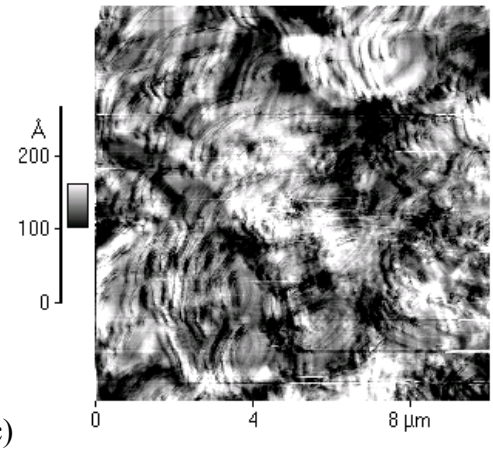

c)

Fig. 5.6 AFM images of *n*AA*n* films deposited on Si/SiO_2 at 155°C. a) and a') 17AA17 film and the height profile scanned along the red line in the image; b) and b') 11AA11 film and height profile; c) 7AA7 film.

Computer simulations were carried out to explore the possible molecular conformation of 11AA11 in a film. The simulations were carried out with Cerius 2 using a combination of geometry optimization with the universal force field and semi-emperical calculations using INDO/2. Fig. 5.7 shows the simulated conformation of 11AA11 molecules in a film.

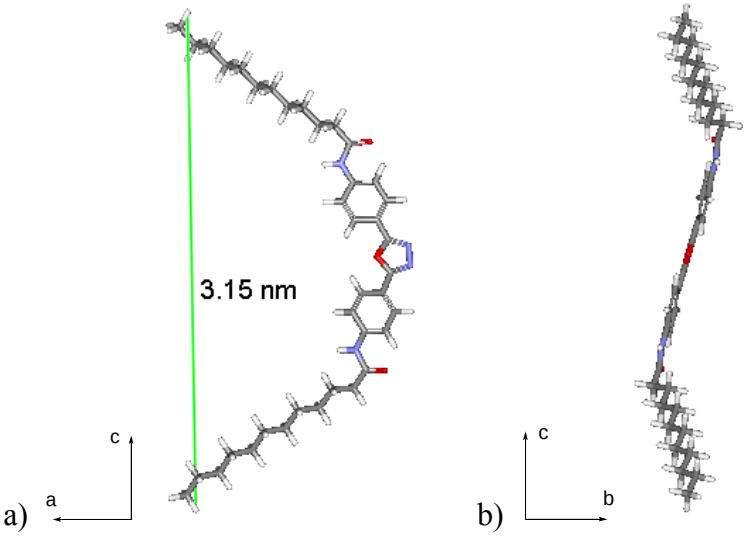

a) b)

Fig. 5.7 Simulated molecular conformation of 11AA11.

In this conformation the carbonyl bonds remain in the plane of the aromatic parts. The aliphatic chain is extended slightly out of the aromatic plane. Viewed from *b* direction the molecule has a banana-shape (Fig. 5.7 a), and a S-shape from *a* direction (Fig. 5.7 b). The molecule lengths for *n*AA*n* were also derived from this conformation and are listed together with the corresponding film periodicities in Tab. 5.2.

Tab. 5.2 Simulated molecule lengths of *n*AA*n* and the corresponding film periodicities derived from XSR measurements.

n	7	11	17
Molecule length (nm)	2.60	3.15	3.80
Film periodicity (nm)	1.3	3.2	3.9

The data in Tab. 5.2 show clearly that the simulated molecule lengths for n = 11 and 17 are in good agreement with the corresponding film periodicities, while in the case of n = 7 the simulated molecular length is much larger than the film periodicity. So it is very likely that 11AA11 and 17AA17 have similar molecular conformations in a film but different with that of 7AA7. The difference could be caused by a different molecule conformation for 7AA7, or by a larger tilt angle for 7AA7 molecules in a film compared with that of 11AA11 and 17AA17. The film periodicities are in agreement with (11AA11 and 17AA17) or smaller (7AA7) than the corresponding simulated molecule lengths, revealing a single molecular layer structure.

The film periodicities were plotted again n in Fig. 5.8. It can be seen from the diagram that the linear dependence of film periodicity on chain length does not exist for *n*AA*n*.

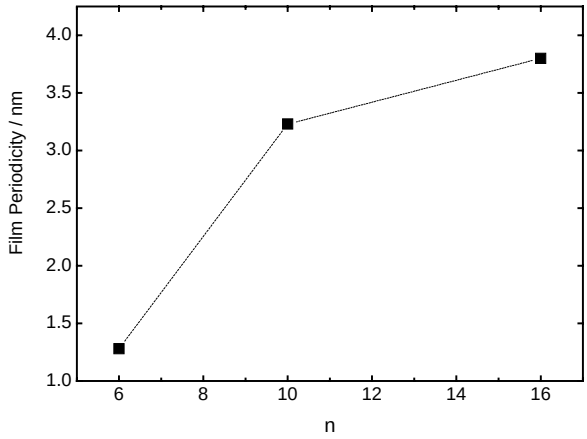

Fig. 5.8 Dependence of the film periodicity on the chain length. The n is the number of methylene unit in the chain. The dash line is only for the guide of eye.

For the *p*CEt*n* series of oxadiazole compounds, the film periodicity depends linearly on the length of the alkyl chain. But such dependence does not exist for *n*AA*n* series. Possible reason for this difference is the strong intermolecular interaction caused by H-bonds between *n*AA*n* molecules (See 5.3.4.2, page 94). When the alkyl chain is short enough, such interaction became dominating and cause the arrangement of molecules different to that of long chains, therefore the film periodicity depends not linearly on the chain length.

5.2 Influence of the head group in oxadiazoles with ether bridge group

The concept of the “head group” was originally used in LB technology. Here we take over this concept for the convenience of the discussion. The head group of the oxadiazole compounds influences the LB film building [18] due to their different hydrophilic abilities. The head groups also play an important role in the VD film formation because the electron donor or acceptor effect of the head group can change the dipole of the whole molecule, the dipole-dipole interactions and consequently the molecular packing. Furthermore, the possible interaction between head groups and/or head groups and other

structures of the molecules can also influence the film structure. By systematically changing the head group in the molecules and investigating their effect on film structure, the contribution of the head group in film building can be studied.

The molecules used in this study are shown in Tab. 5.3. To avoid the influence of intermolecular hydrogen bonds, ether bridge unit was chosen in this study. Unless otherwise mentioned, the lengths of alkyl chains for most substance are chosen to be 16 carbon atoms for the convenience of comparison.

Tab. 5.3 Influence of the head group R on the film periodicity. Molecule length L, obtained by AM1 calculations using the MOPAC in CS Chem3D Pro 5.0, refer to molecules in the extended conformation in vacuum. The film periodicity D is obtained from X-ray measurement.

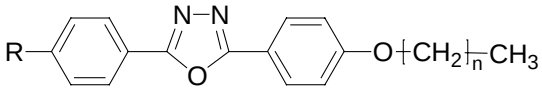

Oxadiazole	R	*n*	Molecule length L [nm]	Film Periodicity D [nm]	D/(2L)
*p*CEt16	-CN(para)	15	3.49	4.8 ± 0.1	0.69
*m*CEt16	-CN(meta)	15	3.46	4.4 ± 0.1	0.64
HEt16	-H	15	3.30	4.9 ± 0.1	0.74
NIEt12	$-NO_2$	11	2.90	4.0 ± 0.1	0.69
MEEt16	$-COOCH_3$	15	3.66	7.1 ± 0.1	0.97
MOEt16	$-OCH_3$	15	3.52	4.5 ± 0.1	0.64

As discussed later in this chapter, the film periodicity could be influenced by physical deposition parameters like substrate temperature, but within a limited range. The data in Tab. 5.3 show that for the substances such as *p*CEt16, MEEt16, MOEt16 and NIEt12, the film periodicities are clearly larger than the corresponding molecule lengths in extended conformation, therefore the films are very likely to have bilayer structures. However the extent to which the film periodicity exceeds the molecule length varied from substance to substance.

Assuming that the molecules have a head-to-head arrangement and the alkyl chains have an all trans conformation in the layer structure, which is illustrated schematically in Fig. 5.9, the D/2L value in Tab. 5.3 can be used to calculate the tilt angle of molecules in film. The tilt angle of the molecules can be calculated according to following equation:

$$\cos(\theta) = D / 2L \qquad 5\text{-}4$$

The tilt angle of the molecules list in Tab. 5.3 were calculated according to equation 5-4 to be 50° to 42°. In this region of tilt angle, the 2,5-diphenyl-1,3,4-oxadiazole part of the molecules can build π-complexes, which exist also in the crystal structures of many oxadiazole compounds (See §2.1.1, page 6) [45].

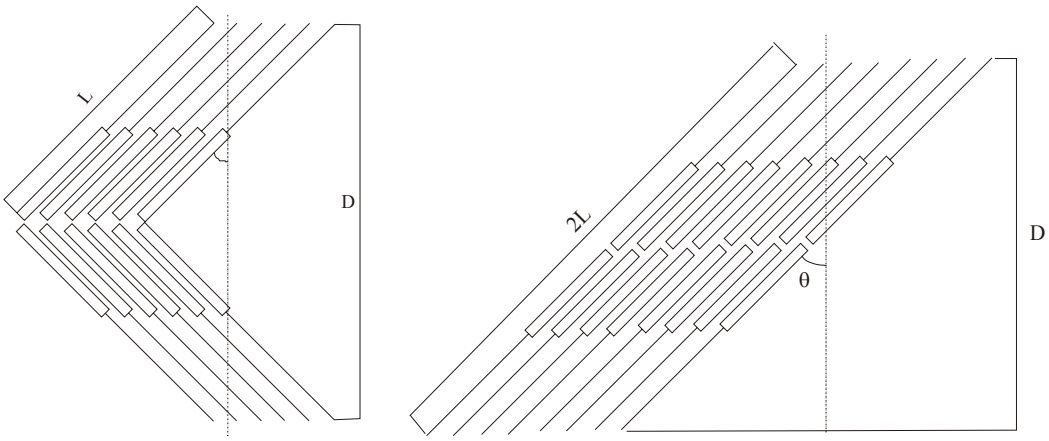

Fig. 5.9 Possible head to head arrangements of the molecules in films with bilayer structure.

The details of the films based on substance in Tab. 5.3 will be discussed in detail in the following sections.

5.2.1 2-(4-Methoxycarbonylphenyl)-5-(4-hexadecyloxyphenyl)-1,3,4-oxadiazole (MEEt16)

5.2.1.1 The film structure of MEEt16

The films of MEEt16 were prepared at T_s ranges from –10°C to 100°C. The growth rate for all films was maintained between 0.5 and 1.1 nm/min. The films were taken out of the deposition set-up and AFM and XSR investigations were applied to investigate the topology and structure of the films. RAIRS was also applied in order to get a deeper insight into the film structure.

The AFM images are shown in Fig. 5.10. The strong influence of T_s on the film topologies can be clearly seen. The film grown at –10°C has a mud like surface dotted with high islands and deep holes, which appears as white and black spots in the image, respectively (Fig. 5.10 a). The height of these islands were obtained by height profile scanning to be between 6~8 nm. The RMS roughness for 10×10 μm^2 is 3.5 nm.

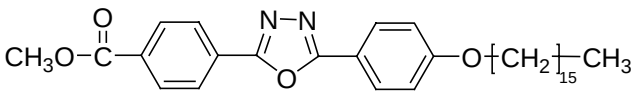

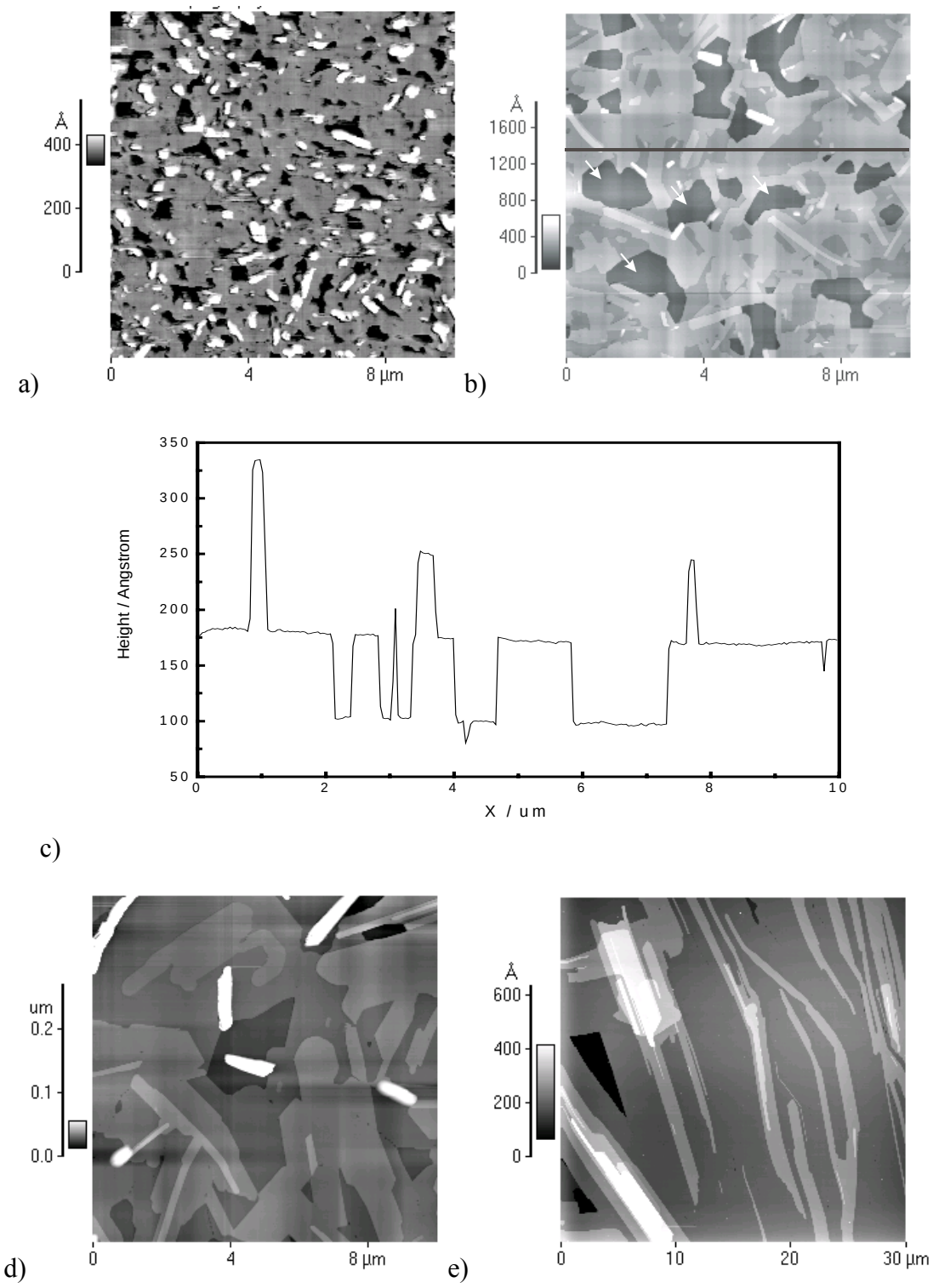

Fig. 5.10 AFM images of MEEt16 films deposited on Si/SiO_2 at T_s = (a) –10°C, (b) 60°C, (d) 85°C and (e) 100°C. The images were taken at room temperature. The growth rates are maintained between 0.5 and 1.1 nm/min. The film thickness for all films measured with quartz micro-balance are 15 nm. Please note that the scale for (e) is 30 µm. (c) is the height profile along the black line in (b), the average terrace height obtained from the profile is 7.4 ± 0.5 nm.

Clear terraces appear when the film is deposited at T_s = 60°C (Fig. 5.10 b). The terrace height is measured by height profile scanning to be 7.3 ± 0.5 nm. The film is not closed, because the height of the boundaries of some dark areas, some of them are denoted with white arrows in the image, are same and are by 25 nm in depth, in agreement with the film thickness (23 nm) obtained from XSR investigation. Such blocks are substrate surface which is not covered by the film.

The films were also prepared at 85°C and 100°C. The higher T_s results in bigger domains. At T_s = 100°C, the size of domains reaches 30 μm, much bigger than the size published for organic molecules, such as OMBD film for sexithienphenyl [24] and quaterthiophene [120]. To illustrate the extremely large domains in the film, an image of 30×30 μm is shown in Fig. 5.10 (e). Surprisingly the three dimensional crystals, which first appear at T_s = 60°C and became higher at T_s = 85°C, disappeared at T_s = 100°C. The domains in the AFM image for films deposited at 100°C have a thread-like form, hinting that the molecules have a much higher chance to order themselves into the narrow end of domains than the long edge.

XSR investigations were also done in order to get an insight into the film structure. The results of XSR measurements for films deposited at –10°C and 100°C are illustrated in Fig. 5.11

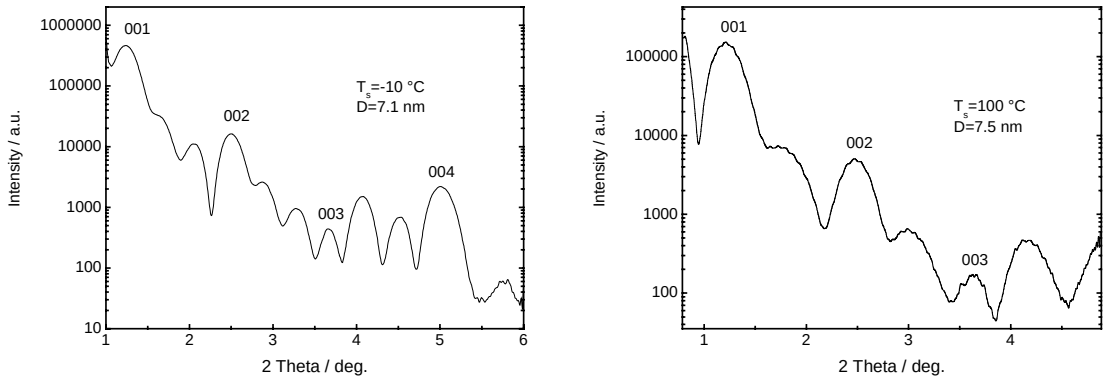

Fig. 5.11 The XSR investigation for MEEt16 film on Si/SiO_2 with T_s = -10°C and 100°C. The film periodicity for T_s = -10 and 100°C are 7.1 ± 0.1 and 7.5 ± 0.1 nm, respectively.

The XSR results reveal the layered structure for the films deposited at all the T_s studied in this work. Even for the film grown at T_s of –10°C, the XSR results shows that the film has layered structure with a film periodicity of 7.1 ± 0.1 nm (Fig. 5.11 left), although in the corresponding AFM image no terrace could be found (Fig. 5.10 a). Elevating the T_s to 20 and 40°C, the corresponding XSR curves do not show any significant change. The film periodicity for films grown at T_s of 100°C amounts to 7.5 ± 0.1 nm.

The study of film structures reveals that the MEEt16 can form layered films on Si/SiO_2 in

the T_s region from –10 to 100°C. The film topography is strongly influenced by T_s. T_s higher than 60°C results in terrace structures in the films and the size of domains increase significantly with the increasing of T_s. The film periodicities for all T_s amounts to almost double the molecule length (3.66 nm) in extended conformation, indicating that the film has a bilayer structure and the molecules arrange with a small tilt angle in the layer. The information obtained by means of AFM and XSR is still not enough for us to get an understanding of the molecular arrangement in the film. The information about the crystal structure of an oxadiazole with analogous structure to MEEt16 may provide more information.

5.2.1.2 Crystal structure of an analogous oxadiazole compound

Reck el al. [133] have investigated the crystal structure of 2,5-di(4-methoxycarbonyl-phenyl)-1,3,4-oxadiazole (MEME), which differs from MEEt16 in that it has two methyl ester groups, instead of a methyl ester and alkoxy chain for MEEt16, attached to each end of a DPO unit. This compound crystallizes under similar conditions in two different orthorhombic crystalline forms. In form 1 (Fig. 5.12) the molecules build up a herring bone structure with infinite stacks along the *a* axis. The plane of the molecule forms an angle of 45° with respect to the stack axis (*a* axis). There are strong π-π electron interactions between adjacent molecular planes.

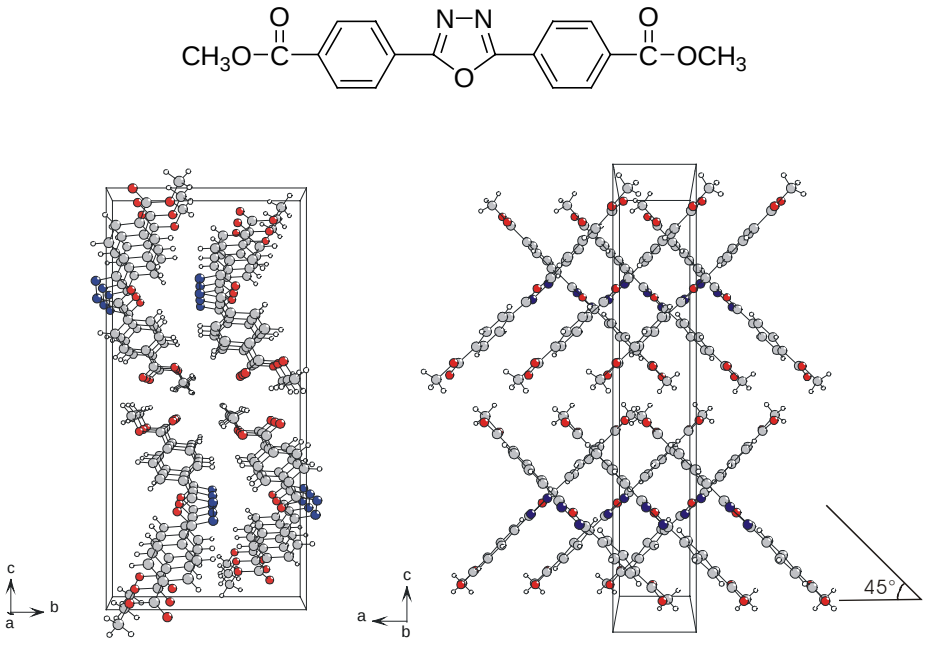

Fig. 5.12 Molecular arrangement of MEME, form 1, viewed along the *a* axis (left) and *b* axis (right). The angle in the figure is the dihedral angle between long axis of molecule and *a* axis.

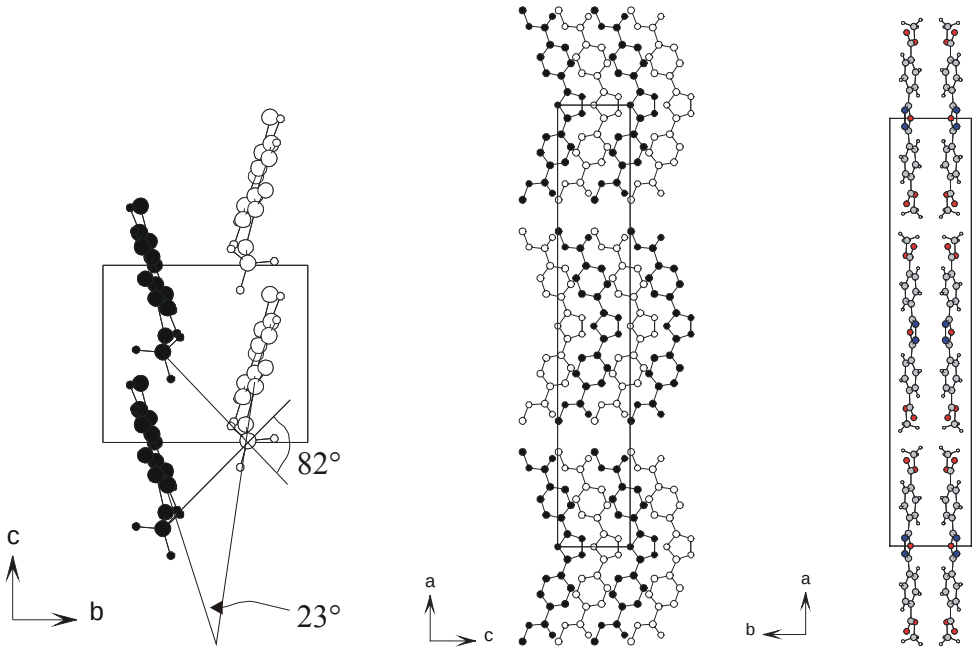

Fig. 5.13 Molecular arrangement of MEME, form 2, viewed along the *a* axis (left, only one layer of molecules are shown for clarity), *b* axis (middle, atoms of front molecules are shown by white circles and those of behind ones are shown by black circles, H atoms are not shown) and *c* axis (right).

In contrast to form 1 no stack interactions are found in crystalline form 2 (Fig. 5.13) as no adjacent molecules are packed with their ring planes parallel to each other. The dihedral angle between oxadiazole ring planes of the adjacent molecules along the *b* axis amounts to 23.2°. The methyl group stay in the plane parallel to the *b* and *c* axis and form a methyl matrix. The angle between two line of methyl group is measured to be 82° (Fig. 5.13 left). The molecules form smectic-like structures comprising of layers stacked along the *a* axis (Fig. 5.13 middle and right). The C=O bonds are located in the plane of the phenyl ring and arranged parallel to each other, i.e. the dipole moments of C=O bonds as well as the oxadiazole ring accumulate along one direction. The intermolecular distances between the oxygen atom in the C=O bond and the H atoms in the methoxy are 3.08, 2.84 and 3.185 Å (Fig. 5.13 middle), respectively, indicating an interaction between the molecules of the neighbouring layers [134].

The topology of the smooth terraces of MEEt16 film shown in the Fig. 5.10 (d) can be further resolved. Fig. 5.14 shows a representative example of an AFM image with a pronounced molecular resolution. The terraces always show a periodic packing of molecules corresponding to an oblique two-dimensional lattice. The angle between two molecule line is 80°, and the lattice constants determined for the two directions are 4.4 Å and 4.8 Å, respectively, in very good agreement with the corresponding value for MEME crystalline form 2, which are 82° and 4.6 Å, respectively. So it is very likely that the MEEt16 film has a similar structure as MEME crystalline form 2.

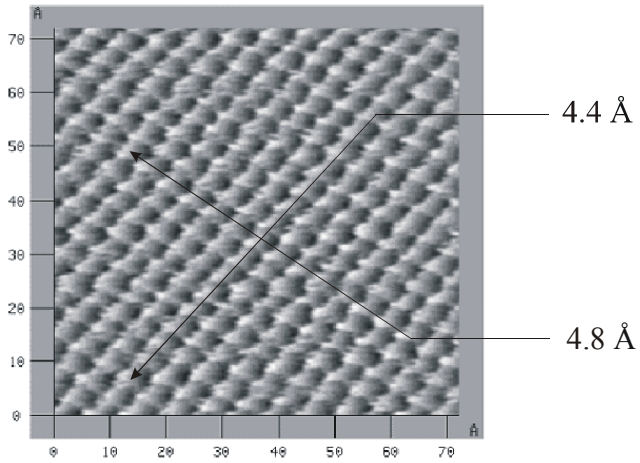

Fig. 5.14 Molecular resolution of the periodic in-plane structure by AFM. The angle between two marked molecule line is 80°. The lattice constants determined for the two directions are 4.4 and 4.8 Å, respectively.

5.2.1.3 IR investigation

The head groups usually have their characteristic absorption band in the IR range. Several factors such as electronic and intermolecular interactions can cause band shifts [135]. The former is determined by the chemical structure, while the latter may vary. By comparison of the band position of functional groups in different states information on the intermolecular interactions can be obtained.

If the MEEt16 molecules in a film have similar molecular arrangements as those found in crystal form 2 of MEME, then the interlayer interaction between C=O bonds and carbon atom in the methoxy group should be reflected in an IR spectra, because the intermolecular interaction concerning C=O bonds can influence its band position. The IR transmission spectra of MEEt16 in KBr, CCl_4 solution (10^{-4} M) and RAIRS spectra of thin MEEt16 films on Si/SiO_2 are shown in Fig. 5.15.

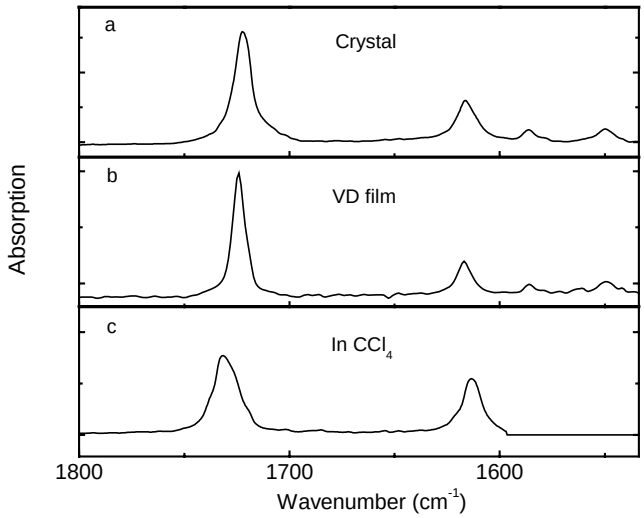

Fig. 5.15 Carbonyl band of MEEt16 in different states. a) crystals in KBr $\nu_{C=O}$ = 1722 cm^{-1} ; b) thin films on $Si(SiO_2)$ $\nu_{C=O}$ = 1723 cm^{-1} ; c) in CCl_4 solution (10^{-3} M), $\nu_{C=O}$ = 1732 cm^{-1}, the latter two spectra are multiplied by 20 and 10 for comparison.

The C=O stretching band ($\nu_{C=O}$) of MEEt16 in crystals appears at 1722 cm^{-1}, similar to that of thin film, which appears at 1723 cm^{-1}. In contrast to solid and film, the $\nu_{C=O}$ for solution appears at 1732 cm^{-1}, c.a. 10 cm^{-1} higher. This shift can be explained by an increase in C=O bond strength in solution. If the aromatic part and the methoxycarbonyl group of MEEt16 molecules have the same arrangement in film as in crystalline form 2 of MEME, then the interaction between oxygen atoms in carbonyl and H atoms in methoxy groups of neighbouring layers can weaken the C=O bond and cause the red shift of $\nu_{C=O}$. Such interaction is the so called C-H···O H-bonding, which have in fact been recognized as important determinants of the stability and specificity of biological systems[136-139]. In the diluted solution, the molecules are separated by solvent and the intermolecular interaction is negligible, thus the C=O bond has relative higher wavenumber.

5.2.1.4 Sructural transformation in the thermal treatment

The intermolecular interaction can be changed by increasing the temperature. Fig. 5.16 shows the temperature dependent RAIRS spectra. Up to 70°C, the spectra remains unchanged. The $\nu_{C=O}$ appears at 1723 cm^{-1}. At 90°C a small shoulder can be seen on the lower wavenumber side of $\nu_{C=O}$. This shoulder became very obvious at 130°C, meanwhile the CH_3 out-of-plane deformation band at 1463 cm^{-1} shifted to higher wavenumber region and merged with CH_2 deformation band, which originally located at 1473 cm^{-1}. Unfortunately, the CH_3 in-plane deformation at 1378 cm^{-1} is too weak to provide any useful information. The change of $\nu_{C=O}$ and CH_3 band is a sign of a dissociation of C-H···O bonding in the thermal treatment.

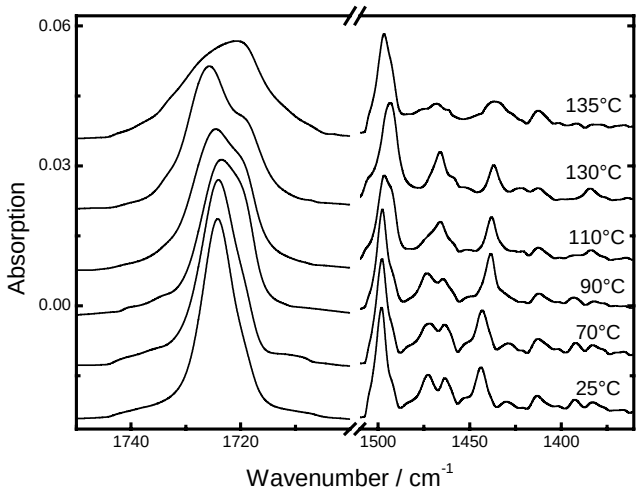

Fig. 5.16 Temperature dependent RAIS spectra of MEEt16 film deposited on Si/SiO_2 with T_s = 20°C. The film thickness is 50 nm. Spectra were scanned during the heating.

The structure and topography of the film were investigated after thermal treatment by means of XSR and AFM, respectively, and the results are shown in Fig. 5.17 and Fig. 5.18.

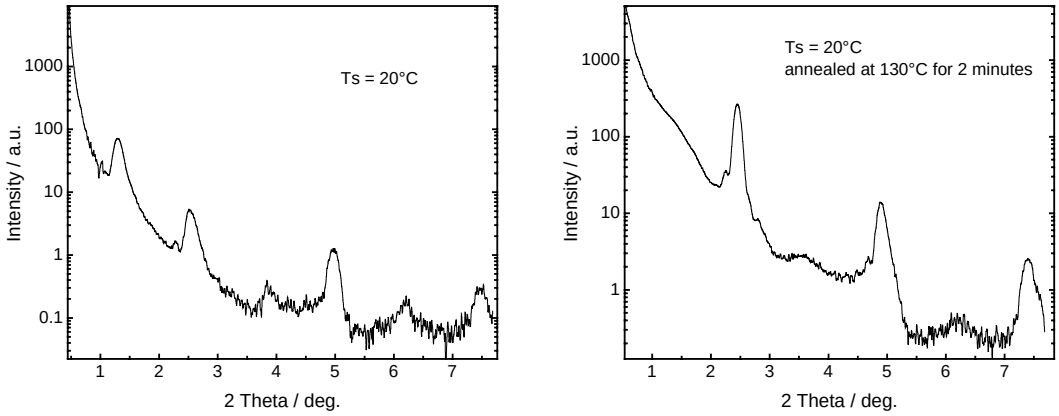

Fig. 5.17 The XSR investigation for MEEt16 film deposited at T_s = 20°C (left) and after being annealed at 130°C for 2 minutes (right). The film periodicities for the film before and after annealing are 7.0 ± 0.1 nm and 3.6 ± 0.1 nm, respectively.

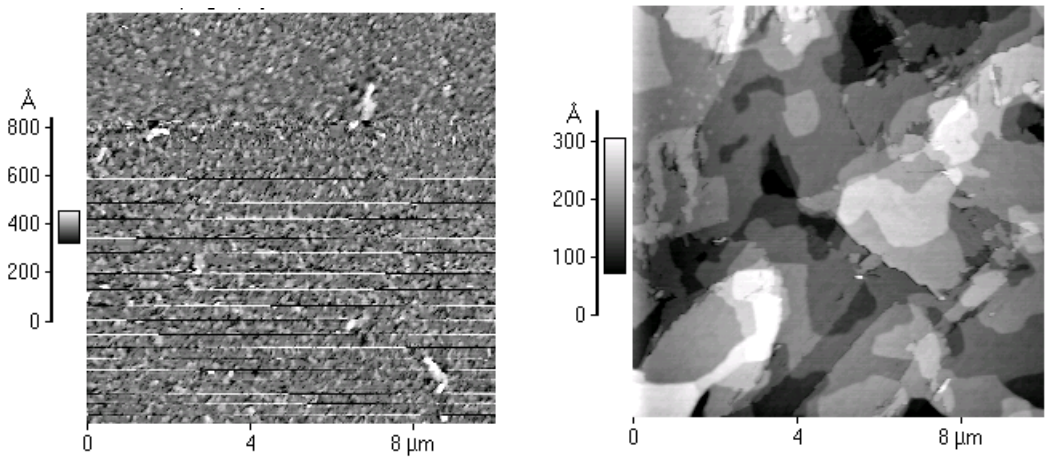

Fig. 5.18 AFM images for MEEt16 film deposited at T_s = 20°C before (left) and after (right) being annealed at 130°C for 2 minutes. The terrace height measured for right image is 3.6 ± 0.5 nm.

The results of XSR as well as AFM show clearly that the molecules performed a reorganization during the annealing. The film periodicity decreased from 7.0 nm to 3.6 nm during the annealing. The latter value is in good agreement with the calculated length of the molecules (3.66 nm), so the film is likely to have a monolayer structure after annealing. An increase in the tilt angle of the molecules can also result in the decrease in film periodicities. Assuming that the film has a bilayer structure, the tilt angle calculated according to equation 5-4 is 60°, which is too big for the formation of intermolecular π- π electron interactions. In crystal form 1 of MEME, which is analogous to MEEt16, the angle between the plane of the molecule and the stack axis (*a* axis, Fig. 5.12) is only 45°.

Based on the aforementioned analysis, a possible film structure of MEEt16 is proposed (Fig. 5.19). In this structure the molecules stand with a tilt angle of about 23° in the film.

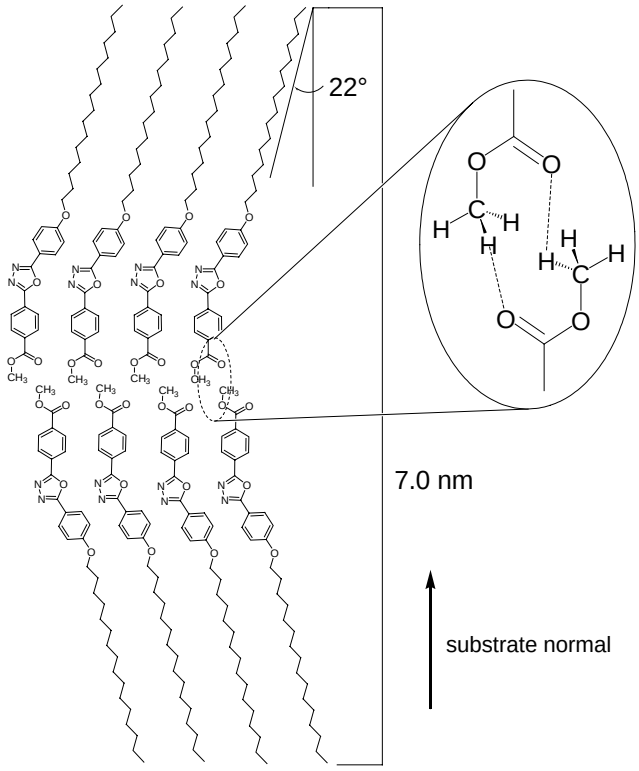

Fig. 5.19 Possible arrangement of MEEt16 molecules in the monolayer of thin film. The aliphatic chains are arranged with a tilt angle of 22°, and C=O bonds are arranged parallel to each other. Interlayer interactions between H atoms and oxygen in the C=O bond is shown as dashed line.

The study of MEEt16 film can be summarized as follows:

The MEEt16 films have a bilayer structure in the investigated T_s range. The film periodicity amounts to nearly double the length of the molecule and the molecules stand at a relative small tilt angle (c.a. 23°) in the film. The presence of an intermolecular interaction induced by the carbonyl and methyoxy group in the methyl ester structure was found in the film. Upon being annealled at 130°C for a short time, the film periodicity was reduced to the length of one molecule. IR investigations during annealling revealed that a change occurs in the intermolecular interactions between the methyoxy and carbonyl groups.

5.2.2 2-(4-Cyanophenyl)-5-(4-hexadecyloxyphenyl)-1,3,4-oxadiazole (*p*CEt16)

5.2.2.1 The film structure of *p*CEt16

The T_s influence on the film topography is described in §4.4.1 (page 33). The film has granular surface at low T_s but smooth terraces structure at high T_s. The XSR

investigations reveal layered structure for all the films, but the film periodicity for $T_s \leq 60°C$ is by about 0.3 nm higher than for $T_s \geq 85°C$. The absolute value of this difference varied slightly in different repeat, but this abruptly decrease of film periodicity does always exist.

5.2.2.2 Crystal structure of an analogous oxadiazole compound

The crystal structure of one oxadiazole with substituent CN group may give us hints in understanding the arrangement of molecules in the *p*CEt16 film. One such molecule whose crystal structure is known (Orgzall [140]) is 2-(4-cyanophenyl)-5-(4-dimethylaminophenyl)-1,3,4-oxadiazole (CDMO). The molecular packing of CDMO is characterized with stacks of molecules along the *b* axis (See Fig. 5.20). In a stack the molecules are packed alternatively π-donor to π-acceptor and π-donor to π-donor, a slightly different molecular arrangement from the structure shown in Fig. 2.1 (page 6). The CN group and dimethylamino group are aligned alternatively at both ends of the molecules of a stack. The CN-CN interaction, which can be proved by measuring the distance between CN groups, may be the main influence leading to this packing. The CN groups of adjacent molecules pack parallel to each other and the distance between them are measured to be 3.88 Å (Fig. 5.20 right), a little bit bigger than that for *n*OCB (3.39-3.57 Å) [141, 142]. This slightly longer CN-CN distance could be the result of the banana-shape of oxadiazole.

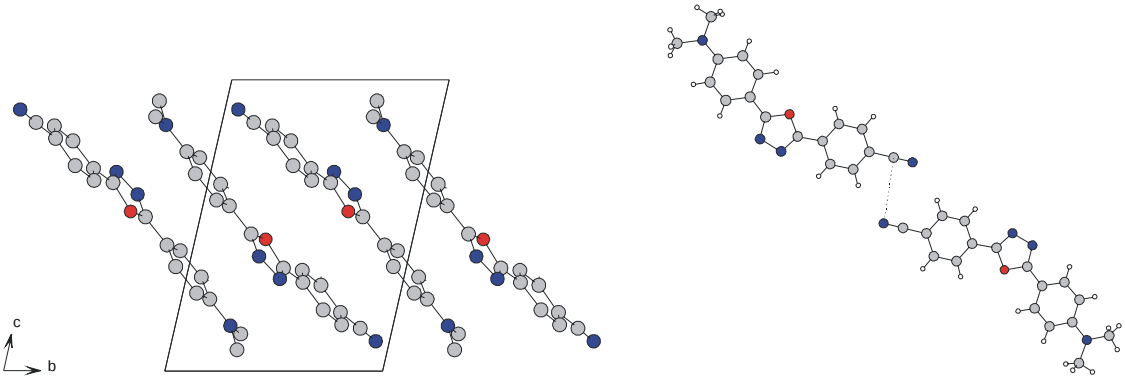

Fig. 5.20 The crystal structure of 2-(4-cyanophenyl)-5-(4-dimethylaminophenyl)-1,3,4-oxadiazole (CDMO) (left) and schematic illustration of CN-CN interaction in CDMO crystal. The distance between N and C atom marked with a dash line amounts to 3.88 Å.

The interaction between CN groups is already well known in the liquid crystal studies of 4-cyano-4'-alkoxy-biphenyls (*n*OCB) and 4-cyano-4'-alkyl-biphenyls (*n*CB). To obtain an understanding of intermolecular interaction between CN groups, Hori et al. [132] has investigated the crystal structures of *n*OCB and found out that smectic-like bilayer structures with infinite networks of closely arranged CN groups are dominant for *n*OCB when $n \geq 9$.

5.2.2.3 IR investigation and film structural transformation during the thermal treatment

The IR investigation reveal the interaction between CN groups [131]. The CN band located at higher position in crystal than in solution. Furthermore, it shifted by several wavenumbers to lower wavenumber region when the crystals are heated over the crystal-nematic or crystal-smectic transform temperature. However, opposite shifts of CN group in IR spectra were also observed when crystals of *n*CB (*n* = 6,7,9,11) were heated over crystal-nematic or crystal-smectic temperature. In addition to *n*CBs, blue shifts of CN band were also found by Zhang et al. [143] in the investigation of *N*-(*p*-cyanobenzylidene)-*p*-octyloxyanline (CBOOA) and 4'-cyanobenzylidene-4-*n*-hexyloxyaniline (CBHA) etc. All of above substance have analog structures with *p*CEt16.

Different shift directions of CN bands in IR spectra hints at different intermolecular interactions concerning the CN groups [131]. Shabatina et al. [144] concluded that dimmers were formed in the mesophase of 8OCB based on the association enthalpy estimated from the CN band. Hori et al. [145] summarized the different types of CN-CN interactions: dimer or tetramer, one-dimensional infinite chains and two-dimensional infinite networks, which are illustrated schematically in Fig. 5.21.

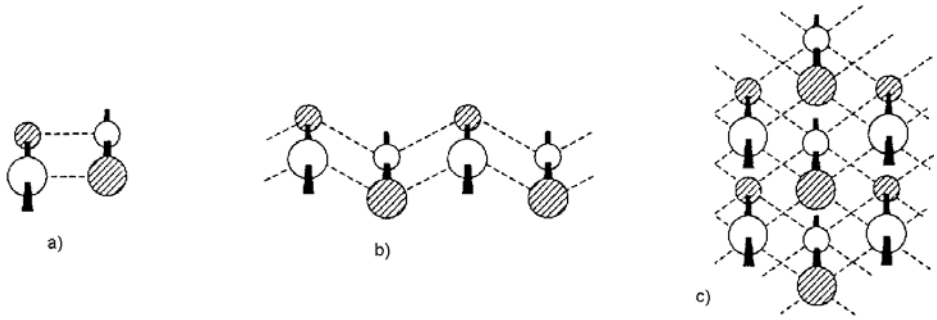

Fig. 5.21 Schematic diagrams of CN-CN interactions: a) a cluster, b) an one dimensional chain and c) a two dimensional network. Nitrogen atoms are shown by hatched circles. Close C···N distances are denoted by dashed line [145].

To obtain information about the environment of the CN group, IR measurements of *p*CEt16 in VD film, crystal and solution (CCl_4 10^{-3} M) were carried out. Matsui et al. has calculated the position of CN group with AM1 method, the results show that when a CN group has a richer electron density, its stretching vibration band shifts to a lower wavenumber position [146]. The results of IR investigation show that the CN band position (ν_{CN}) varied slightly in different condensed states (Fig. 5.21). In dilute (10^{-3} M) CCl_4 solution, in which molecules are isolated to each other, ν_{CN} appears at 2233 cm^{-1}. The same band appears at 2228 cm^{-1} with a small shoulder at 2236 cm^{-1} for solid material crystallized from ethanol and measured in KBr disk, indicating that the electron density in CN group is lower in solution with respect to solid state [146].

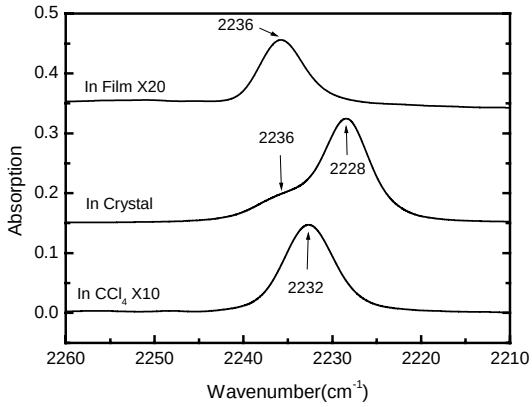

Fig. 5.22 CN band of *p*CEt16 in solid, solution and films. ν_{CN} peaks at 2236, 2228 and 2232 cm^{-1} for thin film (T_s = 25°C), crystal and CCl_4 solution (10^{-3} M), respectively. The spectra for film and solution were multiplied with 20 and 10 for comparison, respectively. Curves are shifted for clarity.

For VD films, ν_{CN} shows a dependence on the substrate temperature. Increasing T_s from 20°C to 85°C, ν_{CN} shifted from 2236 cm^{-1} to 2234 cm^{-1} with a shoulder at 2229 cm^{-1} (Fig. 5.23). The ν_{CN} of the film appear at higher wavenumber region with respect to the solid state, whether the films are deposited at high T_s or low T_s. This difference of CN band is caused by CN-CN or CN-phenyl interactions.

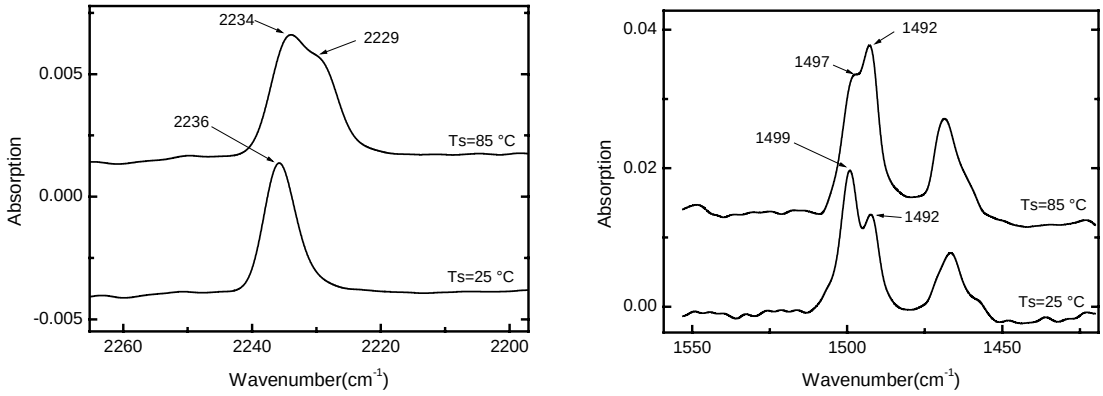

Fig. 5.23. CN (left) and phenyl band (right) of *p*CEt16 in film prepared at high and low T_s. The shoulder at 2229 cm^{-1} for ν_{CN} for T_s = 85 hints a coexistence of two kinds of intermolecular interactions concerning CN group. Phenyl band split as a result of CN-phenyl interaction.

The shoulder of the ν_{CN} form a film with T_s = 85°C hints at the coexistence of two kind of intermolecular interactions concerning the CN group. One is a CN-CN interaction, which is proved by the different CN band positions in solution and solid, the other is the CN-phenyl interaction, in which the CN group has some overlap with the phenyl ring [145]. These two kinds of intermolecular interactions result in two types of molecular arrangements in a layer. The proportion of these two types of arrangements in the film depends on T_s during deposition.

The phenyl stretching band for the film grown at T_s = 25°C appears at 1499 cm^{-1} with a shoulder at 1492 cm^{-1}(Fig. 5.23 right), both bands are a mixture of phenyl semicircle

stretching vibration with CH in plane bending for para substituted benzenes [147]. Usually this mixed band appears around 1490 cm^{-1}, however, due to the overlap of neighbour CN group with phenyl ring, the band splits into two bands. The relative intensity of these two bands reflects the proportion of the two types of molecular arrangement in the film. In the film deposited at T_s = 25°C, the phenyl ring stretching appears mainly at 1499 cm^{-1} with a small shoulder at 1492 cm^{-1}, so the CN-CN interaction mode dominates in the film structure. In the film grown with T_s = 85°C, the phenyl ring stretching appears at 1493 cm^{-1} with a small shoulder at 1498 cm^{-1}, so the proportion of CN-phenyl overlapping mode is higher than for films prepared at T_s = 25°C.

These two type of intermolecular interaction hint that two kinds of crystal structures may exist for *p*CEt16. In the DSC curve (Fig. 5.24) of a *p*CEt16 crystal a peak appears at 78-85°C by heating and at 67-73°C by cooling, indicating a phase transformation. If this transformation is caused by the interaction mentioned above, this should also be reflected in the IR spectra.

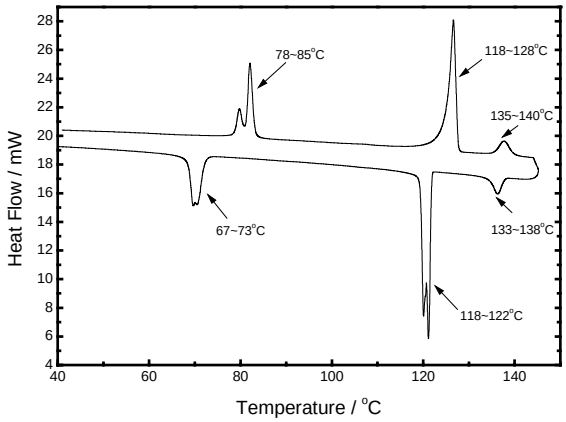

Fig. 5.24 DSC curve of *p*CEt16, second cycle. The heating rate is 10°C/min.

Fig. 5.25 shows the temperature dependent RAIS spectra of a film deposited at T_s = 20°C. The spectra were scanned at the temperature denoted in the figure. Until the film was heated up to 82°C, no obvious change of the CN band and phenyl stretching band could be observed.

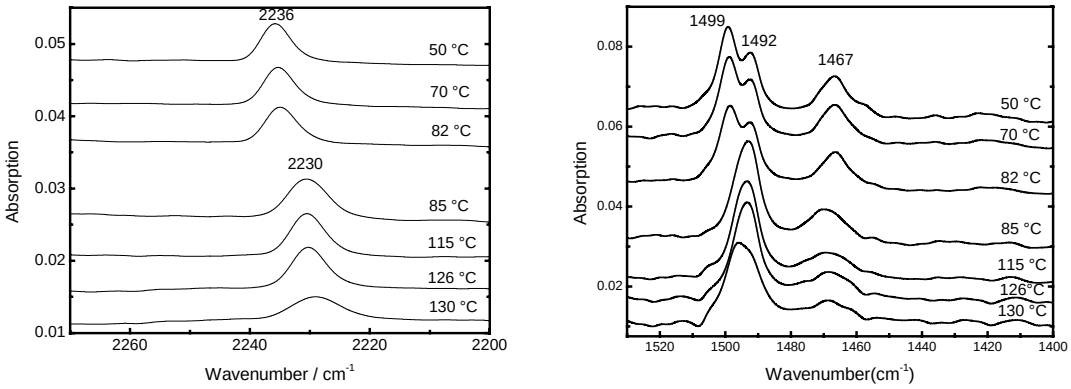

Fig. 5.25 Temperature dependent RAIS spectra of *p*CEt16 film deposited at T_s = 25°C. The film thickness is 50 nm. Spectra were scanned during heating. Curves are shifted for clarity.

When the film was further heated to 85°C, obvious change of spectra occurred. The ν_{CN} shifted from 2236 cm^{-1} to 2230 cm^{-1}, meanwhile the phenyl stretching band at 1499 cm^{-1} disappeared. The phenyl stretching band became a single band at 1492 cm^{-1}. Such change of absorption bands reflects the change of intermolecular interaction. Films deposited at lower temperature have CN-CN interactions, which change to CN-Phenyl interactions when heated up to 85°C.

During this process the CH_2 deformation band at 1467cm^{-1} became weak and broader. The symmetrical and asymmetrical stretching of CH_2 bands shifted to higher wavenumber region, indicating a decrease in the ordering of the aliphatic chain.

The structure change of the film was also measured by XSR, which was carried out simultaneously during the annealing of the film. The results are illustrated in Fig. 5.26.

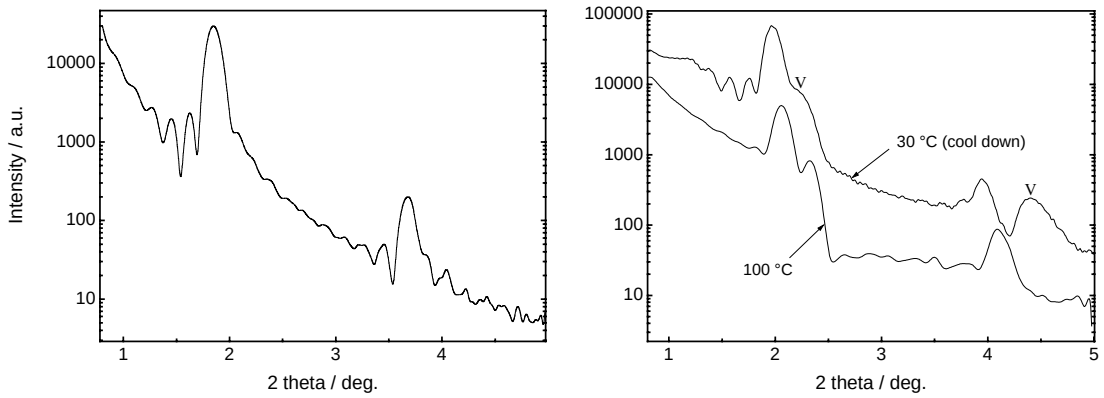

Fig. 5.26 The in-situ XSR investigation of *p*CEt16 films during annealing. The film was deposited at 25°C and measured firstly at 20°C (left), then measured at 100°C (right). Afterwards it was heated up to 130°C and then cooled down to 30°C and measured again (right). The peaks denoted with a 'v' corresponds to film periodicity of 4.0 nm.

The film prepared at T_s = 25°C has film periodicity of 4.8 nm, which upon annealing to 100°C decreased to 4.4 nm (Fig. 5.26 left). This change could not be simply attributed to thermal expansion, otherwise the film periodicity should have been increased. Afterwards the film was cooled down to 30°C and measured again, the film periodicity increased slightly to 4.5 nm. Meanwhile, another group of peaks corresponding to 4.0 nm appeared (Fig. 5.26 right), this shows the coexistence of two types of structure in the film.

Similar to annealing, the film growth process in vacuum is indeed also a cooling process of the materials. In *p*CEt16 crystals the annealing resulted in coexisting structures, while for vacuum deposition only uniform film structures. This difference may be caused by the different energy barriers for the two processes. During the film growth the molecules arriving at the surface encounter relatively lower energy barriers to diffusing on the film or substrate, because they are not as confined by the adjacent molecules, as is the situation for molecules in the film. As a result the molecules are ordered in a thermodynamically more stable structure, thus the film has a uniform structure.

5.2.3 2-(3-Cyanophenyl)-5-(4-hexadecyloxyphenyl)-1,3,4-oxadiazole (*m*CEt16)

*m*CEt16 differs from *p*CEt16 with respect to the position of the substituted CN group. In *m*CEt16 the CN group is attached at the meta position of the phenyl ring instead of the para position for *p*CEt16. Deposited on Si/SiO_2, the films of *p*CEt16 are layered and have a bilayer structure (See §5.1, page 38) and the molecules are oriented with a tilt angle to the substrate. IR investigation has revealed the CN-CN and CN-phenyl interactions between the layers. From a geometrical point of view, the meta position of the CN groups in *m*CEt16 should facilitate the formation of CN-CN or CN-phenyl interaction in films.

5.2.3.1 The film structure of *m*CEt16

A study of the influence of T_s on film based on *m*CEt16 shows that the topography is strongly dependent on T_s. The AFM images of *m*CEt16 films prepared at different T_s are shown in Fig. 5.27:

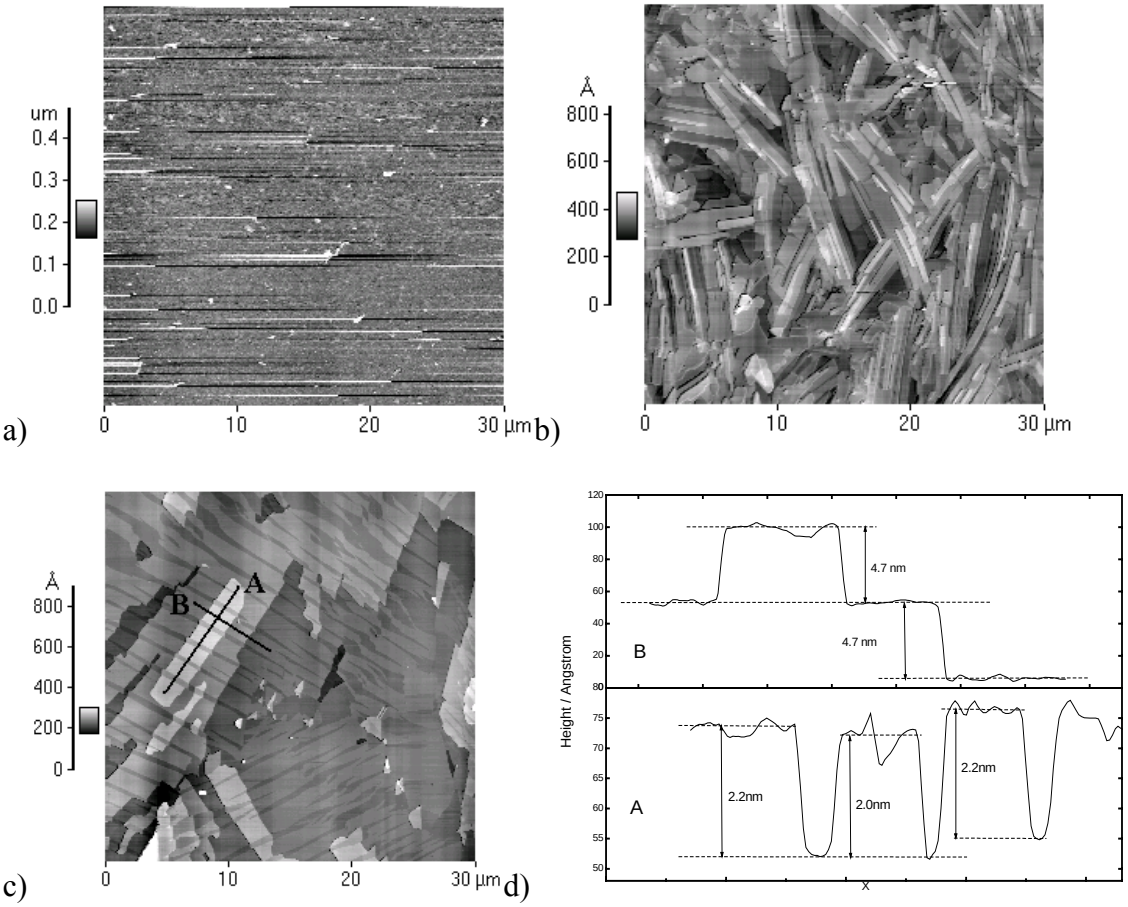

Fig. 5.27 AFM images of *m*CEt16 films deposited at T_s = (a) –10°C, (b) 60°C and (c) 85°C and the height profile along the line A and B lines in (d). The average terrace height obtained from different position is 4.7 ± 0.5 nm. The depths of the cracks varies from 0.8 to 2.4 nm.

The surface of the film grown at T_s = -10°C is characterized by many small particles. The film appears amorphous, the terrace structure can be clearly recognized when T_s is elevated to 60°C (Fig. 5.27 b). Interesting structures can be found in the AFM images of *m*CEt16 films deposited at T_s = 85°C (Fig. 5.27 c). The film topology is characterized with clear terrace structures and long parallel cracks, which divide the domain into many small parallel distributed slices. The height scanning of the AFM image shows that these cracks are not deep into the film, but only within one layer. The depth of these cracks varies from 0.8~2.4 nm, much less than the terrace height, which is obtained by AFM to be 4.7 ± 0.5 nm. In the film plane these cracks extend through the whole domain. It seems that these cracks are caused by the shrinking of film when cooled down at end of deposition. However this hypothesis, can not explain the fact that the cracks occurs at the same place of different layers in the normal direction of the substrate. Furthermore at some places the cracks are so big that it is unlikely to be the result of thermal induced shrink.

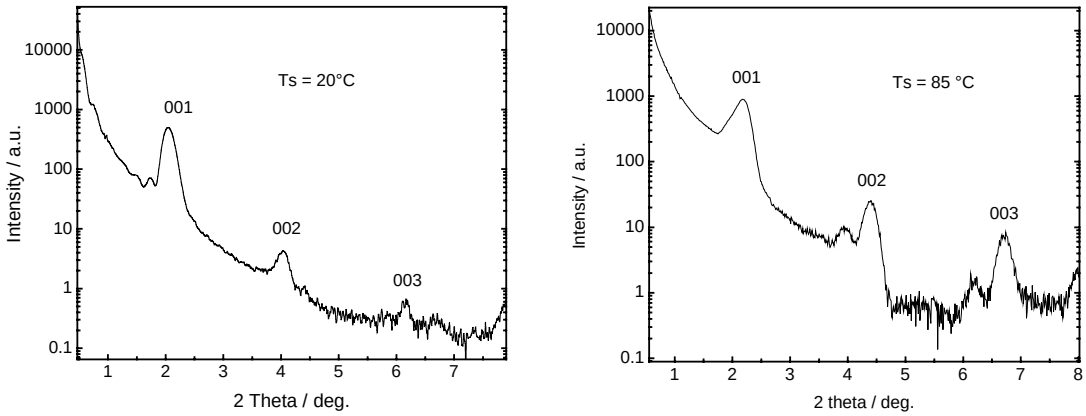

Fig. 5.28 XSR investigation of *m*CEt16 film at T_s = 20°C (left) and 85°C (right). The film periodicities calculated from these curves are 4.4 ± 0.1 and 4.1 ± 0.1 nm for T_s = 20°C and 85°C, respectively.

XSR investigations of film deposited at 85°C revealed a layered film structure. The 002 and 003 peaks in the curve are doubled and the 001 peak is quite broad, so there could be two structures coexisting in the film. One has the film periodicity of 4.4 ± 0.1 nm, another with 4.1 ± 0.1 nm.

5.2.3.2 Thermal treatment and IR investigation of the film

In the DSC curve of *m*CEt16 (Fig. 5.29) small peaks appear before melting process, hint that some structural changes happen. Unlike the peaks in the DSC curve of *p*CEt16, the energies of these peaks are quite small. The peak at 117°C of the heating process has the biggest area, which could be attributed to the melting process.

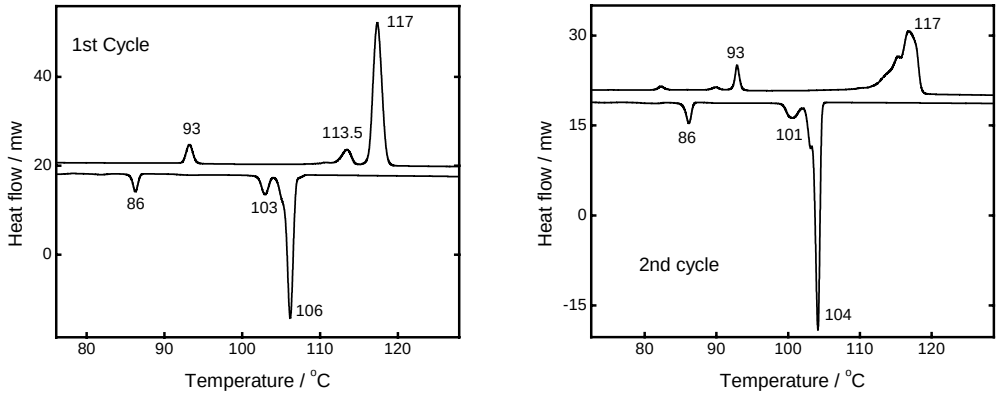

Fig. 5.29 DSC curve of *m*CEt16, the first (link) and second (right) cycle. The heating rate is 10K / min.

IR measurement for *m*CEt16 in dilute solution (CCl_4, 10^{-3} M), in bulk and VD films were carried out. The positions of vibration bands of CN and phenyl ring have been compared with the corresponding bands of *p*CEt16 (Tab. 5.4).

Tab. 5.4 Summary of CN and phenyl band position for *m*- and *p*Et16 under different conditions. The peak with an asterisk appear as shoulder of another band in the same cell of this table.

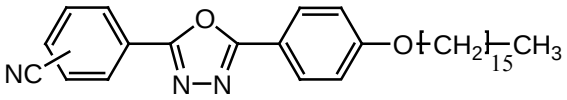

	CN band		Phenyl band	
CN position	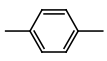		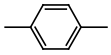	
Solution	2232	2236	1497, 1493	1493
Bulk	2228, 2236*	2234	1492	1497
Film, high T_s	2234, 2229*	2233	1497*, 1492	1493
Film, low T_s	2236	2234	1499, 1492*	1493

In solution the CN band of *m*CEt16 appears at 2236 cm^{-1}, higher than 2232 cm^{-1} of *p*CEt16. According to Matsui et al. [146] CN at the meta position of the phenyl ring has a lower electron density with respect to the para position. This is the result of the electron withdrawal effect of the oxadiazole ring and such effects usually have different influences on different position of phenyl ring.

The ν_{CN} of *m*CEt16 in bulk appears at 2234 cm^{-1} as a symmetrical single band, 2 cm^{-1} lower than in solution. But the ν_{CN} of films deposited at T_s = -10°C and 95°C did not show any significant differences (2234 cm^{-1} and 2233 cm^{-1} for T_s = -10°C and 95°C, respectively, and are symmetrical peaks without any shoulder or split). For all cases ν_{CN} varies between 2236 cm^{-1} and 2233 cm^{-1}, a much smaller range than that of *p*CEt16, which is between 2236 cm^{-1} and 2228 cm^{-1}, indicating that the CN-CN interaction in *m*CEt16 is weaker than that of *p*CEt16.

The phenyl band locate at 1497 cm^{-1} in solid and at 1493 cm^{-1} in solution. For films with T_s = -15°C and 95°C, the phenyl band frequencies are same, 1493 cm^{-1}. In contrast to *p*CEt16 the phenyl band for *m*CEt16 has no shoulder or split. So it is very likely that the CN-phenyl interaction does not exist in the film of *m*CEt16.

Because the endothermal and exothermic processes in the DSC curve are reversible, it is possible that the film structures or intermolecular interaction depends exclusively on the environment temperature. The film prepared at different T_s may have same structure and subsequently the same IR spectra when the samples are measured at room temperature. To make clear whether the CN-CN or CN-phenyl interaction exist in the film, temperature dependent IR spectra of *m*CEt16 bulk material and thin films were performed. The temperature dependence of the CN band for the bulk substance in KBr and films prepared at T_s = -15°C, 95°C are shown in Fig. 5.30 and Fig. 5.31, respectively.

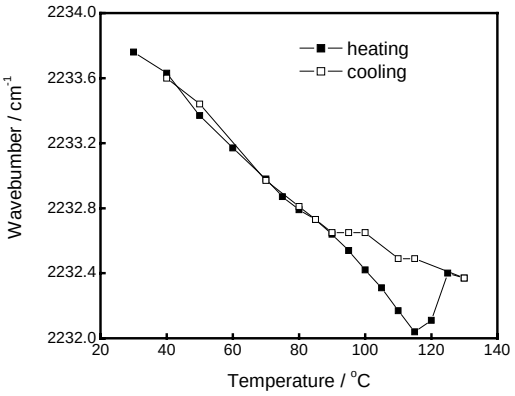

Fig. 5.30 Temperature dependence of CN band of *m*CEt16 bulk substance in KBr. Up to 90°C the CN band remains the same for heating and cooling processes and change linearly with temperature.

During the heating process the ν_{CN} of the bulk substance shifted linearly from 2233.7 cm^{-1} at 30°C to 2232.0 cm^{-1} at 115°C, then shifted slightly to 2232.4 cm^{-1}, when further heated to 125°C. The endothermal peak at 93°C and 113°C in the DSC curve have no influence on the ν_{CN}. The ν_{CN} shifted back to 2233.6 cm^{-1}, when the substance was cooled down to 40°C. No connection between the exothermic peak and a shift of ν_{CN} be found either. Furthermore, for the same temperature the ν_{CN} in the heating and cooling process are almost the same, particularly in the temperature region from 30°C to 90°C.

The temperature dependence of the ν_{CN} for thin films are somewhat different (Fig. 5.31). During the thermal treatment, the ν_{CN} of both films (T_s = -15°C and 95°C) shifted to a lower wavenumber region during heating and back to a high wavenumber region during cooling. Still no clear connection between the peaks in DSC and the shift of ν_{CN} exists. For a given temperature the ν_{CN} in the cooling process is always by about 1.5 cm^{-1} lower than in the heating process. Because the heating rate was very low, the spectra were scanned after the temperature was stable for at least 3 minutes, this difference of ν_{CN} position may indicate that the molecular environments of the CN group during heating and cooling processes are different.

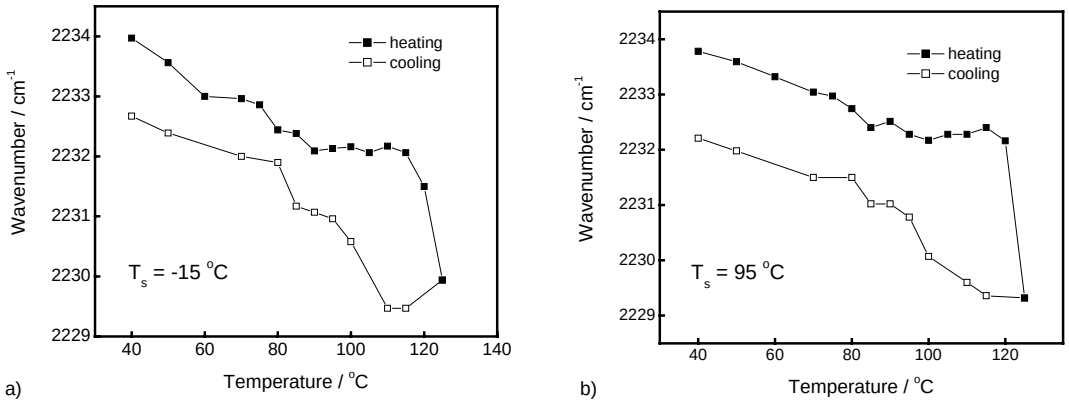

Fig. 5.31 Temperature dependence of ν_{CN} of *m*CEt16 in thin films with T_s = -15°C (a) and 95°C (b). The position of ν_{CN} for both cases are lower in cooling process than heating.

5.2.3.3 Long term stability of the film

After five months of storage the *m*CEt16 films were found to have undergone some topological changes. The surfaces of films deposited at –10°C, 20°C and 40°C are quite different from the fresh prepared films. In Fig. 5.43 the film deposited at T_s = 20°C is presented to illustrate this change.

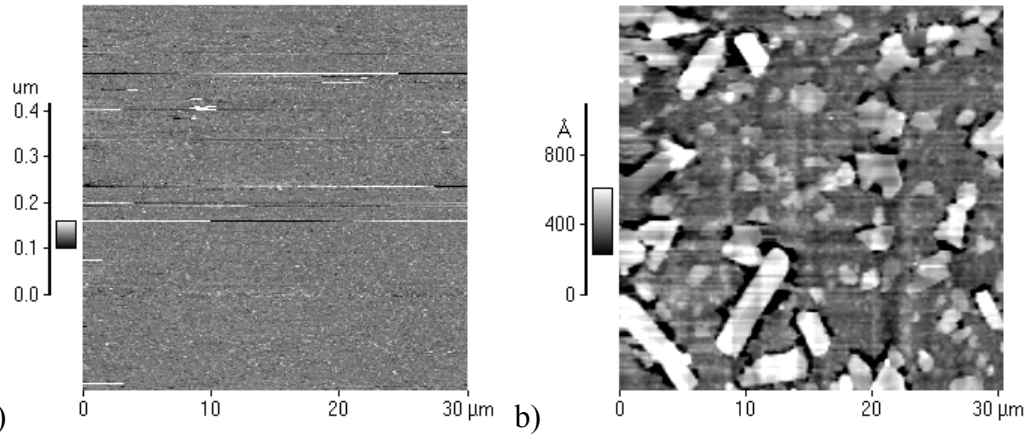

Fig. 5.32 The long term stability of *m*CEt16 film. a) is fresh prepared films at T_s = 20°C and b) is the same films measured after five months of storage.

The AFM image of the freshly prepared film is full of fine particles. After five months of storage, at ambient conditions, long crystals could be found on the surface of the film. Such crystals have grown up to 10 µm in length and are always surrounded with dark areas, indicating that the molecules close by have moved to it and crystallized. This crystallization process began at the edge of the film and slowly extended to the middle. At the edge of the film only crystals could be found in the AFM images and the areas are fully crystalized.

In contrast to the films with low T_s, the films deposited at 60°C and 85°C, which already had clear terrace structures after deposition, do not crystallize, indicating that the films with higher T_s have a more stable structure.

5.2.4 2-(4-Nitrophenyl)-5-(4-dodecyloxyphenyl)-1,3,4-oxadiazole (NIEt12)

5.2.4.1 The film structure of NIEt12

The influence of T_s on film morphology for NIEt12 films was also studied by systematically varying T_s from –10°C to 85°C. The films are prepared with low growth rate between 0.3 and 1.7 nm/min. After the deposition the films were studied with AFM and XSR.

Fig. 5.33 shows the AFM images of NIEt12 films deposited at different T_s. Similar to MEEt16 and *p*CEt16, the film topologies show a strong dependence on T_s. The surface of the films with low T_s (-10°C and 20°C) appear quite rough, and no terrace structures can be found. A terrace with height of 4.1 ± 0.5 nm appears when the T_s is elevated to 40°C. The domains became larger than 30 µm when the film was grown at 60°C. By T_s of 85°C, the highest T_s a film can be obtained at, the size of the domains decreased slightly with respect to those found at T_s = 60°C.

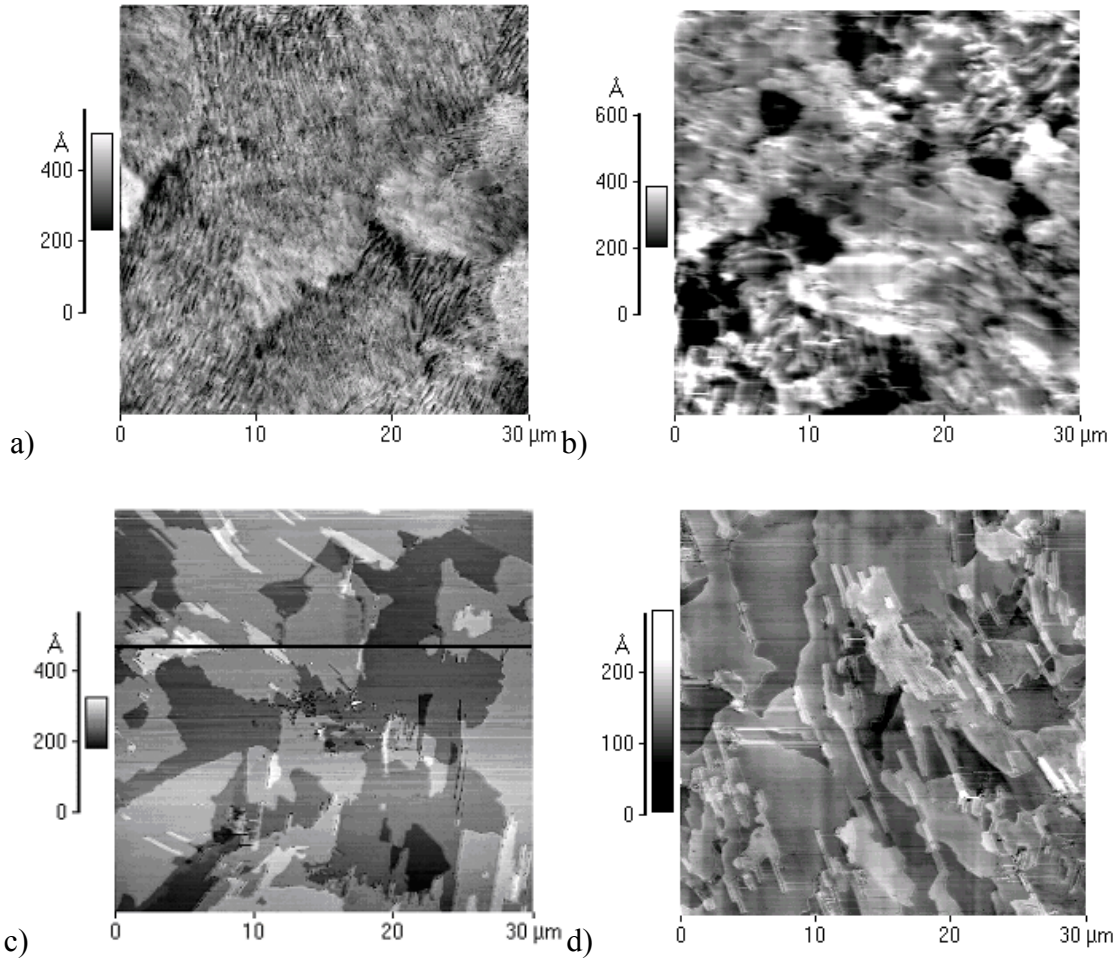

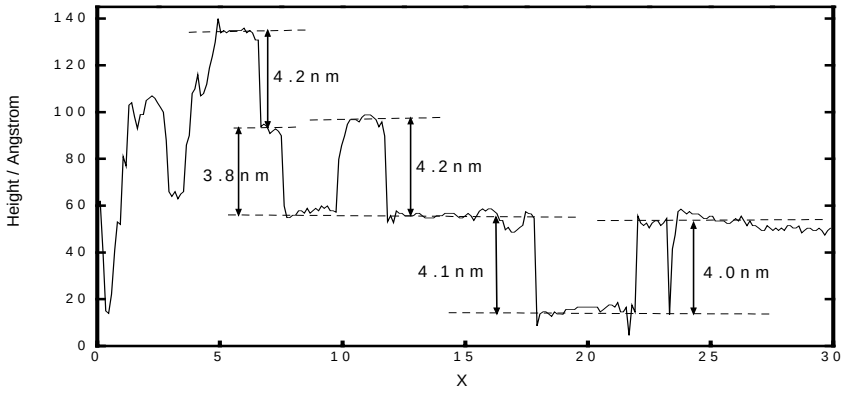

e)

Fig. 5.33 AFM images of NIEt12 films deposited on Si/SiO_2 at T_s = (a) –10°C, (b) 20°C, (c) 60°C and (d) 85°C. The growth rates are maintained between 0.01 and 0.02 nm/min. The film thickness for all films measured with quartz micro-balance are 20 nm. A height profile along the black line in (c) is shown in (e). The average terrace height is 4.1 ± 0.5 nm.

XSR investigations showed the coexistence of two film structures in the film with low T_s (-10°C and 20°C). From the two Bragg peaks in the XSR curve of the film grown at T_s = 20°C film periodicities of 4.0 ± 0.1 nm and 3.0 ± 0.1 nm were calculated, the latter is exactly the length of the NIEt12 molecule in extended conformation, which was determined by AM1 calculations. It is very likely that layers consisting of single molecules exist in the film. The antiphase structure[1] can also result in the peak corresponding to single molecular layers, although the layer is also double molecular layer [148, 149]. Because the terrace height could not be obtained from AFM image, it is impossible for us to determine which structure results in the film periodicity of 3.0 nm.

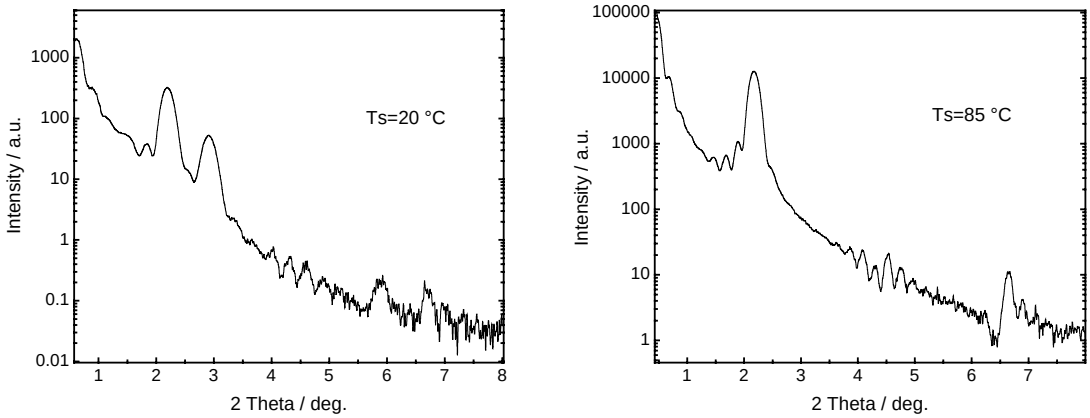

Fig. 5.34 The XSR investigation for NIEt12 film deposited at T_s = 20°C (left) and 85°C (right). The film with T_s = 20°C has film periodicity of 4.0 ± 0.1 and 3.0 ± 0.1 nm. For T_s = 85°C one film periodicity of 4.0 ± 0.1 nm is available.

In contrast to the films deposited at 20°C, the film deposited at T_s = 85°C has a uniform structure. From the Bragg peaks of the XSR curve a film periodicity of 4.0 ± 0.1 nm is obtained.

[1] A concept firstly developed by Reiche to explain the quench of 00*l* peak in XSR curve of some Y-type LB films.

5.2.4.2 Crystal structure of an analogous oxadiazole compound

Orgzall et al. [140] have investigated the crystal structure of 2,5-di(4-nitrophenyl)-1,3,4-oxadiazole (NINI), which differs from NIEt12 in that two nitro groups are attached to the para position of the phenyl ring instead of a nitro group and alkoxy chain for NIEt12. The three-dimensional packing of NINI is characterized by the presence of stacks of molecules along the *a* axis (Fig. 5.35). In a stack the molecules pack parallel to each other and strong π-π interactions exist between the oxadiazole and phenyl rings of adjacent molecules. The plane of the molecule forms an angle of 44° with respect to the stack axis (*a* axis). The tilt angle of the NIEt12 molecules in the VD film was calculated according to equation 5-4 to be 46°, so the angle between molecule and substrate surface is 44°, in good agreement with the angle between the plane of the molecule and the stack axis in the NINI crystal, so it is possible that the packing model of NIEt12 film is similar to that of NINI in crystal.

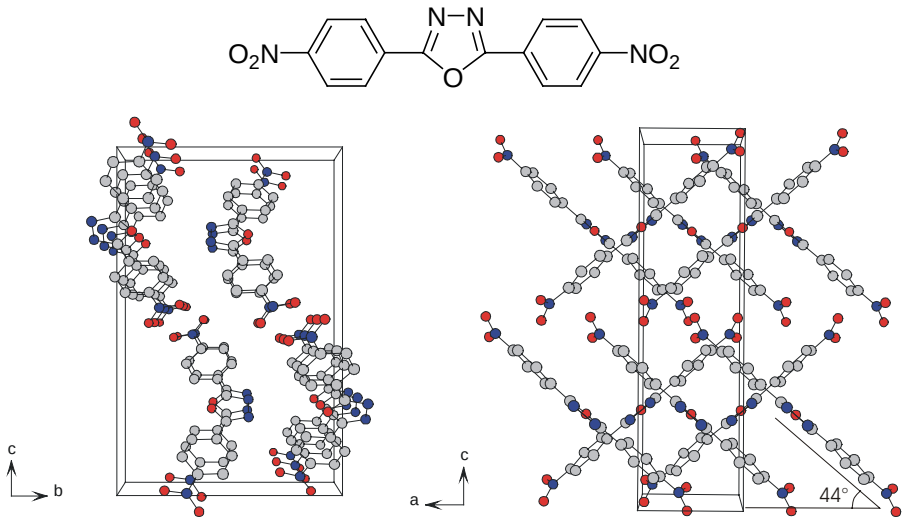

Fig. 5.35 Molecular arrangement of 2,5-di(4-nitrophenyl)-1,3,4-oxadiazole (NINI). View from *a* axis (left) and *b* axis (right).

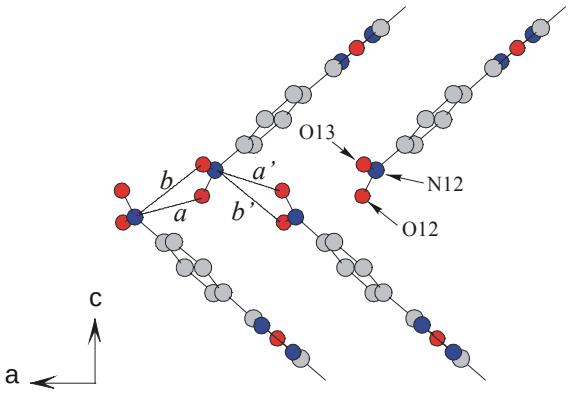

Fig. 5.36 Interlayer interaction between nitro groups in NINI crystal. The interatomic distances in the figure: $a = a' = 3.45$ Å, $b = b' = 3.02$ Å

In the NINI crystal nitro groups occupy the space between the stacks along the *c* axis. The interatomic distances, *a* = *a'* = 3.45 Å, *b* = *b'* = 3.02 Å (Fig. 5.36), are comparable to the expected value for van der Waals contact (3.2 Å), indicating intermolecular contact of the two nitro groups between layers.

The nitro group has a strong dipole moment. A highly polarized system like the nitro group tends to have an interaction with other nitro groups. In fact three nitro-nitro geometries are possible[1], they are illustrated in Fig. 5.37. Considering the charge density difference of N and O atoms in nitro groups and the extra short distance *b* and *b'* (3.02 Å) in the NINI crystal, the existence of electrostatic interactions between nitro groups of adjacent layers seems likely. This nitro-nitro geometry is similar to the packing mode 2 illustrated in Fig. 5.37, where interaction between O of nitro group and N atom of another nitro group is the main reason of nitro-nitro interaction.

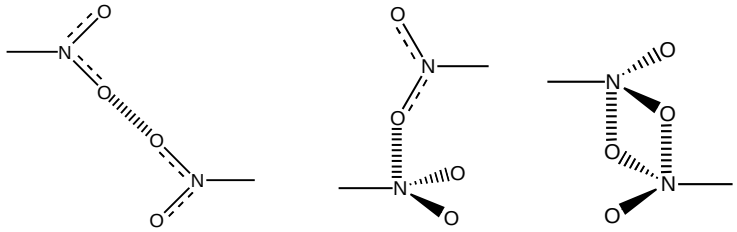

Fig. 5.37 nitro-nitro close interaction geometries. The hashed bonds are only used to illustrate the interaction between nitro groups, they are not real chemical bonding.

5.2.4.3 IR investigation and the structural transformation in the thermal treatment

The films of NIEt12 prepared at different T_s were investigated by means of RAIRS. Nitro groups have two identical NO bonds, which can vibrate asymmetrically or symmetrically, causing strong absorptions at 1556-1545 cm^{-1} (nitro asymmetrical vibration) and 1385-1355 cm^{-1} (nitro symmetrical vibration) [150]. For NIEt12 bulk materials nitro asymmetrical vibrations appear at 1541 cm^{-1} and 1557 cm^{-1}, while symmetrical vibration absorbs at 1365 cm^{-1} and 1352 cm^{-1}. The splitting of the nitro symmetrical vibration band is also described by Epstein et al. [151, 152]. Several theories, including self-association and Fermi resonance, have been proposed to explain the splitting of the symmetrical vibration band of the Nitro group. Ancelin et al. have attributed the splitting to interactions between the nitro group and the substrate surface [153].

The RAIRS investigation of the NIEt12 films deposited at T_s = 25°C and 85°C revealed some differences in the relative intensity of the two bands for the nitro asymmetrical

[1] From Cambridge Crystal Data Center (CCDC).

vibration (Fig. 5.38 left), but the band position remains uninfluenced by the substrate temperature. The intensity and position of the nitro symmetrical vibration are independent of T_s (Fig. 5.38 right).

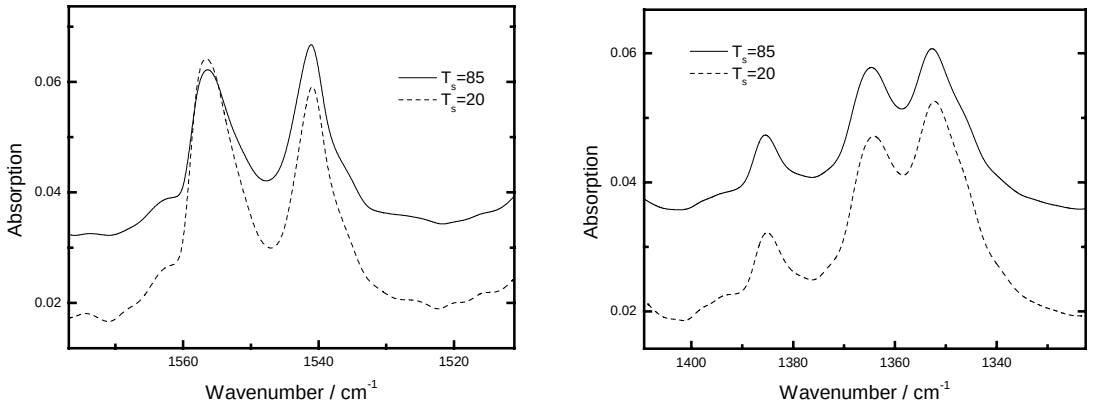

Fig. 5.38 The IR nitro bands of NIEt12 films deposited on Si/SiO_2 with T_s = 20°C (dash line) and 85°C (solid line).

DSC investigation of bulk NIEt12 (Fig. 5.39) crystallized from ethylacetat shows that in the first heating run, two phase transformation peaks appear at 47°C and 125°C, while isotropic transformation occurs at 161°C. In the cooling process, only one peak appears at 158°C. The transformation at 47°C and 125°C in the first heating run is not reversible, in the second heating process only the peak at 161°C appears.

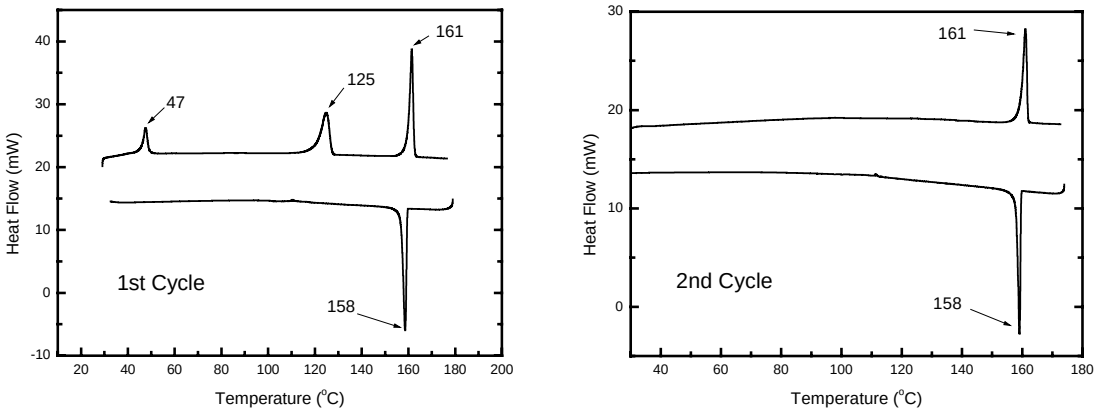

Fig. 5.39 DSC investigation of NIEt12 bulk. The heating rate for first cycle is 10°C/min and 5°C/min for the second cycle.

As revealed by XSR investigation, the film deposited at 20°C has a different structure to that deposited at 85°C (Fig. 5.34, page 66). The phase transform at 47°C and 125°C may have some correlation with this difference, since the growth of VD film is also a kind of crystallization process.

The films were then heated up to 125°C, i.e. the second transform temperature in the first DSC cycle, and temperature dependent RAIRS spectra were obtained simultaneously. In this heating process only the relative intensity of nitro asymmetrical bands undergo some

changes. The film was then further heated to 130°C and a dramatic change occurred in the IR spectra (Fig. 5.40). The nitro asymmetrical band at 1552 cm^{-1} for a temperature of 125°C shifted to 1550 cm^{-1} at 130°C, and its intensity was greatly reduced. Another nitro asymmetrical band at 1537 cm^{-1} visible at 125°C disappeared at 130°C and a new much broader band appeared at 1523 cm^{-1} (Fig. 5.40 link).

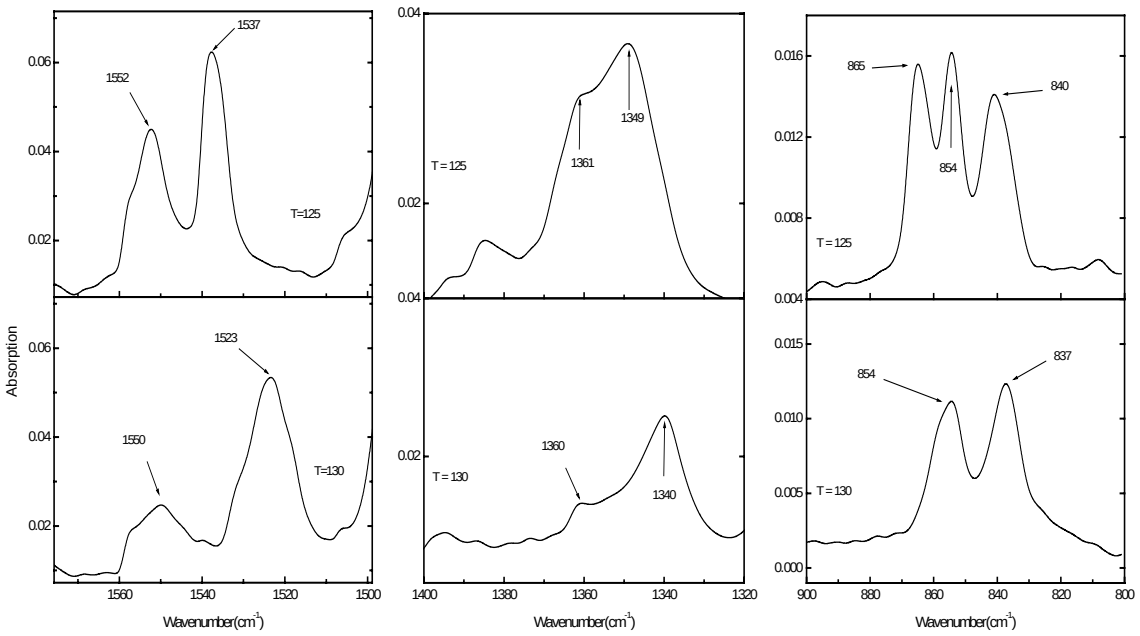

Fig. 5.40 Nitro asymmetrical (left), symmetrical (middle) and C-N (right) band of thin films between 125°C (above) and 130°C (below).

This change in the nitro asymmetrical band is a sign of an environment change for the nitro group, it is also reflected in the symmetrical band of the nitro group [153]. From 125°C to 130°C the most obvious change in the nitro symmetrical band is the decrease of band intensity at 1361 cm^{-1} and 1349 cm^{-1}. The band at 1361 cm^{-1} almost vanished at 130°C while the band at 1349 cm^{-1} shifted to 1340 cm^{-1} (Fig. 5.40 middle). The nitro symmetrical band is no longer a split band. According to the explanation given by Harrand for nitro symmetrical band splitting [154, 155], the change in the spectra is attributed to nitro-nitro disassociation during heating process.

In addition to the nitro symmetrical and asymmetrical bands, the C-N stretching band ($\nu_{(C\text{-}N)}$) of nitro substituted compounds can also provide information about the nitro-nitro interaction. Usually in aromatic compounds like nitrobenzene the $\nu_{(C\text{-}N)}$ is a medium band in the region of 875-830 cm^{-1} [147]. For NIEt12 this band appears at 865 cm^{-1} for bulk materials. During the thermal treatment of the thin film of NIEt12, particularly between 125°C and 130°C, a significant shift of the C-N band to a lower wavenumber region was observed. Above 130°C the C-N stretching band shifted to a lower wavenumber region and overlapped with band at 854 cm^{-1}, which is the nitro scissoring band, so it appears as a shoulder of the latter. The change of C-N stretching band is more evidence for the disassociation of nitro-nitro interaction.

Moreover, the comparison of IR spectra of NIEt12 in solution and in a thin film can also prove this assumption. In a dilute CCl_4 solution (10^{-3} M), the symmetrical band of the

nitro group appears as a single band at 1342 cm^{-1}, a broad and weak shoulder can be seen around 1360 cm^{-1}. Only the band at 1530 cm^{-1} of the nitro asymmetrical vibration can be seen, the band between 1590 cm^{-1} and 1537 cm^{-1} is overlapped by the strong absorption band of CCl_4 in this region (Fig. 5.41). The position as well as the form of the symmetrical band in solution pass very good to that of the thin film at temperature over 130°C. The position and shape of nitro bands at 1530 cm^{-1} also hints that asymmetrical bands of NIEt12 in dilute solution and in thin film heated over 130°C are identical. Thus the environments of NIEt12 molecules in these two states must be similar. In dilute unpolarized solvent like CCl_4, the molecules disperse as unassociated. So the change of IR spectra of thin films during the heating process from 125°C to 130°C reveals the disassociation of nitro-nitro interaction.

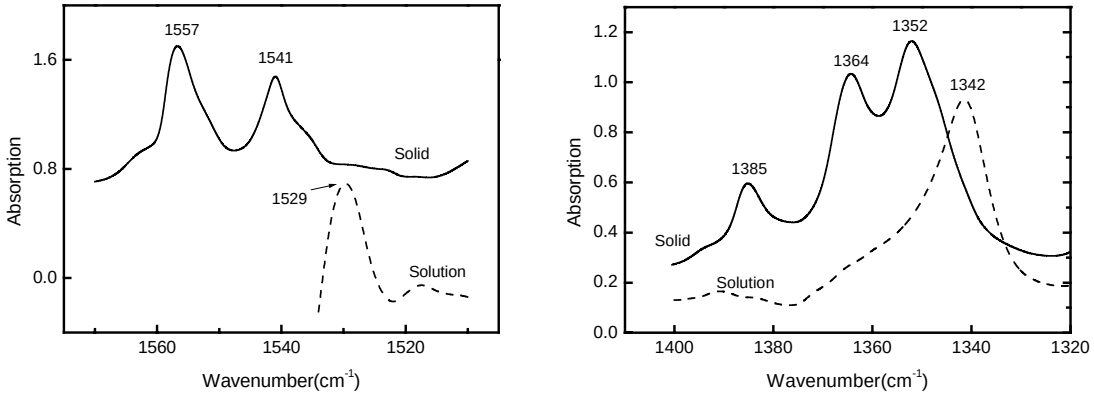

Fig. 5.41 Comparison of nitro asymmetrical (link) and symmetrical (right) bands in solid state (solid line) and CCl_4 solution (dash line). The band position as well as form in solution resemble that of films after thermal treatment. The spectra for solution was multiplied by 25 for comparison. The bands for asymmetrical bands above 1535 cm^{-1} is overlapped by the strong absorption of CCl_4, thus not plotted here.

The structure change induced by annealing was measured with XSR. Films deposited at T_s = 20°C were measured at room temperature before and after annealing at 135°C. After annealing the peak corresponding to film periodicity of 3.0 nm disappeared (Fig. 5.42 right), implying a thermal induced reorganization of molecules in the film.

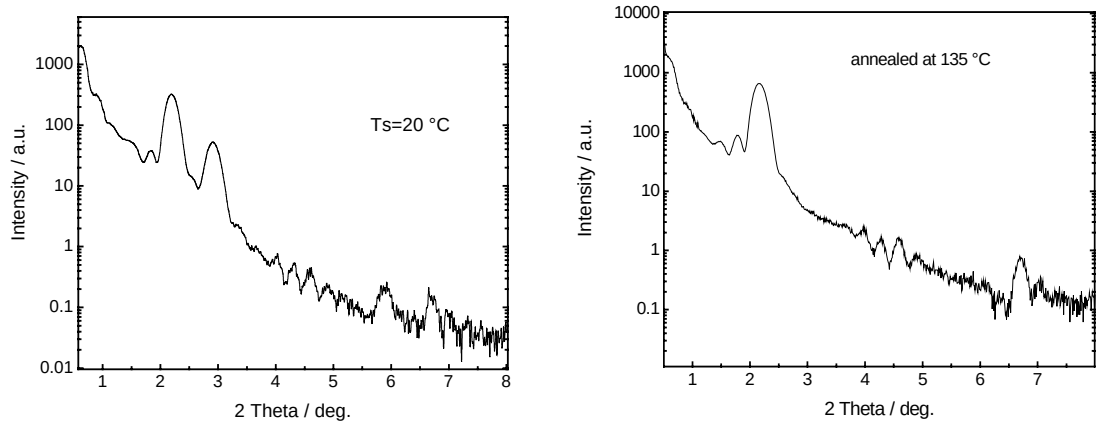

Fig. 5.42 The XSR investigation of NIEt12 film with T_s = 20°C before (left) and after (right) annealling at 135°C. Measurement was done at room temperature. The film periodicity before annealling were 3.0 ± 0.1 nm and 4.0 ± 0.1 nm, after annealing only that of 4.0 ± 0.1 nm remains.

The XSR curve of annealed film (Fig. 5.42 right) is nearly identical with that of films prepared at high T_s (Fig. 5.34 right). The film periodicity of 4.0 nm is much larger than the length of NIEt12 molecules in extended conformation (3.0 nm), and together with the AFM results (Fig. 5.33), it can be concluded that the film has a bilayer structure.

5.2.4.4 Long term stability of the film

After one year of storage the NIEt12 films were re-examined with AFM. Topological changes of varying degrees were observed in the films, in particular the films deposited at T_s = -10°C and 20°C were observed to be considerably different (Fig. 5.43). The surface of NIEt12 films freshly prepared at T_s = -10 and 20°C are characterized with many thread or cloud like structure. No terrace structure could be found. After one year of storage at room temperature, however, clear terrace structures appear in the AFM images of the same films.

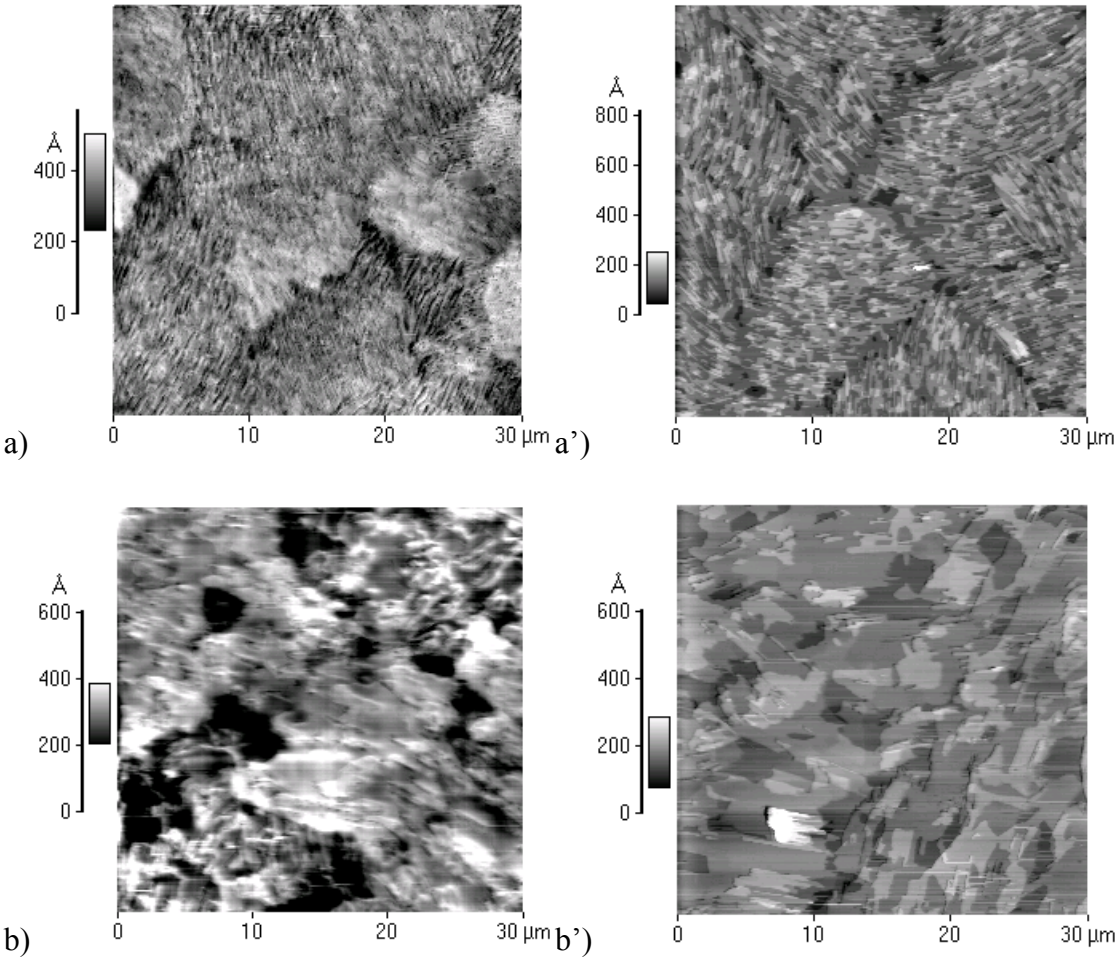

Fig. 5.43 The long term stability of NIEt12 film. a) and b) are fresh prepared films at T_s = -10°C and 20°C, respectively. a') and b') are the same films measured after one year of storage.

The obvious change of film topology show that the films prepared at low T_s were not in a

stable state and as a result, the reorganization of molecules occurs continuously in the film.

The study of NIEt12 films can be summarized as follows:

The structure of NIEt12 films depends strongly on T_s. In the film with T_s = 20°C two structures coexist with film periodicities of 4.0nm and 3.0 nm, while the film with T_s > 60°C has only one film structure with a periodicity of 4.0 nm. The structure of a film with low T_s can be converted irreversibly to that seen at high T_s by simply annealing above 130°C. IR investigations revealed that the nitro-nitro interaction dissociated during the annealing. The films deposited at low T_s are found to have undergone structural changes in storage.

5.2.5 2-(4-Methoxyphenyl)-5-(4-hexadecyloxyphenyl)-1,3,4-oxadiazole (MOEt16)

5.2.5.1 The film structure of MOEt16

MOEt16 was deposited on Si/SiO_2 and the resulting films were investigated with AFM and XSR. Fig. 5.44 shows the AFM images of the MOEt16 films. The surface of the film deposited at –10°C are quite rough, with no apparent structure. Similar topologies are observed for films deposited at 20°C and 40°C. The surface of films deposited at 60°C is characterized by the existence of smooth terraces with a height of 4.7 ± 0.5 nm, higher than the calculated molecule length (3.52 nm), indicating a bilayer-by-bilayer growth mechanism. This step height corresponds to the internal bilayer thickness (4.5 ± 0.1 nm) determined by the XSR measurements (Fig. 5.45).

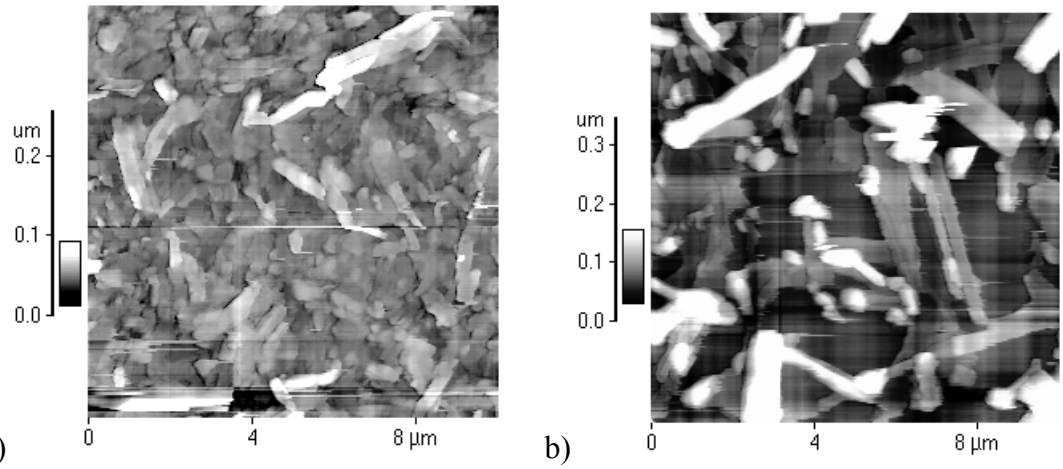

a) b)

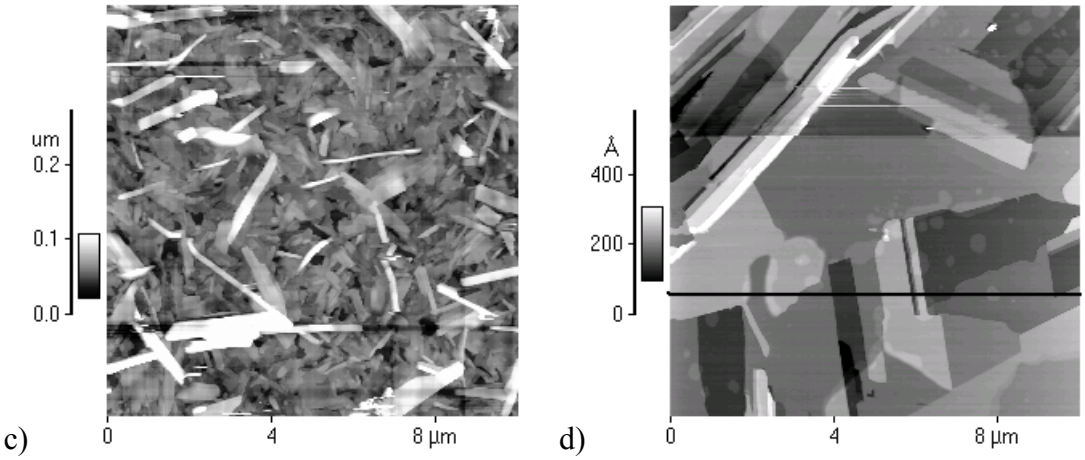

c) d)

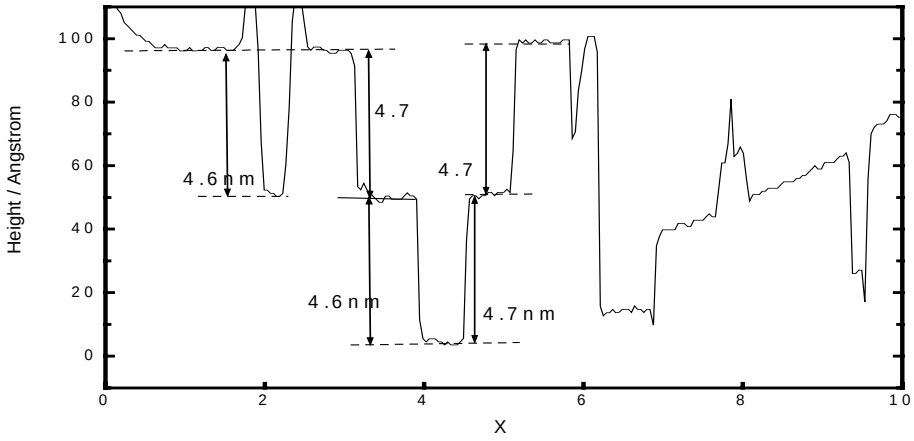

f)

Fig. 5.44 AFM images of MOEt16 films deposited at T_s = (a) –10, (b) 20, (c) 40 and (d) 60°C. The height profile along the straight line in (d) is shown in (f). The average terrace height obtained from different position is 4.7 ± 0.5 nm.

The results of XSR measurements reveal the layered film structure for MOEt16 in the studied T_s ranged from –10°C to 60°C. The film periodicities in direction normal to the substrate surface are same for all the films (4.5 ± 0.1 nm).

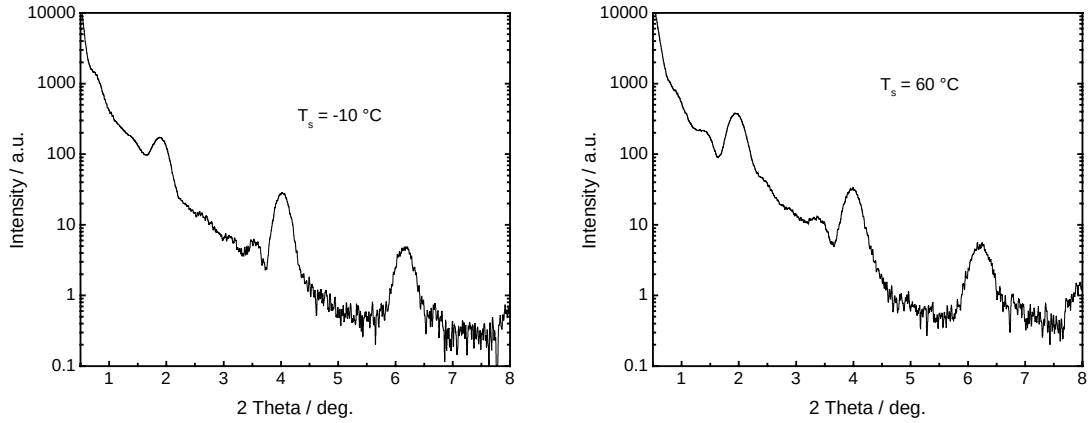

Fig. 5.45 XSR curve of MOEt16 films deposited at T_s = -10°C (left) and 60°C (right). The film thickness is 20 nm. The film periodicity obtained from XSR is 4.5 ± 0.1 nm for both films.

5.2.5.2 Crystal structure of a methoxy substituted oxadiazole

Similar to some other substances discussed in this chapter, the crystal structure of an analogue oxadiazole can provide useful information in understanding the film structure. Orgzall et al. [140] has investigated the crystal structure of 2-(4-methoxylphenyl) -5-(4-aminophenyl)-1,3,4-oxadiazole (MOA), which also has a methoxy group attached at the para position of the phenyl ring. The molecular packing of MOA is characterized by the existence of molecular stacks along the *c* axis (Fig. 5.46).

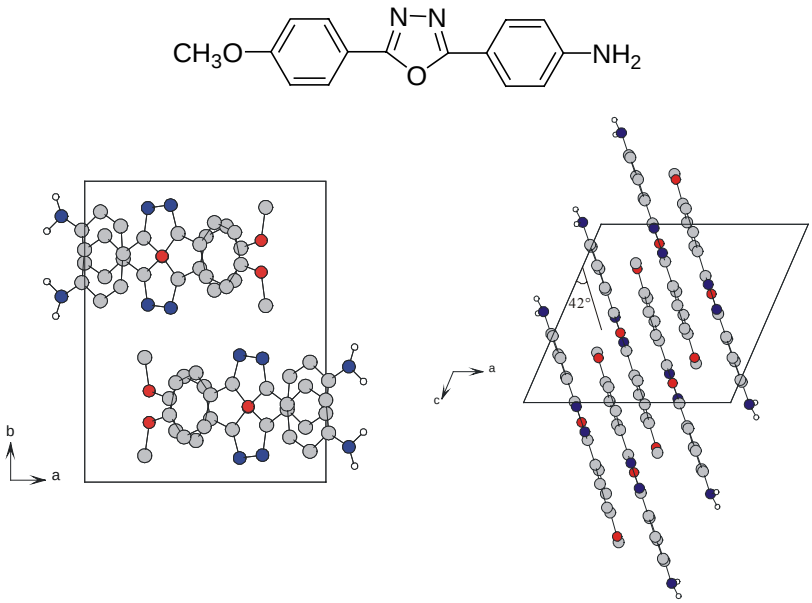

Fig. 5.46 Crystal structure of 2-(4-methoxylphenyl)-5-(4-aminophenyl)-1,3,4-oxadiazole (MOA). Top view (left) and lateral view (right) of the stacks. For clarity only the hydrogen atoms in amino group are plotted.

The adjacent stacks pack parallel to each other. The molecules arrange parallel to each other in the stack and with alternating orientation with respect to the oxadiazole ring. As in the case of the NINI (§5.2.4.2, page 67) and the MEME (§5.2.1.2, page 49) crystal, the strong π-π interactions connects the oxadiazole ring of one molecule and the phenyl ring of the adjacent molecule. The methoxy groups are aligned at the same end of a stack. The long axis of the molecule forms an angle of 42° with the *c* axis and the distance between two adjacent molecule planes is 0.348 nm.

From a chemical point of view, the methoxy groups can not form any strong interactions between each other. However, in the crystal structure and liquid crystal studies of 4-methoxyphenyl 4'-oxcyloxybiphenyl-4-carboxylate, which also has a methoxy head group, Hori et al. have pointed out that a van der Walls contact exists between the methoxy groups. This interaction would maintain the bilayer structure until the thermal agitation overcomes the interlayer interaction at higher temperatures [134]. In the crystal of MOA, the interatomic distance between the O atom of adjacent methoxy groups and C atom in the neighbouring molecule is longer than 5 Å, so no intralayer interaction between methoxy groups in MOA crystal exists.

If the molecules pack themselves in the film in head-to-head model, the tilt angle of molecules can be calculated according to equation 5-4 to be 50°. So the molecules stand with an angle of 40° to the substrate surface, in good agreement with the angle between molecule long axis and the stacking direction in crystal of MOA (42°), indicating that the MOEt16 molecules have similar packing in film as MOA in crystal.

5.2.5.3 DSC and IR investigation

In the heating process of the MOEt16 DSC curve (Fig. 5.47) only one endothermal peak and one exothermic peak appears at 108°C and 88°C, respectively, while in the second cycle a small exothermic peak appears at 88°C of the heating process. The difference between these two peaks amounts to 17°C, indicating that the peak represents the melting process of the crystal. The energy of the peak at 88°C is quite small (3.85KJ·mol^{-1}), and can therefore not be attributed to a phase transform. It is very likely that only very weak or no intermolecular interaction exists for MOEt16, otherwise peaks due to phase transforms would appear in the DSC curve as seen for *p*CEt16, MEEt16 and NIEt12.

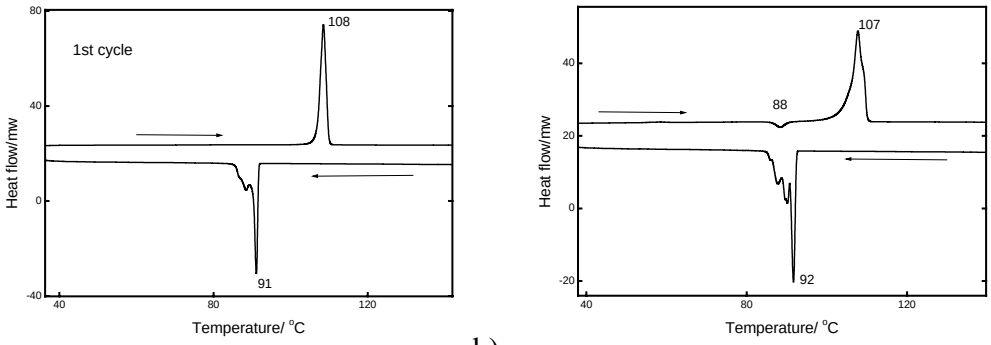

a) b)

Fig. 5.47 DSC measurement of MOEt16. a) first cycle; b) second cycle. The heating rate for both cycles are 10 °C/min.

By comparing the IR spectra of MOEt16 in a diluted solution (CCl_4, 10^{-3} M) and crystal the difference in the molecular environment for the ether unit is revealed. The aromatic ethers usually give rise to two correlatable bands, 1310-1210 cm^{-1} and 1050-1010 cm^{-1} [156-159]. The band between 1310-1210 cm^{-1} can be looked on as an aromatic C-O stretching frequency (also called asymmetrical C-O-C stretching), and the band between 1050-1010 cm^{-1}, as the aliphatic C-O (O-CH_2 or O-CH_3) stretching frequency (also called symmetrical C-O-C stretching) [147].

The IR bands for MOEt16 in a solid and solution (CCl_4, 10^{-3} M) at room temperature are summarized in Tab. 5.5. The asymmetric band consists of two overlapped bands at 1259 cm^{-1} and 1255 cm^{-1}, while the symmetric band appears as an asymmetrical band at 1021 with a shoulder at 1032 cm^{-1}. In a diluted solution, however, both bands are symmetrical single bands located at 1255 cm^{-1} and 1035 cm^{-1} (Fig. 5.48), respectively. Such a

difference in the C-O-C band position in solid and solution reveals that the environments of the ether groups in solid and solution are slightly different.

Tab. 5.5 IR bands concerning ether structure for MOEt16 in solid and solution (CCl_4, 10^{-3} M). The band marked with an asterisk appears as a shoulder.

	Asy. C-O-C	Sym. C-O-C
Solid	1259, 1255	1021, 1032*
Solution (CCl_4)	1255	1035

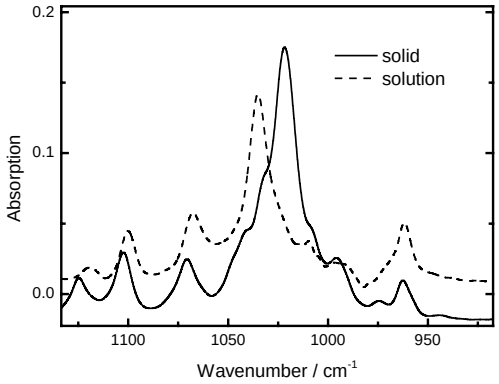

Fig. 5.48 The O-CH_3 band of MOEt16 in Bulk (solid line) and solution (CCl_4 10^{-4} M) (dash line). The band in solution shifted by 14 cm^{-1} to higher frequency region with respect to bulk material.

When the substance is heated over the melting point, the shift of the C-O-C band can also be observed in the IR spectra. However, two different ether substituents, methoxy and hexadecyloxy, exist in the molecule of MOEt16 and it is difficult to assign the shift to any of the two ether structures. In the analog investigation of HEt16, a compound similar to MOEt16 but with a hexadecyloxy substituent, such spectral changes were also observed. So these change can not be specifically ascribed to interaction between methoxy groups.

The study of MOEt16 film can be summarized as follows:

The films deposited in the investigated T_s range have the same bilayer structure, but the film topology depends strongly on T_s. Only at T_s = 60°C can films with a clear terrace structure be obtained. DSC revealed no phase transform and no obvious intermolecular interaction could be found by IR investigation, which may be responsible for the independence of film structure on T_s.

5.2.6 2-Phenyl-5-(4-hexadecyloxyphenyl)-1,3,4-oxadiazole (HEt16)

5.2.6.1 The film structure of HEt16

The topography of HEt16 VD films were measured by means of AFM. A 10×10 μm^2 AFM image of HEt16 film deposited at T_s = -10°C and a height profile along the line in this image are shown in Fig. 5.49 (a) and (a'). It worth pointing out that the film is very unstable and crystallized shortly after deposition. The AFM and XSR measurements were performed on crystallized films. The height of one crystal in the middle of the image was measured to be 250 nm from the height profile. The line RMS obtained from this image is 60 nm. Taking into account that the average thickness is only 20 nm, this film is very rough indeed.

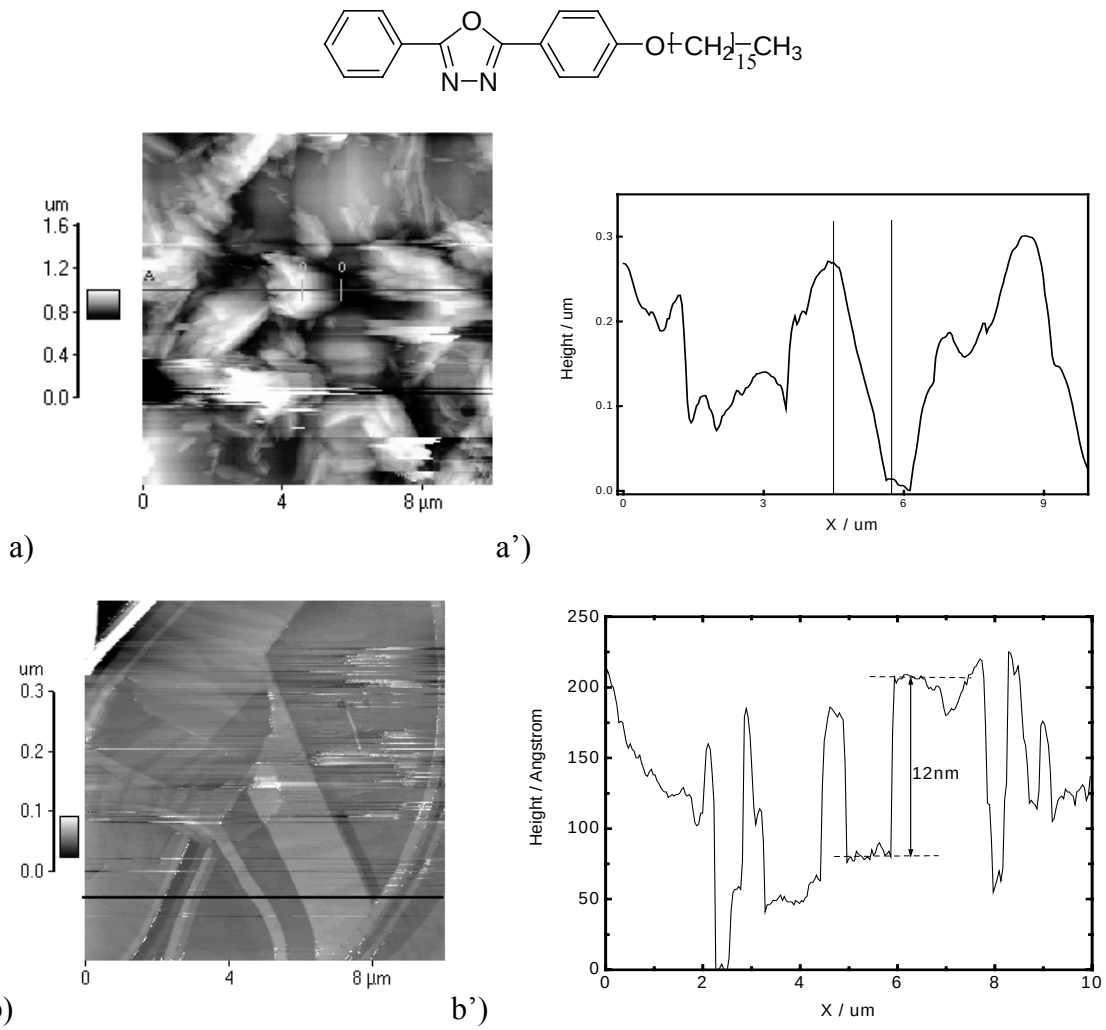

Fig. 5.49. The AFM image of HEt16 films deposited at T_s = -10°C (a) and 60°C (b). a') and (b') are the height profiles along the lines in the corresponding images.

As the T_s was elevated up to 60°C, the film surface was featured with high plateaus. The

relative height of the plateaus was measured to be 12 nm, this value is about four times the length of the molecule (3.3 nm). The RMS roughness alone the line in Fig. 5.49 (b) is 5 nm, much smaller than the RMS for T_s = -10°C.

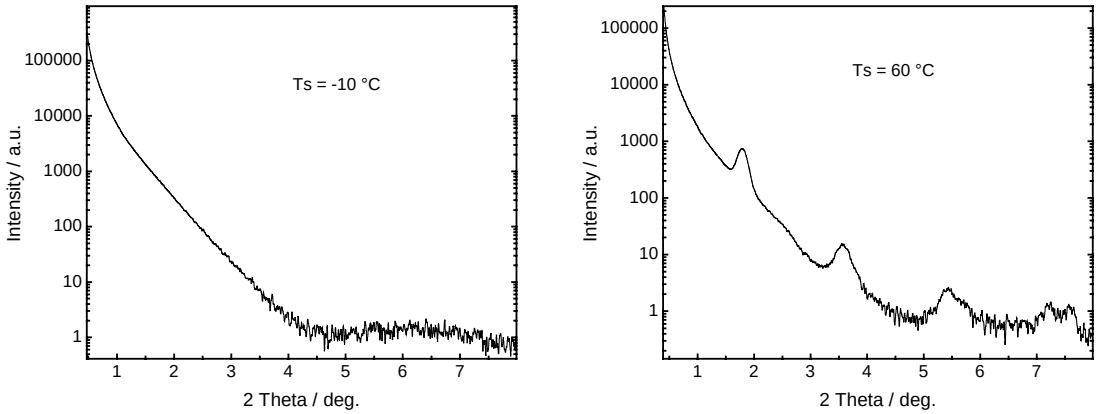

Fig. 5.50 XSR investigation of HEt16 films deposited at T_s = -10°C (left) and 60°C (right). The film periodicity for T_s =60°C is 4.9 ± 0.1 nm.

The XSR investigation reveals a layered film structure for films prepared with T_s = 60°C (Fig. 5.50). The film periodicity for this film obtained from XSR is 4.9 ± 0.1 nm, bigger than the calculated molecule length in extended conformation (3.3 nm), so the film should have a bilayer structure. In contrast to 60°C, the XSR curve for films deposited at T_s = -10°C has no Bragg peaks, indicating that the film does not has a layered structure.

HEt16 has no substituent as head group. DSC investigations showed that no phase transform before the melting point. In the DSC diagram only one peak at 88°C of heating process and one peak at 76°C of cooling process can be observed (Fig. 5.51). The temperature difference between two peaks amounts to 12°C, indicating that these two peaks are caused by the melting and crystallization process.

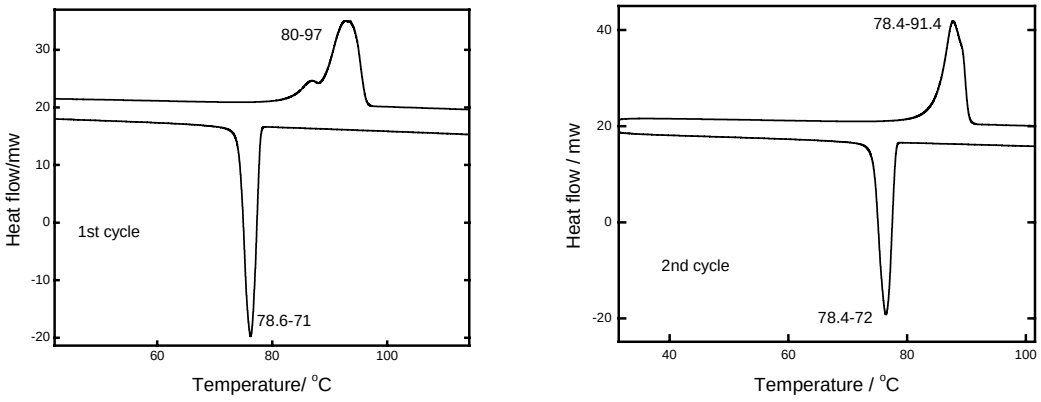

Fig. 5.51 DSC investigation of HEt16 bulk. First cycle (left) and second cycle (right). The heating rate is 10°C/min.

In situ IR investigations during thermal treatment were carried out for HEt16 bulk substance in KBr. The results correlated well with DSC. Although some changes such as intensity decrease or small shift of the band before melting were observed, the most significant changes occurred in the melting or crystallization process.

5.2.6.2 The stability of the film

The films of HEt16 were found to be very unstable. Films freshly prepared at $T_s = -10°C$ were transparent and smooth just after deposition, but crystallized after just 10 minutes at room temperature and became white in colour. Very small crystals formed in the film, and as a result AFM as well as XSR measurement on the fresh prepared film could not be carried out. The films of HEt16 prepared in the investigated T_s range were also found to be unstable in the long term. In Fig. 5.52 the AFM images for a film grown at $T_s = 20°C$, the surface of fresh prepared film was doped with many high crystal structures but the film was closed. After one years of storage the film is fully crystallized, large area of uncovered substrate appeared in the AFM image. The film became spreads of thin crystals. Films prepared at other investigated T_s have undergone similar crystallization process.

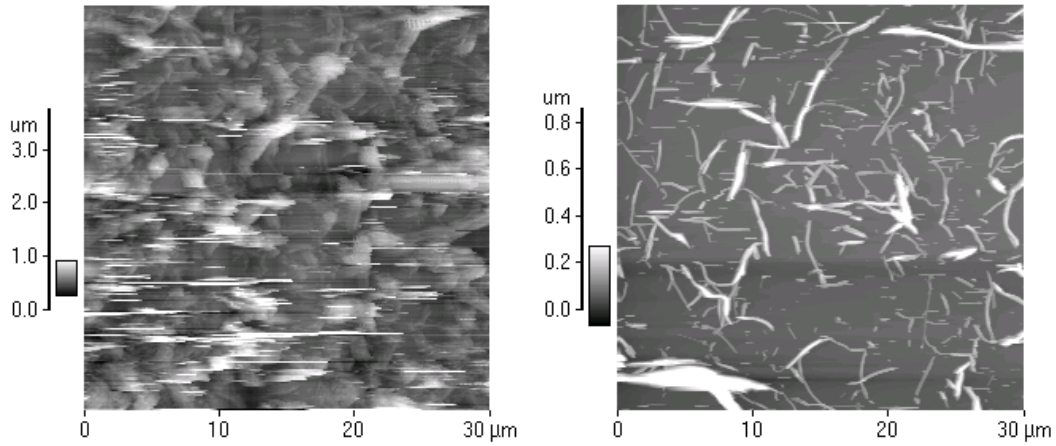

Fig. 5.52 Long term stability of the HEt16 film. 1 day (left) and 1 year (right) after the preparation. The film was deposited at $T_s = 20°C$. The dark area in the right image is bare substrate.

<u>The study of the HEt16 film could be summarized as follows:</u>

The film topology as well as structure depend strongly on T_s and layered films can only be obtained at $T_s > 60°C$. The films deposited on the T_s range from –10°C to 60°C are not stable in the long term, they crystallized quickly after the deposition and the crystallization went on during the storage. Since the only difference between HEt16 and the other oxadiazole compounds discussed in §5.2 is the absence of a head group in the HEt16 molecular structure, the low film stability and special T_s dependence can be attributed to the absence of a head group.

5.2.7 Summary

From the study of VD film structures of oxadiazole compounds with different head groups the following conclusions can be made:

1. Among the investigated oxadiazole compounds, the substances with head groups can form layered films within the whole investigated region of T_s. Layered films of the substance without head group, i.e. HEt16, can only be obtained at relatively high T_s.

2. The film periodicities of the studied substances are larger than the calculated length of the corresponding molecules in extended conformation. These films therefore have a bilayer structure.

3. With the exception of MEEt16, the tilt angle of the molecules calculated according to the head-to-head model ranges between 42° and 50°.

4. The molecules have similar packing in the films as in the crystals, which consist of oxadiazoles substituted with same head group but without an alkyl chain. The exception to this is MEEt16, where the presence of π-π complexes between molecules determined the film structure.

5. The interactions between head groups were found in films based on MEEt16, *p*CEt16 and NIEt12. These interactions are very likely responsible for the extraordinarly high film periodicity of MEEt16 film, the different film periodicity of *p*CEt16 at different T_s and the coexistence of two film structures in NIEt12 films prepared at low T_s.

6. Thermally induced dissociation of intermolecular interactions caused a change in the film structures. The film periodicity of MEEt16 was reduced from double its molecule length to a single molecule length. The film periodicity of *p*CEt16 films was reduced from 4.8 nm to 4.4 nm during the annealing. For films of NIEt12, the film structure corresponding to a film periodicity of 3.0 nm disappeared after being annealled at 135°C.

7. The films of *m*Et16, NIEt12 and HEt16 deposited at low T_s were found to be unstable in the long term and during storage topological changes in the films were observed. The films of HEt16, which has no substituted head group, were found to be the most unstable.

5.3 Influence of the amide bridge group

The head group in the molecules of oxadiazole compounds can influence the formation of layered films. The structure in the molecule which connects the alkyl chain with the phenyl ring, named here as bridge group, has proven to be very important in LB film formation. Freydank et al. [18] investigated the influence of the bridge group of NIA12 on the LB film [16, 64] as well as the VD film stability [63] and concluded that the intermolecular H-bond help to stabilize the LB film on the water surface and the substrate.

The film structure of oxadiazole compounds with an ether bridge group have been discussed in §5.2. In this section focus will be placed on oxadiazole compounds with an amide bridge group. For comparison the oxadiazole compound with ether compounds will also be further discussed.

IR spectroscopy is one of the best methods of detecting H-bonds. In the case of an amide compound, the H-bond has been regarded as an interaction between the H atom in the N-H group and O atom in the carbonyl group. A single H atom is associated with N and O atoms and forms a N-H···O structure. The unbonded N-H stretching band is usually relatively sharp at 3480-3440 cm^{-1} in a solvent which can not form H-bonds with it [135, 147, 159], for example CCl_4. When the H-bond is formed, for example in more concentrated solutions or in the solid state, the N-H stretching band will shift to lower wavenumber region and becomes much broader. The carbonyl band, which is also called as an amide I band, appears for secondary amide at 1680-1630 cm^{-1} [160, 161]. For the similar reason, the amide I band shifts about 30 cm^{-1} to low wavenumber region due to the formation of H-bonds [135].

The amide II band, which is in fact a mix band of C-N stretching vibration and C-N-H bending vibration, appears at 1570-1515 cm^{-1} for secondary amide in the bulk and shifts by about -10 cm^{-1} in solution [135].

5.3.1 2-Phenyl-5-(4-dodecanoylaminophenyl)- 1,3,4-oxadiazole (HA11)

5.3.1.1 Film structure of HA11

Compared with HEt16 (§5.2.6, page 78), HA11 has one amide unit and as a result H-bond can form between neighbouring molecules. The films based on HA11 were prepared at a T_s ranging from 25°C to 100°C. After deposition film topology and structure were investigated with AFM and XSR.

Fig. 5.53 shows the AFM images for HA11 films deposited at different T_s. The effect of T_s

on the film topologies can be clearly seen from the images. The surface of the film prepared at 25°C are characterized with coarse grained structures (Fig. 5.53 a). The film surface underwent significant change when the T_s was further elevated to 75°C and 100°C. Thread like structures were formed on the surface of the film (Fig. 5.53 c). Terrace structure can also be seen in the images, but the heights of these terraces obtained by height profile scanning range from 10 to 20 nm, so they are not formed by layered growth of the film, because the calculated length of HA11 in extended conformation is only 2.8 nm.

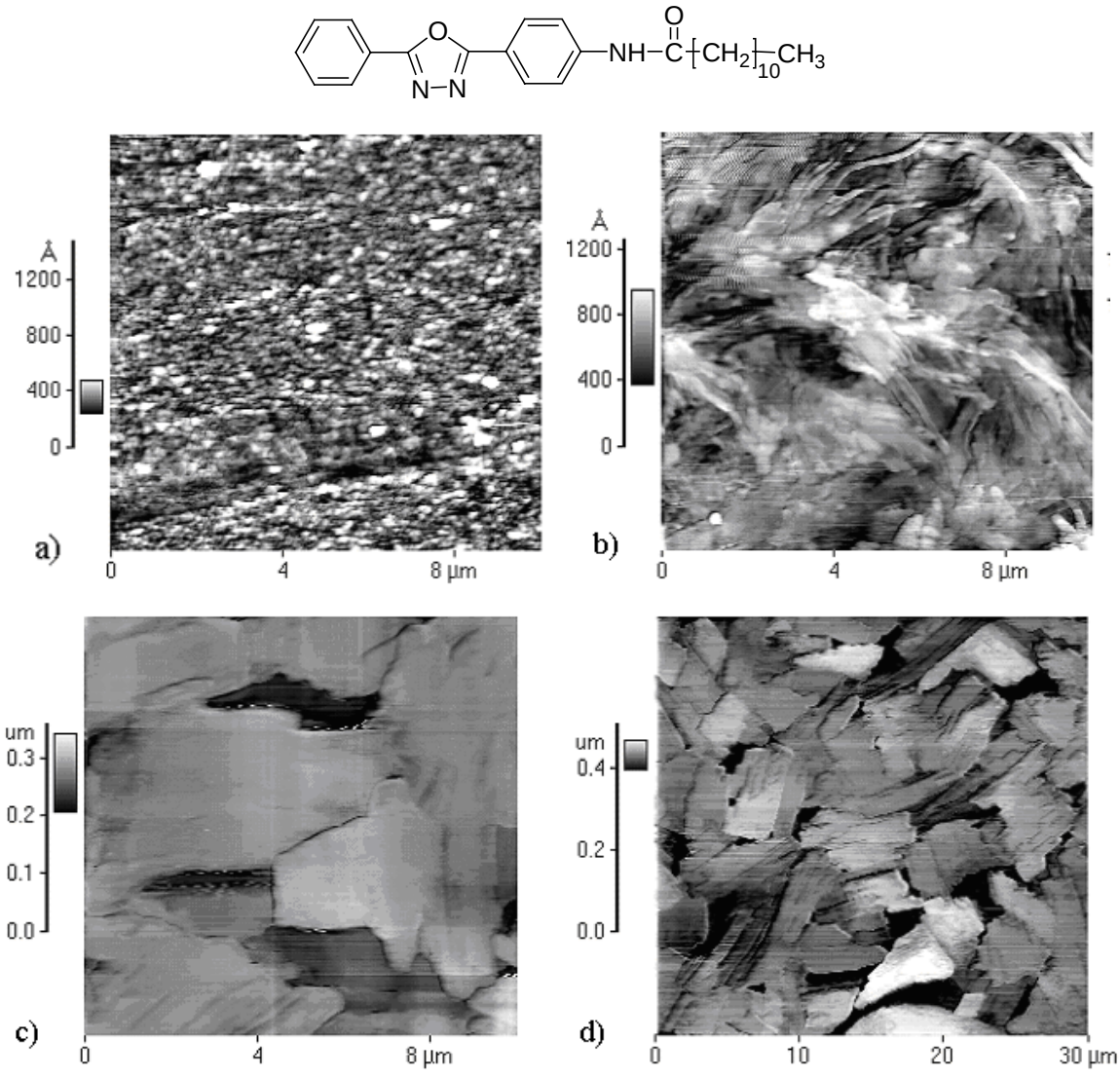

Fig. 5.53 AFM images of HA11 films deposited on Si/SiO_2 at T_s = (a) 25°C, (b) 75°C and (c) (d) 100°C. The growth rates are maintained between 0.12 and 0.38 nm/min. The film thickness for all films measured with quartz micro-balance are 50 nm.

The AFM image for films grown at 100°C shows bigger domains than at lower T_s. To show the size of domains an image with size of 30×30 μm^2 is presented in Fig. 5.53 d). Similar to the film with T_s of 50°C and 75°C, the terrace height obtained from this image

is much larger than the molecule length, implying that the film does not have a layer-by-layer growth mechanism.

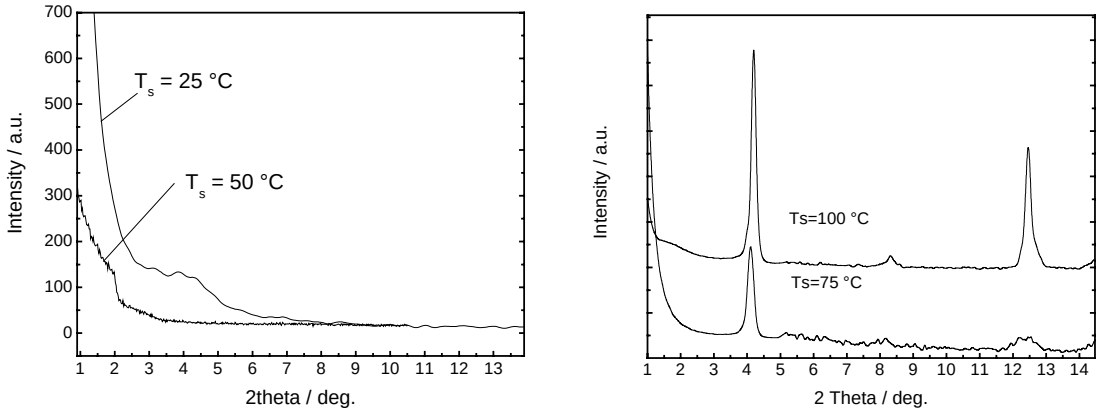

Fig. 5.54 XSR curves of HA11 films deposited at T_s = 25°C, 75°C and 100°C. The films thickness for both films are 50 nm. The film periodicities for T_s = 75°C and 100°C are 2.1 ± 0.1 nm. The data above 5° for T_s = 100 and 75°C are enlarged by factors of 20 and 50, respectively, to make the Bragg peaks in this region clear.

The result of XSR investigation shown in Fig. 5.54 reveal that the films prepared at 25°C and 50°C are amorphous. Bragg peaks with strong intensities appear in the XSR curves for film deposited a 75°C and 100°C, indicating that the films have a layered structure. The film periodicity obtained from XSR is 2.1 ± 0.1 nm, lower than the length of the molecule (2.8 nm), so a layer of the film consists of only one molecule.

5.3.1.2 IR investigation

The IR spectra of HA11 in a solid state and in solution (CCl_4 and $CHCl_3$, 10^{-3}M) were measured. Fig. 5.55 illustrates the difference of $\nu_{N\text{-}H}$ and $\nu_{C=O}$ bands in these two states and the band positions in solution as well as in thin films are also summarized in Tab. 5.6.

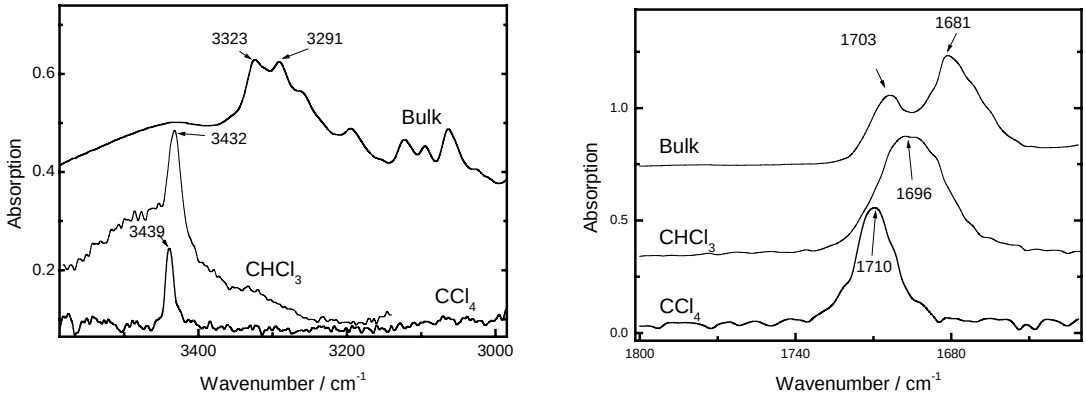

Fig. 5.55 Comparison of ν_{NH} (left) and $\nu_{C=O}$ (right) stretching band for HA11 as bulk and in CCl_4(10^{-3} M). The spectra in CCl_4 is multiplied by 20 for comparison.

Tab. 5.6 Characteristic amide bands for HA11 in different states.

Band (cm^{-1})	CCl_4 (10^{-3} M)	$CHCl_3$ (10^{-3} M)	Bulk	Film (T_s=25°C)	Film (T_s=100°C)
ν_{NH}	3439	3432	3323, 3291	3356	3258
$\nu_{C=O}$	1710	1696	1703, 1681	1702, 1693	1706, 1678
$\nu_{H\text{-}N\text{-}C}$	NA	NA	1528	1529	1540

By comparing the characteristic bands for amide in CCl_4 and in the bulk, an obvious red shift can be observed. The ν_{NH} shifted about 116 cm^{-1} and split into two bands at 3323 cm^{-1} and 3291 cm^{-1}, while $\nu_{C=O}$ shifted about 7 cm^{-1} and split also into two bands at 1703 cm^{-1} and 1681 cm^{-1}. The split of bands may hint that more than one type of H-bond exists in the solid state. This difference is reflected more clearly for films deposited at different T_s (Fig. 5.56). In $CHCl_3$, where the formation of H-bonds between solvent and HA11 is possible, the red shift of amide bands can also be found but the shift is smaller with respect to the bulk material, so the molecules are not H-bonded in CCl_4. The amide II band at around 1530 cm^{-1} overlaps with the strong absorption band of the solvent and is therefore unavailable for analysis.

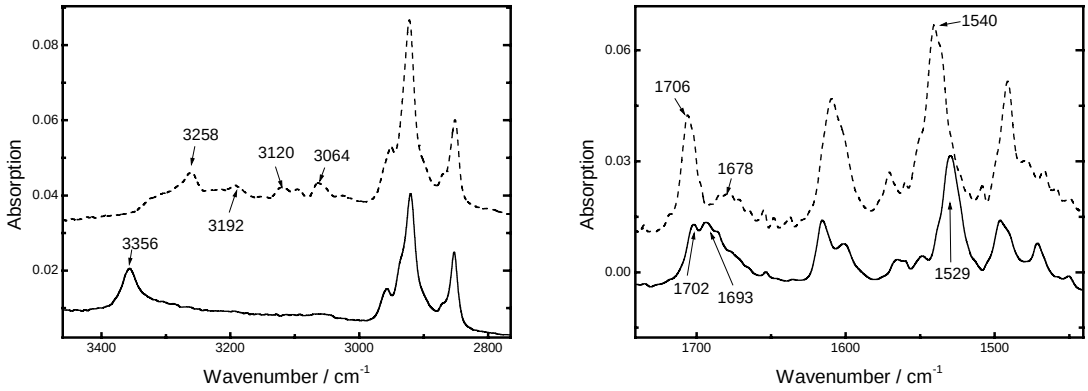

Fig. 5.56 Comparison of RAIRS spectra of HA11 deposited on Si/SiO_2 at T_s = 25°C (solid line) and T_s = 100°C (dash line).

The ν_{NH} for HA11 films grown at T_s = 25°C appears as a single sharp peak at 3356 cm^{-1}, the $\nu_{C=O}$ appears as split band at 1702 cm^{-1} and 1693 cm^{-1}, both bands are lower than in solution, implying a H-bond formation in the film. However the density or the strength of H-bond is still lower than in film with T_s = 100°C, which is a broad band at 3258 cm^{-1}. The $\nu_{C=O}$ of the latter film appears as a sharp band at 1706 cm^{-1} and a broad band at 1678 cm^{-1}. Further evidence of a H-bond content increase is the blue shift of the amide II band from 1529 cm^{-1} (T_s = 25°C) to 1540 cm^{-1} (T_s = 100°C), i.e. a blue shift of 11 cm^{-1}. The so called amide II band arises from N-H bending (60%) and C-N stretching (40%) vibrations [162-164]. When the H-bond holds the H atom of the N-H and increases the force constant of the N-H bending, a blue shift of the amide II band occurs.

The formation of intermolecular H-bonds contributes to the stabilization of LB films [16,

64]. In the case of HA11, the film structure also shows strong correlation with the H-bond formation. The films deposited at lower T_s have a low content of H-bonds and an amorphous film structure, while the films deposited at high T_s are highly H-bonded and have layered structures.

With an amide bridge group in the molecule the long term stability of the HA11 film is greatly improved in comparison to the HEt16 films. The film structure remains unchanged after several months of storage. The intermolecular H-bond increased the energy barrier for molecular movement and the film stability is consequently improved.

5.3.2 2-(4-Cyanophenyl)-5-(4-dodecanoylaminophenyl)-1,3,4-oxadiazole (*p*CA11)

5.3.2.1 Film structure of *p*CA11

Comparing with HA11, *p*CA11 has a CN head group at one end of the molecule.

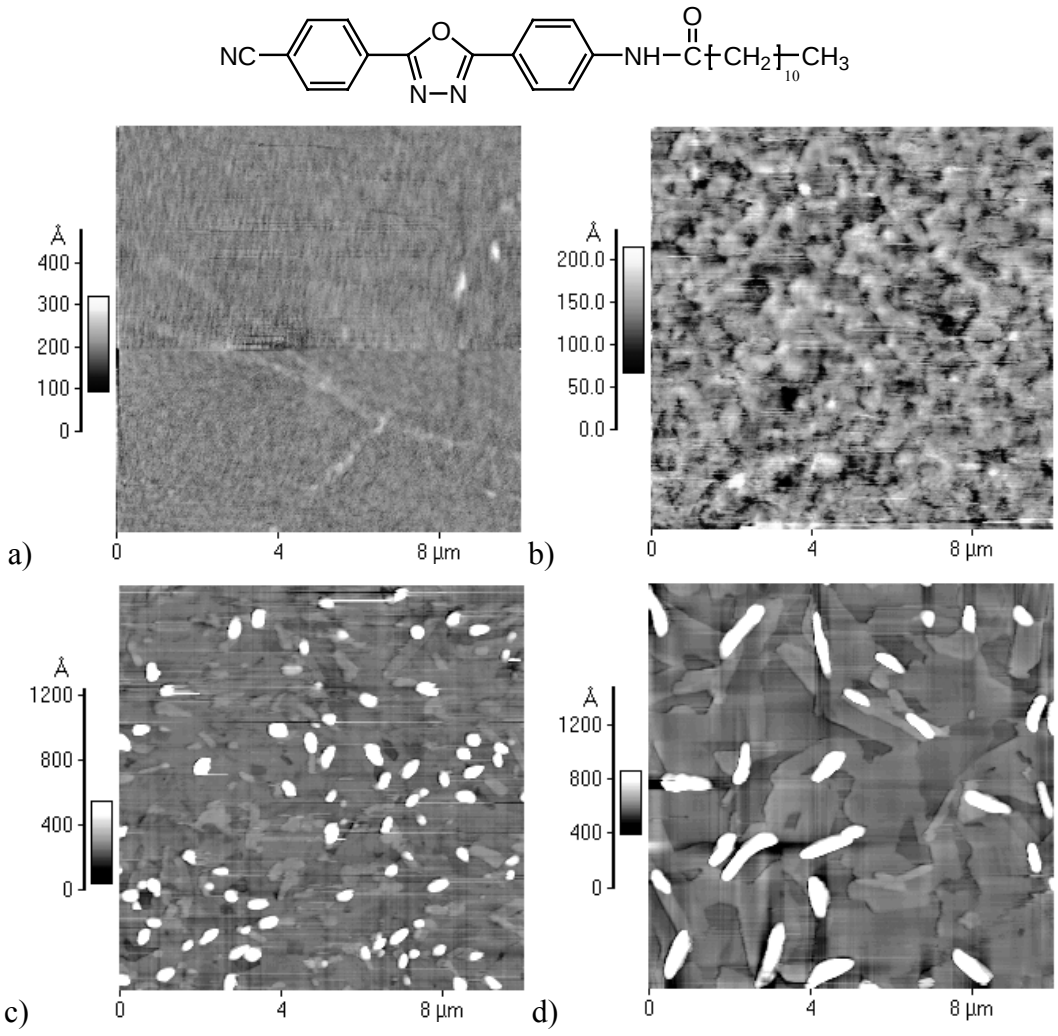

Fig. 5.57 AFM images of *p*CA11 films deposited on Si/SiO_2 at T_s = (a)-10°C, (b)60°C, (c)85°C and (d)100°C. The average terrace height obtained from (d) is 5.3 ± 0.5 nm.

The AFM images of *p*CA11 films show the obvious dependence of film topology an T_s (Fig. 5.57). The films with low T_s has an amorphous surface. The amorphous film structure was also proved by XSR investigation (Fig. 5.58). Besides the terrace structure, there are many crystal-like structures with relative height up to 1 μm. The film deposited at high T_s are characterized by clear terrace structures with an average height of 5.3 ± 0.5 nm, in good agreement with the film periodicity obtained from the XSR curves, which is also 5.3 ± 0.5 nm.

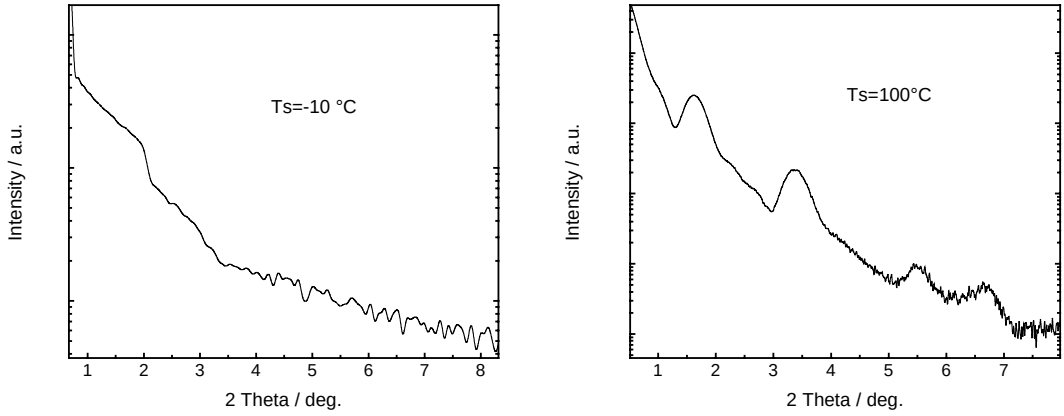

Fig. 5.58 XSR curves of *p*CA11 films deposited at T_s = -10°C and 100°C. The film periodicity for T_s = 100°C is 5.3 ± 0.1 nm.

5.3.2.2 IR investigation

The IR investigation of *p*CA11 in a solid state and in a dilute solution (CCl_4, 10^{-4} M) reveals the presence of H-bonds in the bulk material. Similar to the IR spectra of HA11, the N-H and C=O bands of the bulk material shift to a lower wavenumber region. In the spectra of the bulk substance a small shoulder still remains at 1706 cm^{-1}. This could be attributed to non H-bonded C=O groups, implying that not all molecules are connected by H-bond.

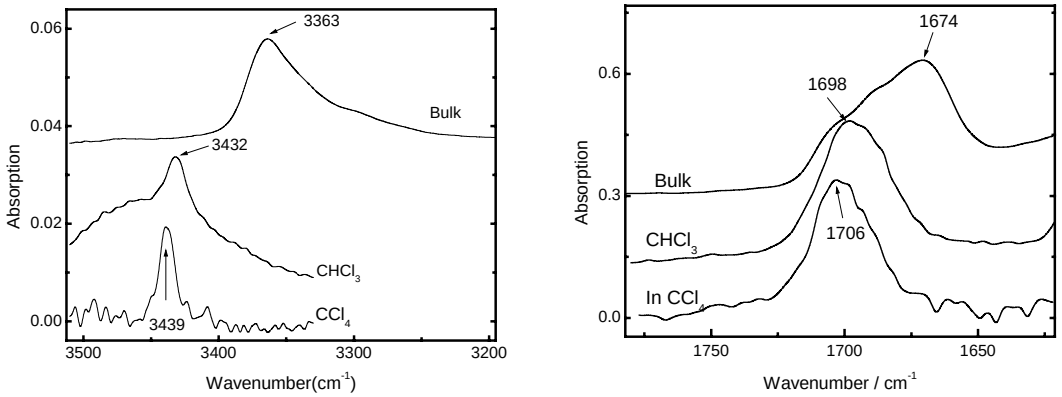

Fig. 5.59 Comparison of *p*CA11 IR spectra in bulk, $CHCl_3$ and CCl_4(10^{-4} M). The spectra in solution is magnified along Y axis for comparison.

The existence of H-bond can be further proved by analysis of ν_{NH} and $\nu_{C=O}$ in different solvents. The characteristic IR bands of *p*CA11 are summarized in Tab. 5.7. In dilute CCl_4 (10^{-4} M) solution, in which no H-bond building possibility exists, ν_{NH} and $\nu_{C=O}$ have shifts of 72 cm^{-1} and 37 cm^{-1}, respectively. These values reduced to 64 cm^{-1} and 22 cm^{-1}, respectively, when *p*CA11 was dissolved in Chloroform ($CHCl_3$), in which the building of H-bond between *p*CA11 and solvent is possible.

Tab. 5.7 Comparison of *p*CA11 IR band in different states. The band denoted with an asterisk appears as a small shoulder.

IR band (cm^{-1})	CCl_4 (10^{-4}M)	$CHCl_3$ (10^{-4}M)	Bulk	Film T_s=-10°C	Film T_s=110°C
ν_{NH}	3439	3432	3367	3362,3342	3368,3315
$\nu_{C=O}$	1711	1698	1706*, 1674	1708,1693	1693,1668
$\nu_{H\text{-}N\text{-}C}$	NA	NA	1522	1527	1525

The formation of H-bond in thin films is somewhat complicated. Both the ν_{NH} and $\nu_{C=O}$ appear as double bands in the IR spectra. The films deposited at higher T_s have ν_{NH} and $\nu_{C=O}$ with relatively lower wavenumbers with respect to films deposited at lower T_s, implying the H-bond in the film deposited at higher T_s is relatively stronger than in the film deposited at lower T_s.

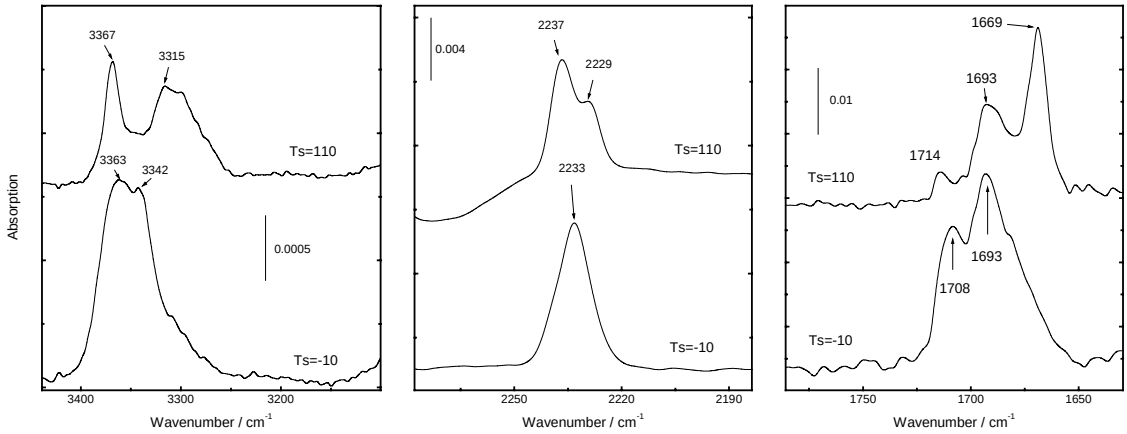

Fig. 5.60 Comparison of ν_{NH} (left), ν_{CN} (middle) and $\nu_{C=O}$ (right) of *p*CA11 films of T_s = -10°C and 110°C.

The ν_{CN} of films deposited at T_s = 110°C appears at 2237 cm^{-1} with an obvious shoulder at 2229 cm^{-1}, while the corresponding band for T_s = -10°C is a single band at 2233 cm^{-1}. The CN band position is influenced by the electron density on the CN group. Higher electron density result in lower wavenumber of CN band [146]. The split of CN band hints, like in the film of *p*CEt16 (See §5.2.2, page 54), the coexistence of two kinds of environments for the CN group.

The N-H and C=O bands are split for higher T_s and the extent of the split is bigger than

that for low T_s. These facts indicate that there are two kinds of H-bonds in the film with higher T_s, one is tight H-bonded while another is relatively loose. The CN-CN interaction also exists in the film.

Temperature dependent IR measurements on the *p*CA11 film were carried out to get an insight into the film structure. When the film was heated above 192°C, i.e. a phase transformation temperature just below the melting point (196°C), an obvious change occurs (Fig. 5.61).

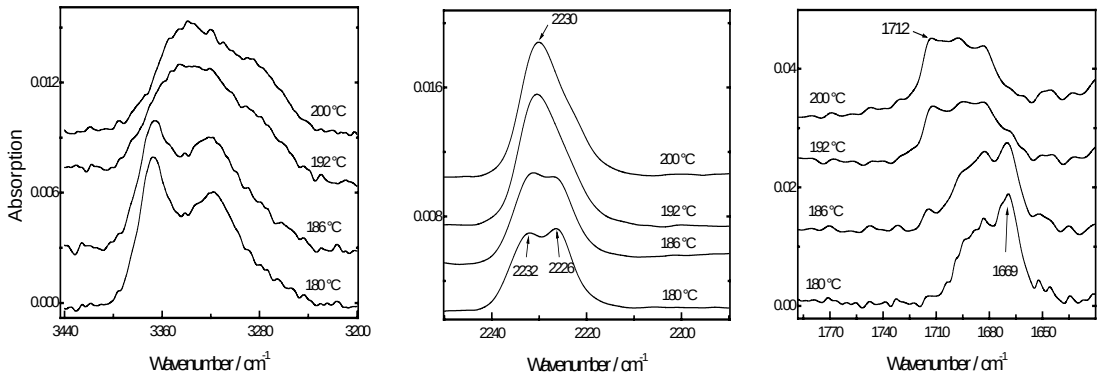

Fig. 5.61 Temperature dependent RAIRS spectra of *p*CA11 film with T_s = 110°C. Only the band for V_{NH}, V_{CN} and $V_{C=O}$ are shown here. The curves are shifted for clarity.

The splitting of the NH and CN band disappeared and the NH band became a broad band around 3338 cm^{-1} and the two band at 2232 an 2225 cm^{-1}, which build up the CN band below 186°C, joined together at 2230 cm^{-1}. Meanwhile the C=O band shifted to higher wavenumber and appears as a broad band. All these changes make the spectra quite similar to the spectra of films deposited at low T_s (Fig. 5.60) and the film structure tends to be uniform after annealing above the melting point. In the AFM images of the annealed film the number of crystalline structures is greatly reduced. The XSR investigation of annealed film reveals a film structure nearly identical to the film deposited at T_s =100°C.

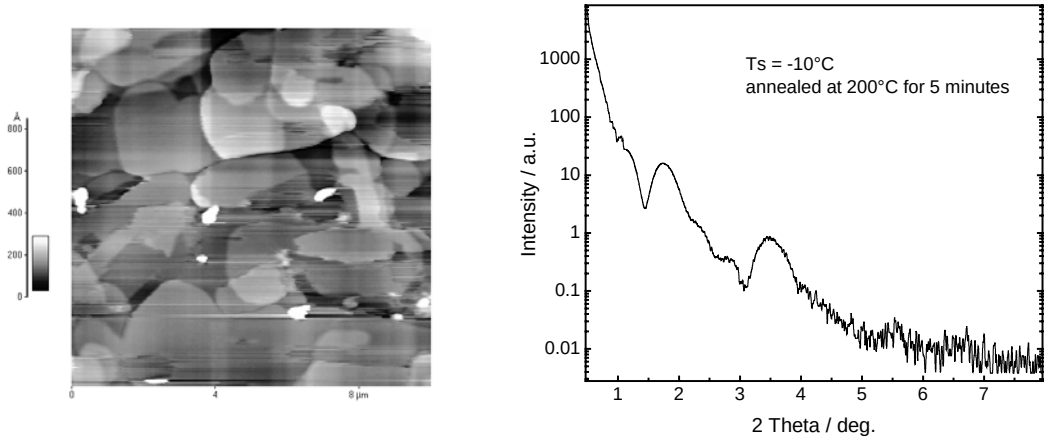

Fig. 5.62 AFM and XSR investigation of film with low T_s after annealed over 200°C for 5 min. The film periodicity obtained from XSR investigation is 5.1 ± 0.1 nm.

The change of film structure in the annealing is irreversible. After cooling down to room temperature, the IR spectra remains unchanged with respect to that at 200°C.

In comparison with *p*CEt16, whose film structure is discussed in §5.2.2, *p*CA11 has H-bonds formed between molecules. The intermolecular H-bond make the film formation behaviour of *p*CA11 more complicated than *p*CEt16. *p*CA11 can form layered films only at relatively high T_s, while *p*CEt16 can form layered films even at T_s = -10°C, the T_s influences only the topologies of *p*CEt16 films. Like in *p*CEt16 film, the CN-CN interaction still exists in the films of *p*CA11, but due to the existence of intermolecular H-bond, the CN-CN interaction becomes more stable. In the case of *p*CEt16, the CN-CN interaction is destroyed as the film is heated over 82°C, which is still far below the melting point of the *p*CEt16. But for *p*CA11, the change of CN-CN interaction occurs only when the film is heated nearly to the melting point (196°C) of *p*CA11.

5.3.3 2-(4-Nitrophenyl)-5-(4-dodecanoylaminophenyl)-1,3,4-oxadiazole (NIA11)

The morphology of VD film based on NIA11 has been studied by Freydank [18] and Reiche et al. [63]. The results are similar to other oxadiazoles discussed in this part. The films deposited at relatively low T_s have an amorphous structure, while those grown at high T_s have layered film structures. The film periodicity was obtained to be 3.4 ± 0.1 nm, which is also longer than the calculated length of molecule (2.87 nm) in extended conformation. The H-bonds were also shown to exist in the film by means of IR investigation and were regarded as the stabilizing factor of film.

Reiche et al. obtained a model of the supramolecular arrangement of the NIA11 molecules by molecular mechanics simulations (Fig. 5.63) [18, 63, 64, 148].

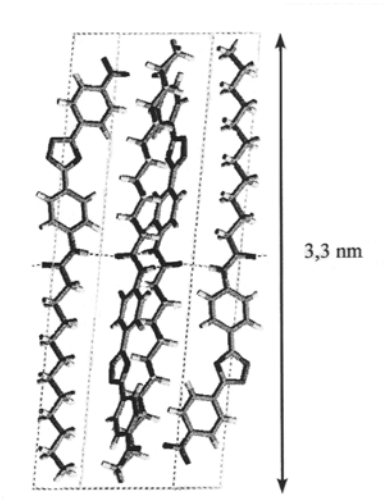

Fig. 5.63 Simulated arrangement of NIA11 molecules in the VD film [64, 148].

This model structure is in good agreement with the experimental data and consists of

layers of NIA11 built up by molecules with alternating orientation with respect to the normal direction of the film. This arrangement allows the formation of hydrogen bonds between the amide groups in the centre of the molecules.

Other oxadiazole compounds with amide structures form amorphous films at low T_s and such amorphous films could be converted to layered films by annealing them over a certain temperature. Furthermore, the resulting films have the same film periodicities as those deposited at high T_s. In a similar study, films of NIA11 prepared at low T_s, which have an amorphous structure, were annealed to see if a layered film could be obtained.

Fig. 5.64 shows the results of XSR investigations of the NIA11 films. The film deposited at 25°C have an almost amorphous structure with only a very weak peak corresponding to a film periodicity of 3.8 nm appearing (Fig. 5.64 a). After annealing by 130°C for 10 minutes, very clear Bragg peaks appear in the XSR curve (Fig. 5.64 b). The film periodicity calculated according to the Bragg peaks is 4.6 ± 0.1 nm, considerably higher than that for film deposited at T_s = 85°C, which is 3.5 ± 0.1 nm (Fig. 5.64 c).

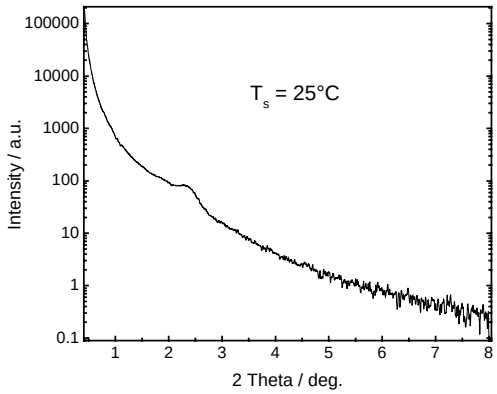

a)

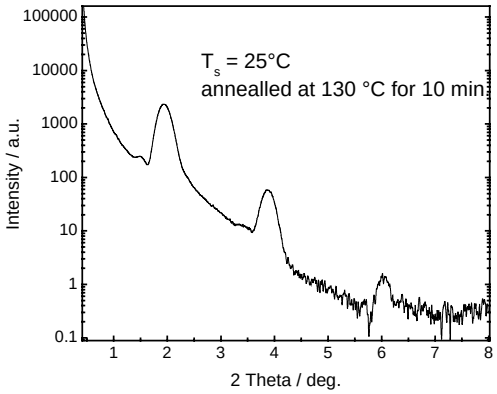

b)

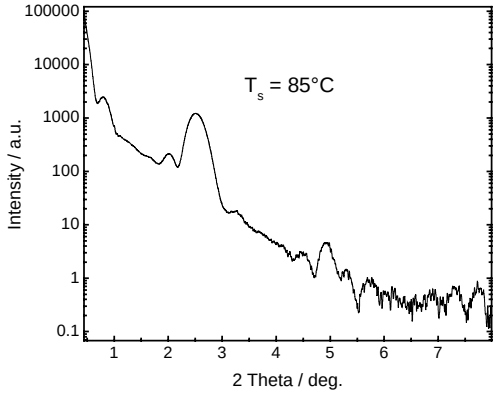

c)

Fig. 5.64 Temperature influence on the film structure of NIA11. a) film prepared at T_s = 25°C and b) after annealing by 130°C. c) The film prepared at T_s = 85°C. The film periodicities for b) and c) are 4.6 ± 0.1 nm and 3.5 ± 0.1 nm.

Reiche [64] and Freydank [18] have studied the influence of temperature on the structure

of a Y-type Langmuir-Blodgett (LB) film of NIA11 consisting of 18 monolayers. The results show that the film can undergo structural transitions while being annealed up to 100°C and 140°C. The original film periodicity of the LB film 5.68 nm at room temperature was reduced to 3.2 nm when the temperature reached 100°C. The evaporation of water in the LB film is regarded to be responsible for this transition. A second transition occurs at about 140°C, in which the film periodicity increased to 4.5 nm.

A model of the structure based on the experimental data and on molecular mechanics simulations was given (Fig. 5.65). In this model the monolayer consists of bilayers of NIA11 interdigitated in the alkyl chain region [64]. Compared with the structure shown in Fig. 5.63, the aromatic and aliphatic regions are separated after being annealed at high temperature (c.a. 140°C). This phase separation is regard to have caused this structure [64]. The intermolecular H-bond was expected to still exist and stabilize the film as it was annealed slightly above 140°C.

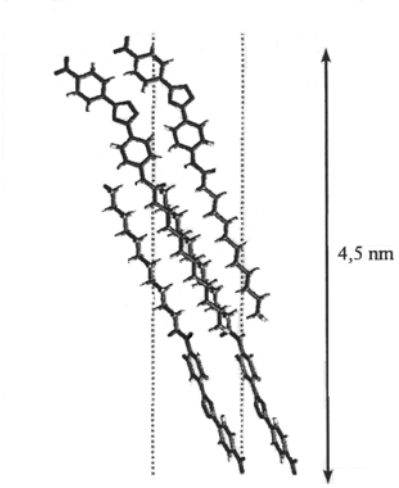

Fig. 5.65 Rough model of the structures resulting from the annealing of LB film of NIA11.

A temperature dependent RAIRS investigation was carried out to monitor possible changes in the interactions between functional groups. The results are illustrated in Fig. 5.66.

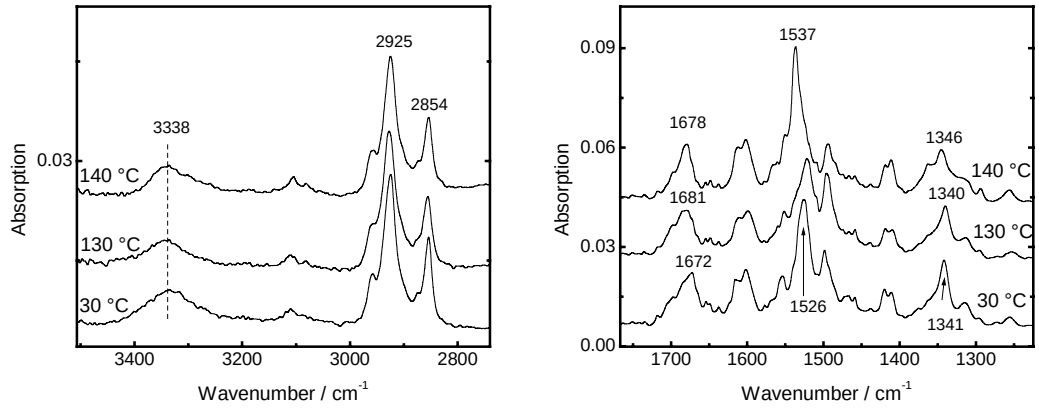

Fig. 5.66 RAIRS spectra of NIA11 film deposited at 25°C. The spectra were scanned at 30, 130 and 140°C.

The characteristic bands for the amide group at 3338 (ν_{NH}) and 1672 cm^{-1} ($\nu_{C=O}$, amide I)

did not undergo obvious changes from 30°C to 210°C. The change of $\nu_{C=O}$ band position is quite small (c.a. 6 cm^{-1}) compared with the corresponding shift of other materials discussed in this section. Furthermore, the $\nu_{C=O}$ band remains stable until 210°C, therefore this shift could not be regarded as evidence of H-bond destruction and indicates that the H-bond remains unchanged during the annealing up to 210°C. This also supports the assumption proposed by Reiche et al. [64].

In contrast to the amide bands, the bands of the nitro group have undergone an obvious shift between 130°C and 140°C. The symmetrical and asymmetrical bands of the nitro group are located at 1526 cm^{-1} and 1341 cm^{-1} at 30°C, respectively, and shifted to 1537 cm^{-1} and 1345 cm^{-1}, respectively. The nitro bands of films deposited at 85°C appear at similar positions to the annealed film. The presence of these shifts indicates that the nitro group environments has changed between 130°C and 140°C.

It is worth comparing the study of the NIA11 and NIEt12 films. Both substances differ in the bridge groups. NIA11 has amide group and has therefore intermolecular H-bonds while NIEt12 does not have. The film periodicity for different T_s and after annealing is listed in Tab. 5.8:

Tab. 5.8 The comparison of film periodicities for NIEt12 and NIA11 films.

T_s (°C)	Film Periodicity (nm)	
	NIEt12	NIA11
20(NIEt12), 25(NIA11)	3.0, 4.0	Amorphous
85	4.0	3.5
Annealed over 130°C	4.0	4.6

For both substances, the film structures resulting from deposition at low T_s are different with those found at high T_s. NIEt12 films grown at low T_s are layered and have film periodicities of 3.0 nm and 4.0 nm, while the corresponding NIA11 film is amorphous. After annealing over 130°C, structural changes occurred in both films. For the NIEt12 film, only the film periodicity of 4.0 nm remains, while a film periodicity of 4.6 nm appeared in the NIA11 film. IR investigations revealed that there is a difference in the nitro group environment above and below 130°C for both films, but the H-bond in NIA11 film is not destroyed by annealing.

In the case of NIEt12, the film periodicity resulting from annealing is the same as that of the film deposited at high T_s, while for NIA11 the resulting film periodicity is considerably higher than that of the film deposited at high T_s. Annealing of NIA11 LB film has similar results [18, 148]. It can therefore be concluded that the NIEt12 film structure formed at high T_s is a thermodynamically stable structure, but the corresponding NIA11 film is not. The change of film structure is likely caused by a change in the nitro-nitro interactions during annealing. The H-bond in the NIA11 film provides an extra energy barrier to the molecule movement, so the film prepared at low T_s is amorphous and even the film with high T_s is not in a thermodynamically stable state.

5.3.4 2,5-Bis(4-dodecanoylaminophenyl)-1,3,4-oxadiazole (11AA11)

5.3.4.1 Film structure of 11AA11

The AFM images of 11AA11 films deposited at T_s ranging from 30 to 175°C is illustrated and discussed in §4.4.2 (Fig. 4.8, page 36). In this section more results of XSR investigation are given.

In the XSR curve for T_s = 30°C, a very weak peak corresponding to a film periodicity of 3.9 ± 0.1 nm could be found (Fig. 5.67). Compared with the peak intensity for films deposited at 85°C, the peak intensity is negligible and the film is nearly amorphous. Up to T_s of 85°C, an obvious peak corresponding to a film periodicity of 3.9 ± 0.1 nm appears in the XSR curve. Taking into account that the film thicknesses are controlled to be same for all the films, the strong Bragg peak intensity provides evidence for improved structural ordering in the films deposited at higher T_s.

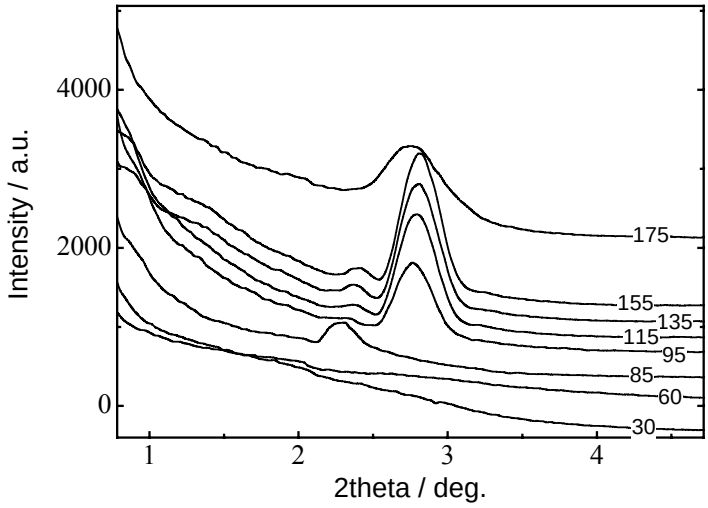

Fig. 5.67 The XSR results of 11AA11 films deposited at T_s from 30°C to 175°C. Curves were shifted along Y axis for clarity. The film periodicities for film deposited below 85°C and above 95°C are 3.9 ± 0.1 nm and 3.2 ± 0.1 nm, respectively.

Peaks in the XSR curve corresponding to film periodicities of 3.2 ± 0.1 nm are observed for all films deposited at 95°C or above, taking into account the simulated molecule length (3.15 nm), it can be concluded that the films have monolayered structure. The film thicknesses obtained from XSR for all films are within 31 ± 2 nm, but the intensities of the Bragg peaks for film prepared at 95°C and above are much higher than those for T_s < 85°C, indicating that the films deposited at T_s > 95°C are better ordered.

The film deposited at 85°C have a larger film periodicity than those grown at 95°C or above. The structure of the former can be converted to that of the latter by simply annealing the film to 130°C, which will be discussed later in this section.

5.3.4.2 IR investigation and structural transformation in the thermal treatment

11AA11 has a chemical structure analogous to HA11, but is symmetrically substituted by two alkyl chains over an amide groups on the phenyl rings. From a chemical point of view, a 11AA11 molecule can form more H-bonds with its adjacent molecules than HA11 can. The existence of intermolecular H-bonds can be proven by comparing the IR spectra of 11AA11 in solid state and in dilute solutions (CCl_4, $CHCl_3$ 10^{-4} M) solution. The N-H and C=O stretching bands are shown in Fig. 5.68.

From Fig. 5.68 the shift of N-H and C=O stretching bands can be clearly seen. The N-H band for 11AA11 in dilute CCl_4 solution appears as two peaks at 3536 cm^{-1} and 3418 cm^{-1}, while in chloroform the same vibration appears at 3434 cm^{-1}. In the spectra of the bulk material the N-H bands are found at 3335 cm^{-1} and 3301 cm^{-1}. The C=O stretching appears for dilute CCl_4 solution at 1705 cm^{-1} with a broad shoulder at higher wavenumber side, at 1696 cm^{-1} for dilute chloroform solution and at 1710 cm^{-1} and 1676 cm^{-1} for bulk materials. The continued red shift of the N-H and C=O stretching band from CCl_4 solution to bulk materials can be explained by the formation of intermolecular H-bonds.

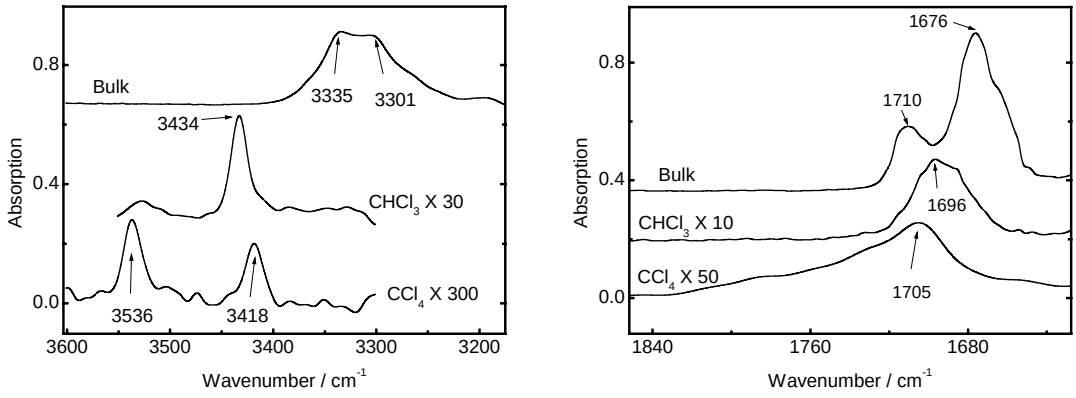

Fig. 5.68 Comparison of 11AA11 NH (left) and C=O (right) IR stretching bands as bulk, in $CHCl_3$ (10^{-4} M) and in CCl_4(10^{-4} M). The spectra for $CHCl_3$ and CCl_4 solution are enlarged by the parameters shown in figure for comparison.

It worth to note that the N-H and C=O band appear as two bands in the bulk and one of the C=O bands even peaks at 1710 cm^{-1}, comparable to the peak in CCl_4 solution. Such a splitting of the bands indicates, similarly to HA11, that two kinds of intermolecular H-bonds exist for 11AA11. The H-bonds may even exist in the dilute CCl_4 solution, because two N-H bands and a broad shoulder at the higher wavenumber side of C=O band can be found. Surprisingly, this phenomenon does not appear when 11AA11 is solved in chloroform.

For the deposited films, the RAIRS spectra clearly reveals the difference in the H-bonding states in the films grown at different T_s (Fig. 5.69). The N-H and C=O bands of films with T_s = 25°C are sharp single peaks at 3304 cm^{-1} and 1661 cm^{-1}, respectively. The low bands position and form illustrates that all the amide groups are H-bonded, almost no free NH or

C=O groups remains in the film. In contrast to that, the film with T_s = 155°C has N-H band at 3335 cm^{-1} and 3299 cm^{-1} and C=O band at 1718 cm^{-1} and 1673 cm^{-1}. Both of them have two peaks in the IR spectra, quite similar to the spectra of bulk materials, indicating that the formation of H-bonds is not complete in the film grown at high T_s.

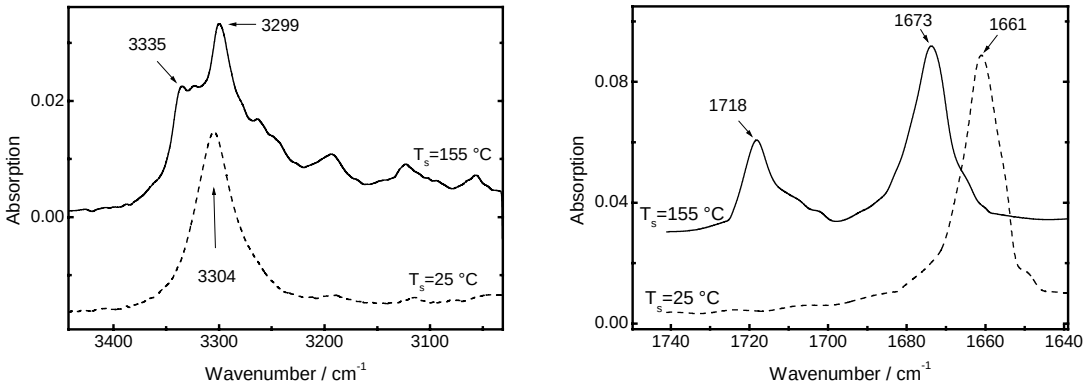

Fig. 5.69 Comparison of RAIRS spectra of 11A11 deposited at T_s = 25°C (dash line) and 100°C (solid line).

The IR investigations reveal that in the film deposited at low T_s nearly all C=O groups are H-bonded. The high density of H-bond forms a high energy barrier to molecular movement on the substrate, thus the film deposited at low T_s has an almost amorphous film structure and a topography typical for amorphous film. On the other hand at high T_s not all C=O groups form H-bonds with NH group and the thermal movement of the molecules is more severe than at low T_s. The molecules can therefore overcome the energy barrier induced by the H-bond formation and arrange themselves in an ordered, thermodynamically stable structure.

If the formation of intermolecular H-bonds thwarts the movement of molecules during deposition and the subsequent formation of layered film structures, then the molecules may undergo reorganization and cause the change of film structure, when the film is thermally treated over a certain temperature. To investigated this films deposited at low T_s were heated and the film structure was studied by means of XSR, AFM and IR.

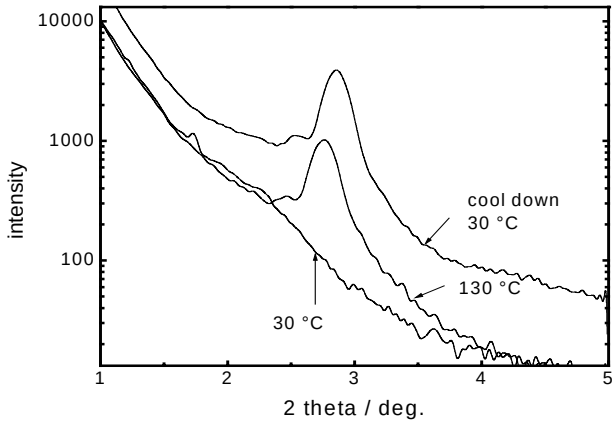

Fig. 5.70 XSR curves of 11bAA11 film deposited on Si/SiO_2 at T_s = 25°C. The XSR measurement is done at 30°C, 130°C, afterwards cool down to 30°C and measured again.

The XSR results are shown in Fig. 5.70. The film was deposited on a Si/SiO_2 substrate with T_s = 25°C. The XSR curve shows that the film is amorphous before being heated and no peaks in the curve can be found. In contrast the XSR reveals a layered film structure after the film is annealed at 130°C. A obvious peak corresponding to film periodicity of 3.2 ± 0.1 nm appeared in the XSR curve. After the film is cooled down to room temperature, the peak remains and the film periodicity decreases slightly to 3.1 ± 0.1 nm, exactly the value for the film deposited at T_s = 155°C. The XSR results reveal that a thermally induced film structure transformation has occured. The film deposited at low T_s has an almost amorphous structure, which can be converted to layered structure by annealing to over 120°C and this process is irreversible.

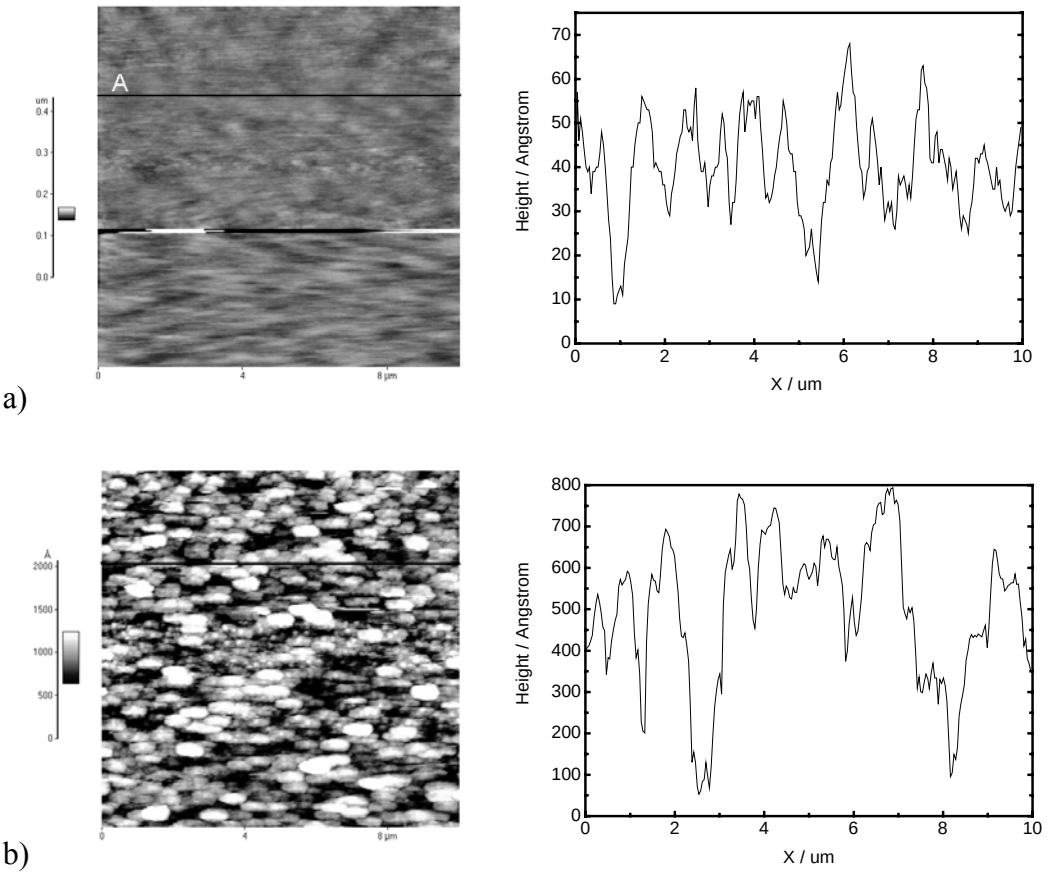

Fig. 5.71 AFM images of 11AA11 film deposited at T_s = 25°C, 30 nm thick. (a) before and (b) after annealing at 160°C for 5 min. The height profile along the black lines in the images are shown right of the corresponding image. The RMS for the film before and after annealing is 2 nm and 17 nm, respectively.

The film topography is also changed by the structural transformation (Fig. 5.71). After thermal treatment the film surface became more rougher with the RMS roughness before and after thermal treatment measured at 2 nm and 17 nm, respectively. The change in surface roughness could be caused by the formation of domain structures. Although the XSR investigation shows ordered film structure after thermal treatment above 120°C, no terrace structure with a height around 3.1 nm can be found in the AFM images, even after the film is further annealed at 160°C for three days. In contrast to that, the surface of films deposited with T_s = 155°C have a clear terrace structure (Fig. 4.8, page 36). Different

mechanisms of film structure formation should be responsible for this difference. In the deposition process the molecules can migrate after they are absorbed on the substrate or film and finally incorporate themselves into the lattice of the already grown layer, while in the case of annealing the migration of molecules must overcome the restriction of neighbouring molecules. The film structure formed during the deposition is therefore more prefect than that obtained by annealing an initially disordered film.

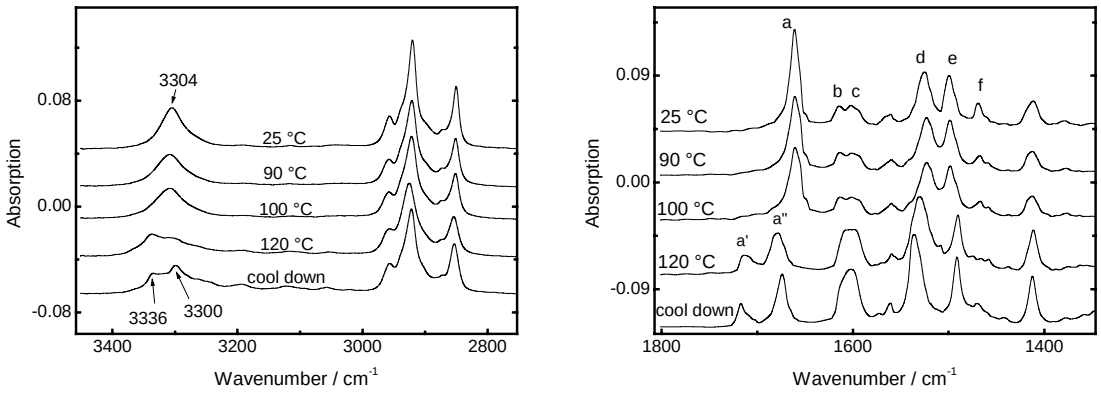

Fig. 5.72 Temperature dependent RAIRS spectra of 11AA11 film deposited at T_s = 25°C. The band in the right figure are : a), a'), a") $\nu_{C=O}$ carbonyl stretching, b) $\nu_{C=N}$ oxadiazole ring, c) ν_{CC} phenyl ring stretching, d) $\nu_{C-N} + \delta_{C-N-H}$, e) phenyl ring stretching, f) δ_{CH2}

Fig. 5.72 demonstrates the influence of temperature on the RAIRS spectra of 11AA11 film. The film was deposited on Si/SiO_2 at 25°C. IR spectra show a complete formation of H-bonds in the film. The NH and C=O bands are sharp single peaks located at low wavenumber region. Obvious changes in IR spectra occurred when the film was heated above 100°C, particularly between 110°C and 120°C (Fig. 5.72). The characteristic amide bands are also summarized in Tab. 5.9.

Tab. 5.9 The change of characteristic amide bands during annealing. The band denoted with an astrisk is higher than another in the same colume.

IR band (cm^{-1})	ν_{N-H}	ν_{C-O}	Amide II
110°C	3304	1660	1522
120°C	3336*, 3300	1713, 1679	1530
30°C (cooled down)	3336, 3300*	1717, 1674	1536

The NH band splits into two band at 3300 cm^{-1} and 3336 cm^{-1}, the position of the first peak is higher than the original NH band. After the film is cooled down to room temperature, the intensity of the peak at 3300 cm^{-1} became higher than 3336 cm^{-1}, the position and the relative intensity is exactly the feature of IR spectra for film deposited at

high T_s. The C=O band (peak a in Fig. 5.72 right) split into two peaks at 1711 cm^{-1} and 1678 cm^{-1} (peak a' and a" in Fig. 5.72 right), both peaks shifted to higher wavenumber during the heating process. The blue shift and splitting of the NH and C=O bands in the heating process reflects the partial dissociation of the N-H···O=C H-bonds and the decrease of strength of the remaining H-bonds in the film.

Although the dissociation of the H-bond could be confirmed, the change in the amide II band position could not be solely explained by the dissociation of the H-bond. Usually the formation of a N-H···O=C H-bond will result in a blue shift of the amide II band [135, 162-166], but the amide II band at 1525 cm^{-1} (peak d in Fig. 5.72 right) shifts to 1537 cm^{-1} during the heating process. Because a band corresponding to free C=O bond appears at 1712 cm^{-1}, but a new NH band appears at 3300 cm^{-1}, which is lower than the NH band position before thermal treatment, so it is very likely that the H atom in NH bond form H-bond with the atom other than O in carbonyl bond. In the 11AA11 molecule the only candidate for such interaction formation is the N and O atoms in oxadiazole ring. The change in the C=N stretching band (peak b in Fig. 5.72 right) of the oxadiazole ring [167] may reflect the formation of such a H-bond. However, due to the lack of further information, the existence of such a H-bond can not be confirmed.

The study of the 11AA11 VD film reveals that, like other amide substituted oxadiazole compounds discussed in this chapter, films with layered structure can only be obtained by deposition at high T_s. The H-bond formation shows a correlation with T_s as well as film structure. Nearly all the NH are H-bonded with C=O in the films grown at low T_s, while free C=O bonds exist in film grown at high T_s. Moreover, the strength of the H-bond for films grown at low T_s is also higher than that seen in films grown at high T_s. The amphorous film deposited at low T_s could be converted to a layered film by annealing over 120°C.

5.3.4.3 An analogous oxadiazole without amide groups

To further investigate the influence of the H-bond on the film formation, an analogous substance to 11AA11, 11EsEs11, whose chemical structure shown in Fig. 5.73, was studied. The VD films of 11EsEs11 were deposited on Si/SiO_2 at T_s ranging from 30 to 110°C. The film topography shows an obvious dependence on T_s. The films prepared at T_s = 30°C show a granular surface structure (Fig. 5.73 a), while the surface of films grown at T_s = 70°C is characterized by a clear terrace structure (Fig. 5.73 b). The terrace height was measured to be 3.6 ± 0.5 nm.

Unlike 11AA11, which shows amorphous film growth at low T_s and layered growth at high T_s, 12EsEs12 can form layered films on Si/SiO_2 even at room temperature. Although AFM investigations showed a granular surface for the 12EsEs12 film, XSR investigation reveal a layered structure for films prepared at T_s = 30°C as well as at 70°C (Fig. 5.74). The film periodicities obtained from XSR for both films are the same, namely 3.2 ± 0.1 nm.

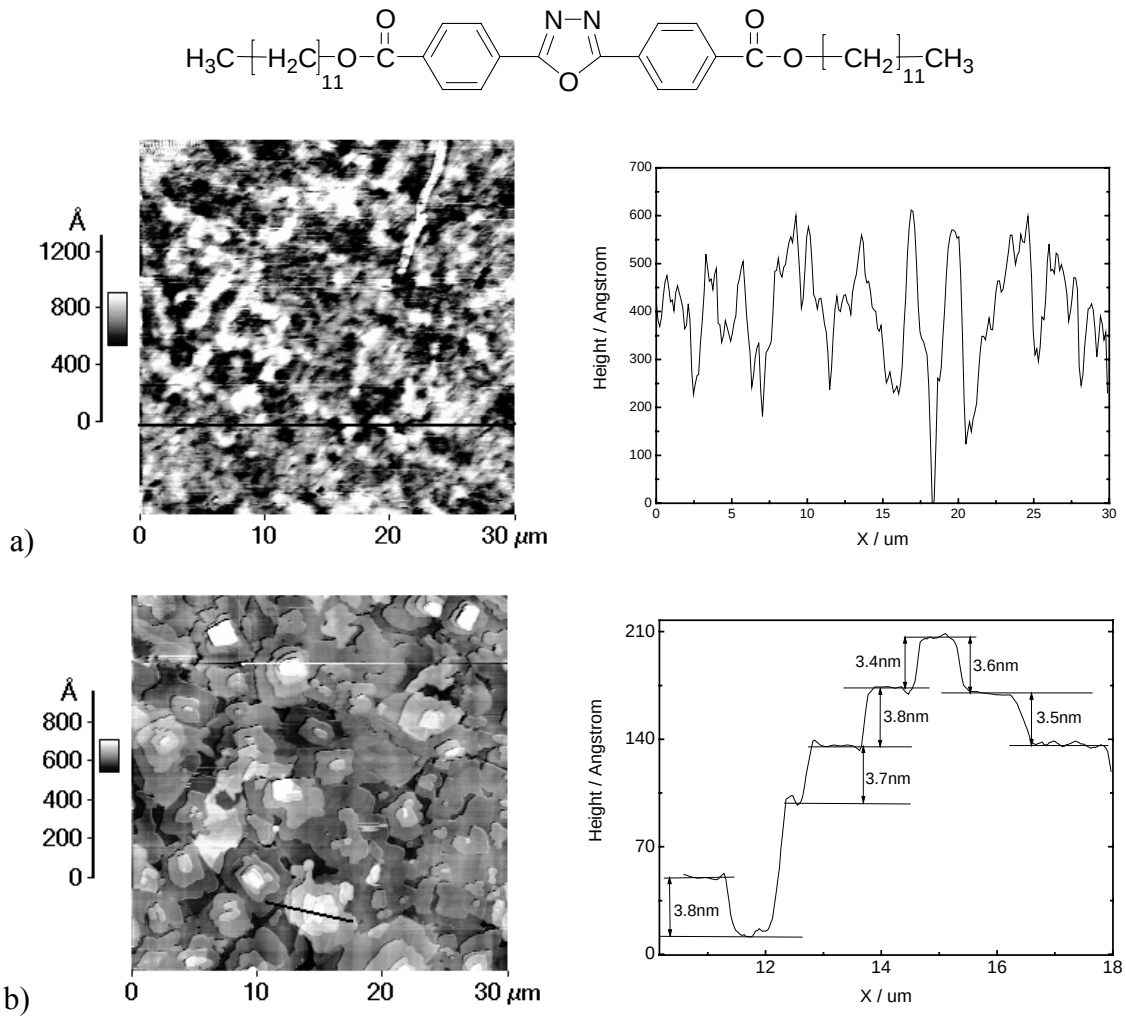

Fig. 5.73 AFM images of 12EsEs12 films deposited at T_s = 30°C (a) and 70°C (b). The terrace height of film in (b) are measured to be 3.6 ± 0.5 nm.

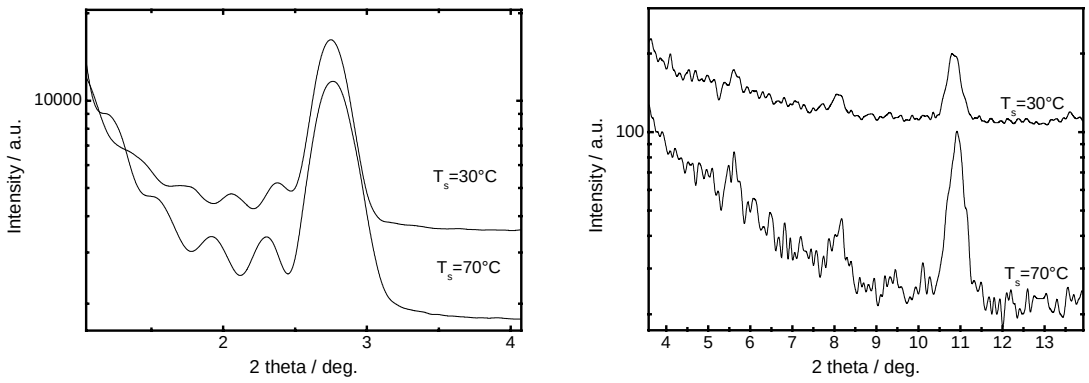

Fig. 5.74 XSR curves of 12EsEs12 film deposited on Si/SiO_2 with T_s = 30°C and 70°C. The film periodicities of both films obtained from XSR are 3.2 ± 0.1 nm.

IR investigations of 12EsEs12 were also performed to find if H-bonds exist between the molecules. The characteristic bands for the ester group is the carbonyl stretching band

($\nu_{c=o}$) and the band involving interacting C-C, C-O and O-C bonds, for simplicity, it is called the stretching band of the C-O ($\nu_{c=o}$) next to C=O. For 12EsEs12 solid state, $\nu_{c=o}$ and ν_{c-o} appear at 1719 cm^{-1} and 1278 cm^{-1}, respectively. The comparison of the ester characteristic bands for 12EsEs12 in dilute CCl_4 solution and solid state (KBr disk) is shown in Fig. 5.75.

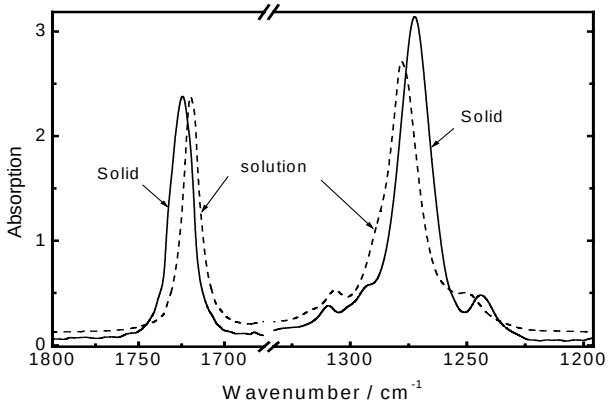

Fig. 5.75 Comparison of ester characteristic bands for 12EsEs12 in dilute CCl_4 solution (10^{-3} M) (dash line) and solid state (solid line). The band difference for $\nu_{c=o}$ and ν_{c-o} are 4 and 6 cm^{-1} , respectively.

The $\nu_{c=o}$ and ν_{c-o} band positions are slightly different in solution and solid state. The $\nu_{c=o}$ band in solution is 4 cm^{-1} lower than in solid, whilst the ν_{c-o} band is 6 cm^{-1} higher. It is likely that there is no interactions between the ester groups, because the shifts of the corresponding bands are quite small. To further confirm this temperature dependent RAIRS investigations were carried out. The result spectra are shown in Fig. 5.76. The $\nu_{c=o}$ is not influenced by the temperature and its position remains unchanged up to 150°C, which is the melting point for 12EsEs12. The ν_{c-o} shifts slightly to a lower wavenumber region, but the shift is only 4 cm^{-1}. Combining the results of the IR investigation for solution, solid state and VD film, it can be concluded that there is no intermolecular interaction caused by the ester group in 12EsEs12.

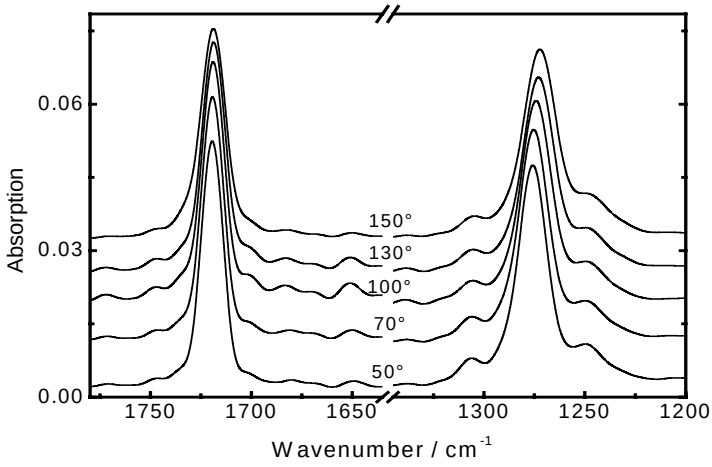

Fig. 5.76 Temperature dependent RAIRS investigation of 12EsEs12 film deposited at T_s = 25°C. Only the characteristic bands for ester group are shown here. The curves are shifted for clarity.

Both 11AA11 and 12EsEs12 are oxadiazole compounds with a symmetrically substituted alkyl chain. Though the chains in the 12EsEs12 molecules are one methylene unit longer than that in 11AA11, no large difference in film formation behaviour could be attributed to this difference (See §5.1). Another structural difference between the two substance is their bridge groups. The 11AA11 has an amide as a bridge group, while 12EsEs12 has an ester as a bridge group. In the IR study discussed in this chapter, H-bond is found and the state of H-bond are influence by the T_s by film deposition as well as the environment temperature by the ex-situ thermal treatment. The temperature, at which the change in the H-bond state occurs, is the same temperature at which film structure transformation occurs. The fact that 11AA11 can form a layered film only when T_s is higher than a certain temperature while films of 12EsEs12 are always layered, can be attributed to the presence of intermolecular H-bonding for 11AA11.

5.3.5 Summary

The study of the film formation of oxadiazole compounds with an amide bridge group can be summarized as follows.

1. In the film, intermolecular H-bonds are found between the amide groups. All the substances form amorphous films at low T_s and layered films could be obtained only at high T_s.

2. The state of H-bonds in films of HA11, *p*CA11 and 11AA11 depends on the T_s, but such a dependence is not observed for NIA11. The HA11 and *p*CA11 films deposited at low T_s have a low content of H-bonds, while the films deposited at high T_s are highly H-bonded. In contrast nearly all the molecules in 11AA11 film deposited at low T_s are H-bonded, while only a part of the molecules are H-bonded in film deposited at high T_s.

3. For the substances with head groups, the film periodicity is larger than the corresponding molecule length in extended conformation. The films have therefore bilayer structures. For HA11, which has no substitute head group, and 11AA11, which is symmetrically substituted by two alkyl chains, the film periodicity is smaller than the molecule length in extended conformation. Their films have therefore single layer structure.

4. The amorphous films of *p*CA11 and 11AA11 could be converted to layered films by annealing them above certain temperature. The resulting films have the same film periodicity with those deposited at high T_s. Such structural changes are always accompanied by a change in the H-bond. Comparison with the corresponding oxadiazole compounds with ether groups, it can be concluded that the change in intermolecular H-bonds has induced the change of the film structure.

5. During the annealing of the NIA11 film, the H-bond remains stable, but the interaction between nitro groups is disassociated. At the same temperature the film has undergone structural change. The change of the NIA11 film is very likely to be caused by the disassociated of interlayer interaction between nitro groups. The resulting film has a layered structure and the film periodicity is much larger than that of the films obtained by deposition.

6. Replacing the amide groups in 11AA11 with ester groups, i.e. 12EsEs12, the T_s dependence of the film structure does not exist any longer. The films of 12EsEs12 deposited at all investigated T_s range have monolayered structure.

6 Effects of structure change on the optical properties of the VD film

Aromatic substituted 1,3,4-oxadiazoles are well known fluorescence substances widely applied in OLED development (See §2.1.2, page 7). To optimize the performance of OLEDs, it is essential to understand the influence of the chemical and physical structure of the film on its optical properties. Kaminorz [168] has systematically investigated the relationship between the chemical structure and absorption (UV) as well as the fluorescence (PL) properties of 1,3,4-oxadiazole compounds. The influence of film structure on the optical properties of oxadiazole is still not investigated, although the optical and electrical properties are believed to be strongly influenced by the film morphology [24, 26, 127, 169-171].

The optical properties of films of were investigated in this work. Among all the investigated films, the optical properties of 11AA11 films show the most obvious dependence on the film structure. For this reason 11AA11 will be taken as an example to illustrate the dependence of the optical properties on the structure of the oxadiazole films.

6.1 Absorption and PL properties of the VD films

As described in §5.3.4, the film structure of 11AA11 depends strongly on T_s. The dependence of film structure on T_s is summarized in Tab. 6.1.

Tab. 6.1 The dependence of 11AA11 film structure on the T_s.

T_s /°C	30~60	85	95~175
Film Periodicity/nm	amorphous	3.9	3.2

The UV/Vis absorption and fluorescence spectra of 11AA11 in chloroform solution and as drop-casted film (drop solution on quartz and dried up) are presented in Fig. 6.1. The peaks at 270 nm and 312 nm in the absorption spectra of the solution can be assigned to the $n\pi^*$ and the S_o-S_1 transition of the $\pi\pi^*$ delocalization in the π electron system, respectively. This assignment follows from investigations of the structural analogous diphenyl-1,3,4-oxadiazoles in solution by Popova et al. [172] and by Feygelman et al. [173]. The absorption and fluorescence spectra do not overlap each other, therefore re-absorption effects can be neglected. In the absorption as well as emission spectra, the position of the maxima of the VD film grown at T_s = 30°C is strongly red shifted with respect to that of the solution.

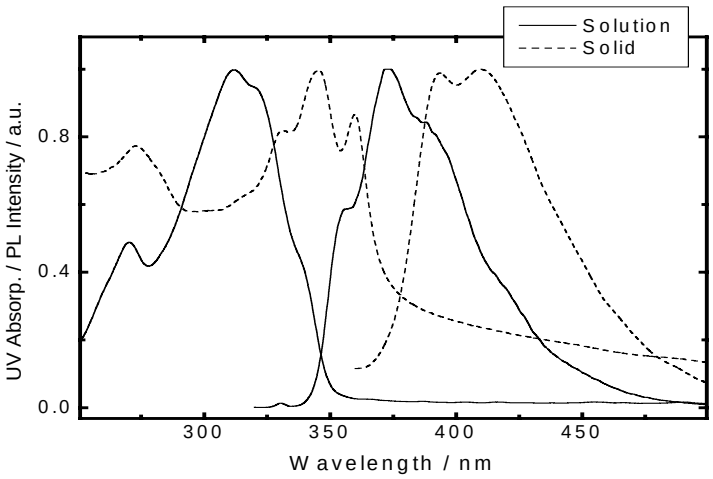

Fig. 6.1 Absorption and fluorescence spectra of 11AA11 in solution ($CHCl_3$, 10^{-5}M) and in solid state. The absorption of a drop-casted film was measured in reflection. The fluorescence of the film was measured in a front-face arrangement.

There are several explanations for the red shift. One such explanation was given at the molecular level is that the red shift is attributed to an increase of the π electron system of the molecule in the crystal compared with that in the diluted solution, in which the rings of the molecules can rotate freely around the bonds connecting them. In a solid state the three aromatic rings in the molecule adopt a nearly coplanar geometry, the wave functions of the π electrons overlap more, so the bandwidth of the delocalized S_0 and S_1 decreases, which leads to a lowering of the transition energy [174-176].

Another explanation given by Birks [177] at the supermolecular level is that the red shift of the absorption and emission spectra results partly from the influence of the surroundings as a continuum and partly from the interactions with neighbours. In most of the investigated oxadiazole crystals the molecules arrange parallel to each other (§2.1.1, page 6). The overlap of the wave functions of the neighbouring molecules are favoured in this arrangement. The increased delocalization of the electrons implies a broadening of the energy levels, which involves a decrease of the transition energy [45, 178, 179].

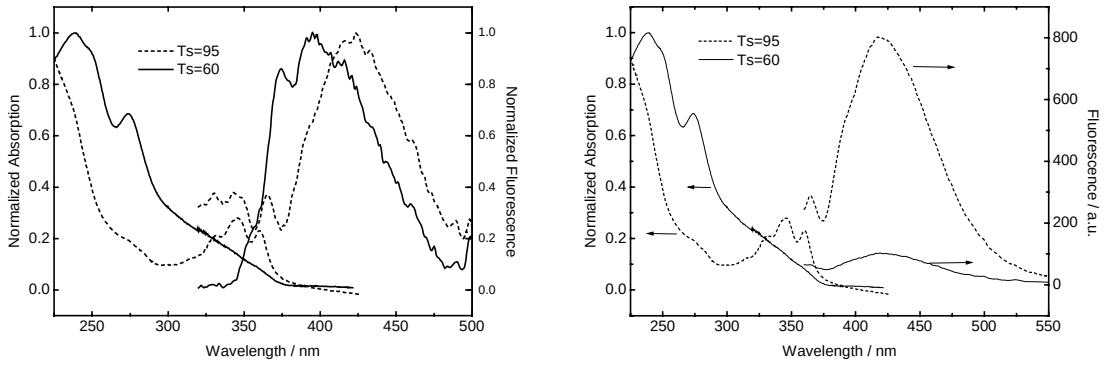

Fig. 6.2 Absorption and fluorescence spectra of 11AA11 VD films. The fluorescence spectra were excited with light of wavelength of 275 (left) and 345 nm (right).

In the case of 11AA11, the intermolecular π-π interactions is mostly likely to be

responsible for the red shift of the red shift. Because the VD films grown at low T_s are nearly amorphous and those grown at high T_s as well as drop-casted film have layered structures and the red shift was not observed for the VD films grown at low T_s. For the VD film grown at T_s = 60°C, the peak represents a ππ* transition delocalized along the molecule and is not as intense as the peak for $n\pi^*$ transition (Fig. 6.2). The former appears just as a slope around 325 nm. For the film deposited at 95°C, three peaks appeared at 330 nm, 345 nm and 360 nm, which also appear in the absorption spectra of crystal state films, indicating the formation of the π-π intermolecular interaction.

When excited by light with a wavelength of 275 nm, the maxima of the emission spectra of the film grown at T_s = 95°C have a red shift of 30 nm in relation to that of T_s = 60°C. Excited by light with wavelength of 345 nm, the film grown at T_s = 95°C luminesces much intensive than that grown at T_s = 60°C.

The obvious difference in the optical properties of the films deposited at different T_s hints that the molecular arrangements in the two films are also different, in agreement with the results obtained from XSR measurement, which showed that the film deposited at 60°C is amorphous while that at 95°C is layered (See §5.3.4.1, page 94).

6.2 The change of optical properties during the film structure transformation.

11AA11 films deposited at T_s < 85°C and T_s > 95°C exhibit different film structures. It was found that the structure of films deposited at T_s < 85°C could be converted to that seen at T_s > 95°C by simply annealing the film over 120°C (see §5.3.4.2, page95). IR investigations during the annealing revealed that the intermolecular H-bonds have undergone some changes (see §5.3.4.2). UV and PL measurements were also applied in-situ during annealing to examine if the structural transformation has any impact on the optical properties of the film.

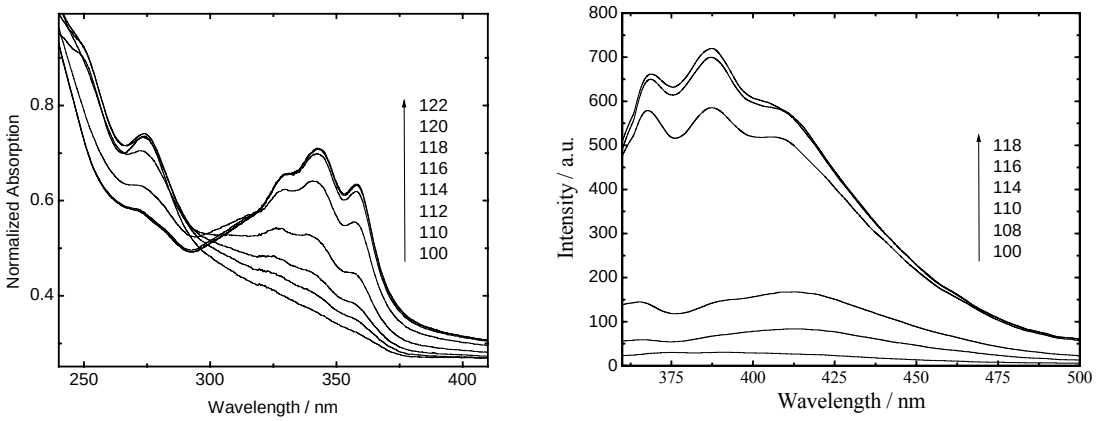

Fig. 6.3 UV (left) and PL (right) spectra of 11AA11 film with T_s = 60°C during annealing. The temperature at which the spectrum were scanned is denoted along the arrow in the corresponding figure. The excitation wavelength for PL is 345 nm.

The UV and PL spectra obtained simultaneously during annealing are shown in Fig. 6.3. The peak at 275 nm vanished during annealing and three new peaks appeared at 330 nm, 345 nm and 360 nm, when the film grown at T_s = 60°C was heated over 120°C. This is an indication of a change in the film structure, also seen by XSR investigation. The corresponding energies of peaks at 330 nm, 345 nm,and 360 nm are 3.76 eV, 3.59 eV and 3.44 eV, respectively. It is worth mentioning that this structural transformation is irreversible. After cooling to room temperature, the position of the maxima remains unchanged, although the small peaks have undergone some change in intensity.

It has been found that the temperature for structural transitions is somewhat different for film deposition and annealing. The film deposited at 95°C has an already layered film structure with film periodicity of 3.2 nm and absorbs at 345 nm, while the structural transition occurs between 110°C and 120°C by annealing a film deposited at T_s = 60°C. This difference could be explained by the different energy barriers for molecules to move in the two situations. For movement in the film a molecule must overcome the energy barrier resulting form the intermolecular interaction. For 11AA11 this energy barrier is enforced by the intermolecular H-bonds. During the film deposition, such an energy barrier is much smaller than annealing afterwards, because a molecule just arriving at the substrate does not have many neighbouring molecules and the intermolecular H-bonds are still not formed.

The study of the optical properties of 11AA11 film illustrates a strong correlation between the optical properties and the film structure. The films prepared at T_s < 85°C absorb at 275 nm and do not fluoresce when excited by light with wavelength of 345 nm. In contrast, the films grown at T_s > 95°C absorb at 345 nm and fluoresce strongly when excited by light of 345 nm. The optical properties of the former films could by converted to that of latter films by annealing over 120°C.

7 Summary and future work

7.1 Summary

In this work the correlations between the chemical structures of the 2,5-diphenyl-1,3,4-oxadiazole compounds and their corresponding VD film structures were systematically investigated for the first time. Oxadiazole compounds based on the 2,5-diphenyl-1,3,4-oxadiazole as core, substituted with a variety of head groups and alkyl chains with different lengths attached over ether, amide or ester units were synthesised (Fig. 7.1). The VD films based on these substances were prepared on Si/SiO_2 and the film topography, the film structure and possible intermolecular interactions were characterized by means of AFM, XSR and IR spectroscopy, respectively.

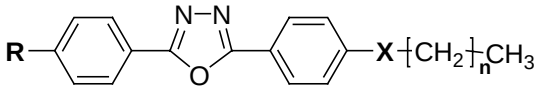

Fig. 7.1 General structure of studied oxadiazoles. R: head group; X: bridge group.

For a given molecule, the film structure could be controlled through the variation of the physical deposition parameters such as the film growth rate, the substrate temperature (T_s) and the vacuum. The study of the influence of these deposition parameters on film formation provides the possibility of controlling molecular arrangement and the subsequent physical properties of the films.

From a comparison of VD films based on 2-(4-cyanophenyl)-5-(4-hexadecyl-oxyphenyl)-1,3,4-oxadiazole (*p*CEt16) in HV and UHV, it was found that the film structures were not significantly influenced by the base vacuum and HV is adequate for the study of film morphology. The film grow rate and substrate temperature (T_s) both influence the film topology, the difference is that the effect of the latter is much more obvious than the former. The films grown at low rate and high T_s tend to have a layered structure, clear domains and terraces. The effect of T_s also depends on the chemical structure of the substance being deposited, which will be summarized later.

The influence of the length of the alkyl chain was studied with alkyloxy (*p*CE*t*n) and acylamino (*n*AA*n*) substituted oxadiazole series. It was found that an alkyl chain attached to the aromatic part of the molecule can help the layer-by-layer growth of the film. For the alkyloxy substituted molecules, the molecule with a short chain of $n = 5$ can form a layered film, while the molecule without a substituted alkyl chain formed only islands on the substrate. The results also show that, for $5 \leq n \leq 16$, the film periodicity depends linearly on n, indicating that the tilt angle of the molecules in the film is not determined by the alkyl chain. According to this linearly dependence, the tilt angle of the alkyl chain was calculated to be 33°. For the *n*AA*n* series of oxadiazoles, which have intermolecular H-bonds formed in the film, the linear dependence of film periodicity on the length of the

substituted alkyl chain does not exist for $7 \leq n \leq 17$. A possible reason is the strong intermolecular interactions induced by H-bonds, which dominate when the alkyl chain is short enough and result in a different molecular arrangement in comparison with those of long alkyl chains. The film periodicity therefore does not depend linearly on the chain length.

The influence of head groups on film formation was studied using oxadiazole derivatives with ether bridge groups. Most of the investigated oxadiazole compounds can form layered films within the whole investigated T_s region (-10°C to 100°C, depends on molecules) with T_s only influencing the topologies of the deposited films. Films prepared at relatively low T_s (usually below 40°C) have amorphous like surfaces, while high T_s (usually above 60°C) results in films with smooth domains and clear terrace structures. The only exception is the oxadiazole without a head group (HEt16), which can only form a layered film at high T_s. The film periodicities of the studied films exceed the calculated length of the corresponding molecules, implying the films have a bilayer structure.

The intermolecular interactions between head groups such as methyl ester in MEEt16, *para*-cyano in *p*CEt16 and *para*-nitro in NIEt12 have been found by IR investigation. These interactions are very likely responsible for the extraordinarly high film periodicity of MEEt16 film, the different film periodicity of *p*CEt16 at different T_s and the coexistence of two film structures (film periodicities of 4.0 and 3.0 nm) in NIEt12 film prepared at low T_s. During the thermal treatment of the films, the thermally induced change in the intermolecular interactions caused a change of film structure. The high film periodicity of MEEt16, which was twice as long as its molecule length, was reduced to the value of single molecule length. The film periodicity of *p*CEt16 films was reduced from 4.8 nm to 4.4 nm during the annealing. For films of NIEt12, the film structure corresponding to a film periodicity of 3.0 nm disappeared after being annealed at 135°C.

In spite of the aforementioned facts, the tilt angle of most molecules is, however, not determined by the interactions between head groups. With the exception of MEEt16, the tilt angle of the molecules calculated according to the head-to-head model amounts to between 42° and 50°. The molecules have similar packing in the films as in crystals, which consist of oxadiazoles substituted with the same head group but without an alkyl chain. Except for MEEt16, the presence of π-π complexes between the molecules basically determined the tilt angle of molecules.

The influence of the amide bridge group on the film formation was investigated by comparing the film formation behaviour of oxadiazole derivatives with amide, ether and ester bridge groups. Films of amide bridged oxadiazoles prepared at low T_s were amorphous, layered films could only be obtained at high T_s, while, as summarized earlier, ether and ester bridged oxadiazole formed layered film within the whole investigated T_s region. This difference was attributed to the intermolecular H-bonds, which were only found to exist in the films based on amide bridged oxadiazoles.

When head groups were present in the molecules, the film periodicities of amide bridged oxadiazoles were larger than the corresponding molecule length in extended conformation, indicating bilayer structure of the films. For HA11, which is asymmetrically substituted and has no substituted head group, and 11AA11, which is symmetrically substituted by two alkyl chains, the film periodicity is smaller than the molecule length in extended conformation, indicating single layer structure for their films.

The states of the H-bonds in films of HA11, *p*CA11 and 11AA11 varies with T_s, but such a dependence was not observed for NIA11. NIA11 forms the most stable multilayers of the investigated oxadiazoles in the LB technique. The HA11 and *p*CA11 films deposited at low T_s have a low content of H-bonds and an amorphous film structure, while the films deposited at high T_s are highly H-bonded and have layered structures. In contrast nearly all the molecules in 11AA11 film deposited at low T_s are H-bonded and the film is amorphous, while only a fraction of the molecules are H-bonded in film deposited at high T_s and the film is ordered.

The amorphous films of *p*CA11 and 11AA11 could be converted to layered films by annealing them over a certain temperature. The resulting films have the same film periodicities as those found for films deposited at high T_s. Such structural transformations were always accompanied by a change in the H-bond state. Comparing with the oxadiazole compounds with ether bridge groups, it can be concluded that the change in intermolecular H-bonds has induced the change of film structure.

During the annealing of the NIA11 film, the H-bond remains stable, while an interaction between nitro groups is disassociated. Meanwhile, the film has undergone a structural change. The change of the NIA11 film is therefore very likely caused by the disassociation of interlayer interactions between nitro groups. The resulting film has a layered structure and the film periodicity is much larger (4.6 nm) than that of the films obtained directly from deposition (3.5 nm). Such a transformation of the film structure was also observed during the annealing of Y-type LB films of NIA11.

The study of the optical properties of 11AA11 films illustrates a strong correlation between the optical properties and the film structure. The films prepared at $T_s < 85°C$ absorb at 275 nm and do not fluoresce when excited by light with a wavelength of 345 nm. In contrast films deposited at $T_s > 95°C$ absorb at 345 nm and fluoresce strongly when excited by light of 345 nm. The optical properties of the former films could be converted to that of latter films by annealing over 120°C, this process is irreversible.

7.2 Future work

Several questions are still open at the end of this work which can be followed in the future work. The questions are related with substrate effect on film formation, physical properties, film characterization methode and computer simulation.

The investigations in this work focus on the influence of chemical structure on the formation of films, which are relative thick. The influence of the substrate on the film structure are not taken into consideration. In-situ characterization methods like LEED and RHEED and STM/AFM are required for this study. Two aspects should be taken into consideration for this study, the orientational effect of substrate on the first monolayer of films and the dependence of film structure on the film thickness.

The in-plane structure of the films still remains to be investigated for the future. The grazing incidence diffraction (GID) provides the possibility. The difficulty for such investigation for the VD film is that the film is not so good ordered as LB films, so the signal-noise ratio of the spectrum is too low to interpret, which remains a problem to solve in the future.

Many oxadiazole derivatives are mesogens. Up to now, the relationship between the liquid crystal properties and the film formation still remains unknown or has not attracted any interest at all. Taking into account that in both processes, formation of mesophase and film, the molecules perform self-organization and form a certain kind of organization, some correlation between these two processes may exist.

The influence of the film structure on its physical properties, esp. electrical properties, remains to be intensively investigated in the future work. The work in this direction is of great importance for the application of oxadiazoles and for the understanding of electronic band structure of the films.

It has been shown that Reflection Absorption Infrared Spectroscopy (RAIRS) is a very powerful mothod for investigating the film structure and the molecule-substrate interaction. Polarized RAIRS, in particular the microscopic RAIRS, will contribute greatly in the investigation of molecule orientation induced by substrate.

Computer modelling was proved to be a very powerful tool for understanding the film structure. In this work the development of an appropriate approach to the film structure simulation of the substituted 2,5-diphenyl-1,3,4-oxadiazole is very demanding. The electronic band structure can also be calculated, which can provide very useful information in the study of electrical properties of films.

8 References

[1] Inganäs, O. In *Organic Electroluminescent Materials and Devices*, S. Miyata; H. S. Nalwa, eds.; Gordon and Breach Publishers: Amsterdam, **1996**, pp. 147-176.

[2] Faraggi, E. Z.; Chayet, H.; Cohen, G.; Neumann, R.; Avny, Y.; Davidov, D. *Advanced Materials*, **1995**, *7*, 742.

[3] Schulz, B.; Kaminorz, Y.; Brehmer, L. *Synthetic Metals*, **1997**, *84*, 449-450.

[4] Schulz, B.; Bruma, M.; Brehmer, L. *Advanced Materials*, **1997**, *9*, 601.

[5] Schulz, B.; Brehmer, L.; Knochenhauer, G. *Mat. Sci. and Engin.-Biomim. Mat. Sensors and Systems*, **1995**, *C3*, 169.

[6] Schulz, B. *Molecular Crystals & Liquid Crystals Science & Technology Section A-Molecular Crystals & Liquid Crystals*, **1994**, *240*, 135.

[7] Schulz, B.; Leibnitz, E. *Acta Polymerica*, **1992**, *43*, 343.

[8] Salimgareeva, V.; Polevoi, R.; Ponomareva, V.; Sannikova, N.; Kolesov, S.; Leplyanin, G. *Russian Journal of Applied Chemistry*, **2003**, *76*, 1655-1658.

[9] Malimath, G.; Chikkur, G. *Applied Radiation and Isotopes*, **1994**, *45*, 143-147.

[10] Peng, Z.; Bao, Z.; Galvin, M. E. *Advanced Materials*, **1998**, *10*, 680-684.

[11] Wang, J. F.; Jabbour, G. E.; Mash, E. A.; Anderson, J.; Zhang, Y. *Advanced Materials*, **1999**, *11*, 1266.

[12] Chen, J. P.; Markiewicz, D.; Lee, V. Y.; Klaerner, G.; Miller, R. D.; Scott, J. C. *Synthetic Metals*, **1999**, *107*, 203.

[13] Bao, Z.; Rogers, J.; Dodabalapur, A.; Lovinger, A.; Katz, H.; Raju, V.; Peng, Z.; Galvin, M. *Optical Materials*, **1999**, *12*, 177-182.

[14] Xu, C.; Kaminorz, Y.; Reiche, J.; Schulz, B.; Brehmer, L. *Synthetic Metals*, **2003**, *137*, 963-964.

[15] Kaminorz, Y.; Xu, C.; Schulz, B.; Stiller, B.; Reiche, J.; Regenstein, W.; Brehmer, L. *Synthetic Metals*, **2002**, *127*, 217-220.

[16] Reiche, J.; Schulz, B.; Knochenhauer, G.; Dietzel, B.; Freydank, A.; Zetzsche, T.; Brehmer, L. *Thin Solid Films*, **1997**, *295*, 241-5.

[17] Giebler, R.; Schulz, B.; Reiche, J.; Brehmer, L.; Wu, M.; Woell, C.; Smith, A. P.; Urquhart, S. G.; Ade, H. W.; Unger, W. E. S. *Langmuir*, **1999**, *15*, 1291-1298.

[18] Freydank, A.; Thesis, *Herstellung und Charakterisierung supramolekularer Architekturen auf der Basis amphiphier aromatischer 1,3,4-Oxadiazole,* University Potsdam: Potsdam, **1998**.

[19] Forrest, S. R. *Chemical Review*, **1997**, *97*, 1793-1896.

[20] An, H.; Hou, J.; Chen, B.; Shen, J.; Liu, S. *Thin Solid Films*, **1998**, *326*, 201-204.

[21] Azim-Araghia, M. E.; Campbell, D. *Thin Solid Films*, **1998**, *320*, 320-323.

[22] Cocchi, M.; Virgili, D.; Giro, G.; Fattori, V.; Marco, P. D. *Applied Physics Letters*, **2002**, *80*, 2401-2403.

[23] Yang, A.; Kuroda, M.; Shiraishi, Y.; Kobayashi, T. *Journal of Chemical Physics*, **1998**, *109*, 8442-8450.

[24] Muccini, M.; Murgia, M.; Biscarini, F.; Taliani, C. *Advanced Materials*, **2001**, *13*, 355-358.

[25] Fraxedas, J. *Advanced Materials*, **2002**, *14*, 1603-1614.

[26] Ammermann, D.; Boehler, A.; Rompf, C.; Kowalsky, W. *Personal Communication*, **1995**.

[27] Saalfrank, R. W.; Weiss, B.; Peters, K.; Schnering, H. G. v. *Chemische Berichte-Recueil*, **1985**, *118*, 4026-4034.

[28] Franco, O.; Reck, G.; Orgzall, I.; Schulz, B. *Journal of Physical Chemical Solids*, **2002**, *63*, 1805-1813.

[29] Orgzall, I.; Franco, O.; Reck, G.; Schulz, B. *Journal of Molecular Structure*, **2003**, *649*, 219-230.

[30] Reck, G.; Schulz, B.; Orgzall, I.; CCDC; Vol. *152152*.

[31] Reck, G.; Schulz, B.; Orgzall, I.; CCDC; Vol. *160022*.

[32] Stockhause, S.; Schulz, B.; CCDC; Vol. *151852*.

[33] Kuznetsov, V. P.; Patsenker, L. D.; Lokshin, A. I.; Tolmachev, A. V. *Crystallog. Reprots*, **1998**, *43*, 430-438.

[34] Stockhause, S.; Wickleder, M. S.; Meyer, M.; Orgzall, I.; Schulz, B. *Journal of Molecular Structure*, **2001**, *561*, 175-183.

[35] Mikat, J.; Franco, O.; Regenstein, W.; Reck, G.; Knochenhauer, G.; Schulz, B.; Orgzall, I. *High Pressure Research*, **2000**, *18*, 311-318.

[36] Orgzall, I.; Lorenz, B.; Mikat, J.; Reck, G.; Knochenhauer, G.; Schulz, B. *Journal of Physical Chemical Solids*, **1999**, *60*, 1949-1965.

[37] Reck, G.; Schulz, B.; Orgzall, I.; Schulz, B.; CCDC; Vol. *152146*.

[38] Reck, G.; Schulz, B.; Orgzall, I.; Schulz, B.; CCDC; Vol. *152147*.

[39] Reck, G.; Schulz, B.; Orgzall, I.; Schulz, B.; CCDC; Vol. *152148*.

[40] Reck, G.; Schulz, B.; Orgzall, I.; Schulz, B.; CCDC; Vol. *152149*.

[41] Reck, G.; Schulz, B.; Orgzall, I.; Schulz, B.; CCDC; Vol. *152150*.

[42] Reck, G.; Schulz, B.; Orgzall, I.; Schulz, B.; CCDC; Vol. *152151*.

[43] Schulz, B.; Stiller, B.; Zetzsche, T.; Knochenhauer, G.; Dietel, R.; L, B. *Chemistry of Materials*, **1995**, *7*, 1041-1044.

[44] Schulz, B.; Stiller, B.; Zetzsche, T.; Knochenhauer, G.; Dietel, R.; Brehmer, L. *Molecular Crystals and Liquid Crystals*, **1994**, *248*, 35-42.

[45] Franco, O.; Thesis, *Structural and Spectroscopical Study of Crystals of 1,3,4-oxadiazole Derivatives at High Pressure,* University Potsdam: Potsdam, **2002**.

[46] Glusker, J. P.; Lewis, M.; Rossi, M. *Crystal Structure Analysis for Chemists and Biologists*, VCH **1994**.

[47] Berggren, M.; Gustafsson, G.; Inganäs, O.; Andersson, M. R.; Hjertberg, T.; Wennerström, O. *Journal of Applied Physics*, **1994**, *76*, 7530.

[48] Hamada, Y.; Adachi, C.; Tsutsui, T.; Saito, S. *Japanese Journal of Applied Physics Part 1*, **1992**, *31*, 1812.

[49] Hamada, Y.; Adachi, C.; Tsutsui, T.; Saito, S. *Optoelectr.*, **1992**, *7*, 83.

[50] Tsutsui, T.; Aminaka, E.-I.; Fujita, Y.; Hamada, Y.; Saito, S. *Synthetic Metals*, **1993**, *55-57*, 4157.

[51] Hamada, Y.; Adachi, C.; Tsutsui, T.; Saito, S. *Japanese Journal of Applied Physics*, **1992**, *31*, 1812-1816.

[52] Liang, F.; Wang, L.; Ma, D.; Jing, X.; Wang, F. *Applied Physics Letters*, **2002**, *81*, 4-6.

[53] Zheng, M.; Ding, L.; Gurel, E. E.; Lahti, P. M.; Karasz, F. E. *Macromolecules*, **2001**, *34*, 4124-4129.

[54] Kim, J. H.; Park, J. H.; Lee, H. *Chemistry of Materials*, **2003**, *15*, 3414-3416.

[55] Adachi, C.; Tsutsui, T.; Saito, S. *Applied Physics Letters*, **1990**, *56*, 799.

[56] Lee, J.-G.; Park, B.; Woo, H.-S.; Kim, Y.; Ha, C.-S.; Lee, C.-M.; Jeong, K.; Ha, J.-H.; Kim, Y.-R. *Solid State Communications*, **1997**, *102*, 895.

[57] Chung, S.-J.; Kwon, K.-Y.; Lee, S.-W.; Jin, J.-I.; Lee, C. H.; Lee, C. E.; Park, Y. *Advanced Materials*, **1998**, *10*, 1112.

[58] Jiang, X.; Liu, Y.; Song, X.; Zhu, D. *Solid State Communications*, **1996**, *99*, 183.

[59] Sun, R. G.; Masuda, T.; Kobayashi, T. *Japanese Journal of Applied Physics Part 2-Letters*, **1996**, *35*, L1434.

[60] Kido, J.; Ohtaki, C.; Hongawa, K.; Okuyama, K.; Nagai, K. *Japanese Journal of Applied Physics Part 2*, **1993**, *32*, L917.

[61] An, H.; Chen, B.; Hou, J.; Shen, J.; Liu, S. *Journal of Physics D: Applied Physics*,

1998, *31*, 1144-8.

[62] Johansson, N.; Salbeck, J.; Bauer, J.; Weissörtel, F.; Bröms, P.; Andersson, A.; Salaneck, W. R. *Advanced Materials*, **1998**, *10*, 1136.

[63] Reiche, J.; Freydank, A.; Helms, A.; Geue, T.; Schulz, B.; Brehmer, L.; Stiller, B.; Knochenhauer, G. *Materials Science and Engineering: C*, **1999**, *8-9*, 237-242.

[64] Reiche, J.; Knochenhauer, G.; Dietel, R.; Freydank, A.; Zetzsche, T.; Geue, T.; Barberka, T. A.; Pietsch, U.; Brehmer, L. *Supramolecular Science*, **1997**, *4*, 455-9.

[65] Dimitrowa, K.; Hauschild, J.; Zaschke, H.; Schubert, H. *J. Prakt. Chem.*, **1980**, *322/6*, 933-944.

[66] Parra, M.; Fuentes, G.; Vera, V.; Villouta, S.; Hernandez, S. *Bol. Soc. Chil. Quim.*, **1995**, *40*, 455-460.

[67] Parra, M.; Belmar, J.; Zunza, H.; Zuniga, C.; Fuentes, G.; Martinez, R. *Journal für Praktische Chemie*, **1995**, *337*, 239-241.

[68] Hetzheim, A.; Wasner, C.; Werner, J.; Kresse, H.; Tschierske, C. *Liquid Crystal*, **1999**, *26*, 885-891.

[69] Karamysheva, L. A.; Agafonova, I. F. *Molecular Crystals and Liquid Crystals A*, **1999**, *332*, 2527-2536.

[70] Aguilera, C.; Parra, M.; Fuentes, G. *Zeitschrift für Naturforschung B, Journal of Chemical Sciences*, **1998**, *53*, 367-370.

[71] Sato, M.; Ujiie, S. *Advanced Materials*, **1996**, *8*, 567-569.

[72] Dingemans, T. J.; Samulski, E. T. *Liquid Crystal*, **2000**, *27*, 131-136.

[73] Bechhoefer, J.; Hutter, J. L. *Physica A*, **1998**, *249*, 82-87.

[74] Itaya, A.; Watanabe, K.; Imamura, T.; Miyasaka, H. *Thin Solid Films*, **1997**, *292*, 204-212.

[75] Itaya, A.; Imamura, T.; Hamaguchi, M.; Tsuboi, Y.; Miyasaka, H.; Asahi, T.; Masuhara, H. *Thin Solid Films*, **1997**, *311*, 277-285.

[76] Imamura, T.; Watanabe, K.; Tsuboi, Y.; Miyasaka, H.; Itaya, A. *Thin Solid Films*, **1999**, *338*, 243-251.

[77] Sumiyoshi, T.; Takahashi, I.; Tsuboi, Y.; Miyasaka, H.; Itaya, A.; Asahi, T.; Masuhara, H. *Thin Solid Films*, **2000**, *370*, 285-293.

[78] Athouel, L.; Froyer, G.; Riou, M. T.; Schott, M. *Thin Solid Films*, **1996**, *274*, 35.

[79] Horowitz, G.; Bachet, B.; Yassar, A.; Lang, P.; Demanze, F.; Fave, J.-L.; Garnier, F. *Chemistry of Materials*, **1995**, *7*, 1337-1341.

[80] Horowitz, G.; Kouki, F.; Valat, P.; Romdhane, S.; Bouchriha, H.; Delannoy, P.; Monge, J.-L. *Synthetic Metals*, **1997**, *90*, 187-192.

[81] Servet, B.; Ries, S.; Trotel, M.; Alnot, P.; Horowitz, G.; Garnier, F. *Advanced Materials*, **1993**, *5*, 461-464.

[82] Porzio, W.; Destri, S.; Mascherpa, M.; Brueckner, S. *Acta Polymerica*, **1993**, *44*, 266.

[83] Siegrist, T.; fleming, R. M.; Haddon, R.; Laudise, R. A.; Lovinger, A. J.; Katz, H. E.; Bridenbaugh, P.; Davis, D. D. *Journal of Materials Research*, **1995**, *10*, 2170-2173.

[84] Kouji Hamano; Tetsuyuki Kurata; Kubota, S.; Koezuka, H. *Japanese Journal of Applied Physics*, **1994**, *33*, L1031-L1034.

[85] Timpanaro, S.; Sassella, A.; Borghesi, A.; Porzio, W.; Fontaine, P.; Goldmann, M. *Advanced Materials*, **2001**, *13*, 127.

[86] Servet, B.; Horowitz, G.; Ries, S.; Lagorsse, O.; Alnot, P.; Yassar, A.; Deloffre, F.; Srivastava, P.; Hajlaoui, R.; Lang, P.; Garnier, F. *Chemistry of Materials*, **1994**, *6*, 1809-1815.

[87] Tavazzi, S.; Meinardi, F.; Borghesi, A.; Sassella, A.; Tubino, R. *Synthetic Metals*, **2001**, *124*, 71-73.

[88] Kanemitsu, Y.; Shimizu, N.; Suzuki, K.; Shiraishi, Y.; Kuroda, M. *Physical Review B*, **1996**, *54*, 2198-2204.

[89] Lang, P.; Hajlaoui, R.; Gamier, F.; Desbat, B.; Buffeteau, T.; Horowitz, G.; Yassar, A. *Journal of Physical Chemistry*, **1995**, *99*, 5492-5499.

[90] Lang, P.; El Ardhaoui, M.; Horowitz, G.; Garnier, F.; Wittmann, J. C.; Lotz, B.; Straupe, C.; Dallas, T. P. *Synthetic Metals*, **1997**, *84*, 605-606.

[91] Lovinger, A. J.; Davis, D. D.; Ruel, R.; Torsi, L.; Dodabalapur, A.; Katz, H. E. *Journal of Materials Research*, **1995**, *10*, 2958.

[92] Mena-Osteritz, E. *Advanced materials*, **2002**, *14*, 609-616.

[93] Mushrush, M.; Facchetti, A.; Lefenfeld, M.; Katz, H. E.; Marks, T. J. *Journal of America Chemical Society*, **2003**, *125*, 9414-9423.

[94] Hotta, S.; Ichino, Y.; Yoshida, Y.; Yoshida, M. *Journal of Physical Chemistry B*, **2000**, *104*, 10316-10320.

[95] Sassella, A.; Borghesi, A.; Pinotti, E.; Tubino, R.; Destri, S.; Porzio, W. *Journal of Crystal Growth*, **1999**, *201/202*, 1044-8.

[96] Hetzheim, A.; Möckel, K. *Advances in Heterocyclic Chemistry*, **1966**, *7*, 185.

[97] Hetzheim, A. In *Mothoden der Organischen Chemie*, Houben-Weyl, ed.; Georg Thieme Verlag: Stuttgart, **1994**; Vol. *E 8c*, pp. 526 ff.

[98] Hill, J. In *Comprehensive Heterocyclic Chemistry II*, Storr Elseoris, ed.: Oxford, **1996**; Vol. *4*, pp. 267-287 (905-1006).

[99] Hill, J. In *Comprehensive Heterocyclic Chemistry*, A. R. Katritzky; C. W. Rees, eds.; Pergamon: Oxford, **1984**; Vol. *6*, pp. 426 pp.

[100] Kern, W. *Journal of the Electrochemical Society*, **1990**, *137*, 1887.

[101] Herman, M. A.; Sitter, H. *Molecular Beam Epitaxy*, Springer **1996**.

[102] M. Henzler, W. Göpel. *Oberflächenphysik des Festkörpers*, Teubner Stuttgart **1991**.

[103] Venables, J. A.; Spiller, G. D. T.; Hanbucken, M. *Rep. Prog. Phys.*, **1984**, *47*, 399.

[104] Maroncelli, M.; Qi, S. P.; Strauss, H. L.; Snyder, R. G. *Journal of America Chemical Society*, **1982**, *104*, 6237-6247.

[105] Pelletier, I.; Laurin, I.; Buffeteau, T.; Desbat, B.; Pézolet, M. *Langmuir*, **2002**, *19*, 1189-1195.

[106] Bain, C. D.; Whitesides, G. M.; Nuzzoj, R. G.; Troughton, E. B.; Tao, Y.-T.; Evall, J. *Journal of America Chemical Society*, **1989**, *111*, 321-335.

[107] Hostetler, M. J.; Stokes, J. J.; Murray, R. W. *Langmuir*, **1996**, *12*, 3604-3612.

[108] Hostetler, M. J.; Green, S. J.; Stokes, J. J.; Murray, R. W. *Journal of America Chemical Society*, **1996**, *118*, 4212-4213.

[109] Desiraju, G. R. *Crystal Engineering: The Design of Organic Solids*, Elsevier: Amsterdam **1989**.

[110] Desiraju, G. R.; Gavezzotti, A. *Acta Crystallographica Section B*, **1989**, *45*, 473-482.

[111] Desiraju, G. R. *Angewendete Chemie, Int. Ed.*, **1995**, *34*, 2311-2327.

[112] Biscarini, F.; Zamboni, R.; Samorí, P.; Ostoja, P.; Taliani, X. *Physical Review B*, **1995**, *52*, 14868-14877.

[113] Rovira, C.; Novoa, J. J. *Chemical Physics Letters*, **1997**, *279*, 140.

[114] Heuzé, K.; Fourmigué, M.; Batail, P.; Canadell, E.; Auban-Senzier, P. *Chemistry A European Journal*, **1999**, *5*, 2971-2976.

[115] Mattheus, C. C.; Thesis: *Polymorphism and electronic properties of pentacene*, University of Groningen, **2002**.

[116] Schoonveld, V. A.; Thesis: Transistors based on ordered organic semiconductors, University of Groningen, **1999**.

[117] Yoshida, Y.; Takiguchi, H.; Hanada, T.; Tanigaki, N.; Han, E. M.; Yase, K. *Applied Surface Science*, **1998**, *130-132*, 651-657.

[118] Seidel, C.; Poppensieker, J.; Fuchs, H. *Surface Science*, **1998**, *408*, 223-31.

[119] Staub, R.; Toerker, M.; Fritz, T.; Schmitz-Huebsch, T.; Sellam, F.; Leo, K. *Surface*

Science, **2000**, *445*, 368-79.

[120] Podesta, A.; Toccoli, T.; Milani, P.; Boschetti, A.; Innotta, S. *Surface Science*, **2000**, *464*, L673-80.

[121] Schlettwein, D.; Tada, H.; Mashiko, S. *Thin Solid Films*, **1998**, *331*, 117-130.

[122] Sassella, A.; Borghesi, A.; Tubino, R.; Destri, S.; Porzio, W.; Barbarella, G. *Synthetic Metals*, **2000**, *115*, 69-73.

[123] Tanigaki, K.; Kuroshima, S.; Ebbesen, T.; Ichihashi, T. *Molecular Crystals and Liquid Crystals*, **1992**, *B2*, 179-192.

[124] Böhler, A.; Dirr, S.; Ammermann, D.; Johannes, H.-H.; Kowalsky, W. *Synthetic Metals*, **1997**, *91*, 95-97.

[125] Botta, C.; Destri, S.; Porzio, W.; Sassella, A.; Borghesi, A.; Tubino, R. *Optical Materials*, **1999**, *12*, 301-305.

[126] Vincett, P. S.; Popovic, Z. D.; McIntyre, L. *Thin Solid Films*, **1981**, *82*, 357.

[127] Yoshida, Y.; Takiguchi, H.; Hanada, T.; Tanigaki, N.; Han, E.-M.; Yase, K. *Journal of Crystal Growth*, **1999**, *198/199*, 923-8.

[128] Fuchigami, H.; Tanimura, S.; Uehara, Y.; Kurata, T.; Tsunoda, S. *Japanese Journal of Applied Physics*, **1995**, *34*, 3852-7.

[129] Schulz, B.; Stiller, B.; Zetzsche, T.; Knochenhauer, G.; Dietel, R.; Brehmer, L. *Chemistry of Materials*, **1995**, *7*, 1041-1044.

[130] Leadbetter, A. J.; Frost, J. C.; Gaughan, J. P.; Gray, G. W.; Mosley, A. *Journal de Physique*, **1979**, *40*, 375.

[131] Hori, K.; Kuribayashi, M.; Iimuro, M. *Physical Chemistry Chemical Physics*, **2000**, *2*, 2863-2868.

[132] Hori, K.; Wu, H. *Liquid Crystal*, **1999**, *26*, 37-43.

[133] Reck, G.; Orgzall, I.; Schulz, B.; Dietzel, B. *Acta Crystallographica Section C*, **2003**, *59*, in press.

[134] Oki, M.; Hori, K. *Bulletin of the Chemistry Society of Japan*, **1998**, *71*, 543-548.

[135] Günzler, H.; Böck, H. *IR-spektroskopie*, VCH **1983**.

[136] Matsuura, H.; Yoshida, H.; Hieda, M.; Yamanaka, S.-y.; Takanori Harada; Shin-ya, K.; Ohno, K. *Journal of America Chemical Society*, **2003**, *125*, 13910-13911.

[137] Musah, R. A.; Jensen, G. M.; Rosenfeld, R. J.; McRee, D. E.; Goodin, D. B. *Journal of America Chemical Society*, **1997**, *119*, 9083-9084.

[138] Wahl, M. C.; Sundaralingam, M. *Trends of Biochemistry Science*, **1997**, *22*, 97-102.

[139] Senes, A.; Ubarretxena-Belandia, I.; Engelman, D. M. In *Proc. Natl. Acad. Sci.*: USA, **2001**; Vol. *98*, pp. 9056-9061.

[140] Orgzall, I. *unpublished results*.

[141] Hori, K.; Kurosaki, M.; Wu, H.; Itoh, K. *Acta Crystallographica Section C*, **1996**, *52*, 1751-1754.

[142] Hori, K.; Koma, Y.; Uchida, A.; Ohashi, Y. *Moleuclar Crystals and Liquid Crystals*, **1993**, *225*, 15-22.

[143] Zhang, X. L.; Gilpin, R. K. *Moleuclar Crystals and Liquid Crystals*, **1993**, *231*, 57-68.

[144] Shabatina, T. I.; Vovk, E. V.; Khasanova, T. V.; Andreev, G. N.; Sergeev, G. B. *Supramolecular Science*, **1997**, *4*, 485-489.

[145] Kuribayashi, M.; Hori, K. *Liquid Crystal*, **1999**, *26*, 809-815.

[146] Matsui, E.; Nito, K.; Yasuda, A. *Liquid Crystal*, **1994**, *17*, 311-322.

[147] Lin-Vien, D.; Colthup, N. B.; Fateley, W. G.; Grasselli, J. G. *The Handbook of Infrared and Raman Characteristic Frequencies of Organic Molecules*, Academic Press **1991**.

[148] Reiche, J.; Thesis, *Beiträge zur Strukturaufklärung organischer Mono- und MultischichtenUniversity,* Potsdam: Potsdam, **1996**.

[149] Reiche, J. *Thin Solid Films*, **1996**, *284-285*, 453-455.

[150] Kross, R. D.; Fassel, V. A. *Journal of America Chemical Society*, **1956**, *78*, 4225-4229.

[151] Epstein, L. M.; Shubina, E. S.; Ashkinadze, L. D.; Kazitsyna, L. A. *Spectrochimica Acta Part A*, **1982**, *38*, 317-322.

[152] Bertran, J. F.; Hernandey, M.; Serna, B. L. *Spectrochimica Acta Part A*, **1982**, *38*, 149-151.

[153] Ancelin, H.; Briody, G.; Yarwood, J.; Lloyd, J. P.; Petty, M. C. *Langmuir*, **1990**, *6*, 172-177.

[154] Harrand, M. *Journal of Raman Spectroscopy*, **1975**, *4*, 53-73.

[155] Harrand, M. *Journal of Raman Spectroscopy*, **1979**, *8*, 161-164.

[156] Sax, K. J.; Saari, W. S. *Journal of Organic Chemistry*, **1960**, *25*, 1590.

[157] Katrizky, A. R.; Coats, N. A. *Journal of Chemistry Society, Lonon*, **1959**, 2062.

[158] Briggs, L. H.; Colebrook, L. D.; Fales, H. M.; Wildman, W. C. *Analytical Chemistry*, **1957**, *29*, 904.

[159] Colthup, N. B.; Daly, L. H.; Wiberley, S. E. *Introduction to Infrared and Raman*

Spectroscopy, Academic Press **1990**.

[160] Suzuki, I. *Bulletin of the Chemistry Society of Japan*, **1960**, *33*, 1359-1365.

[161] Suzuki, I. *Bulletin of the Chemistry Society of Japan*, **1962**, *35*, 1279-1293.

[162] Maeda, Y.; Higuchi, T.; Ikeda, I. *Langmuir*, **2000**, *16*, 7503-7509.

[163] Maeda, Y.; Nakamura, T.; Ikeda, I. *Macromolecules*, **2001**, *34*, 1391-1399.

[164] Maeda, Y.; Nakamura, T.; Ikeda, I. *Macromolecules*, **2001**, *34*, 8246-8251.

[165] Urai, Y.; Ohe, C.; Itoh, K. *Langmuir*, **2000**, *16*, 3920-3926.

[166] Katsumoto, Y.; Tanaka, T.; Sato, H.; Ozaki, Y. *Journal of Physical Chemistry A.*, **2002**, *106*, 3429-3435.

[167] Bottino, F. A.; Pasquale, G. D.; Iannelli, P. *Macromolecules*, **2001**, *34*, 33-37.

[168] Kaminorz, Y. In *Mathematisch-Naturwissenschaftlichen Fakultät*; Universität Potsdam: Potsdam, **1998**, pp. 100.

[169] Tokuhisa, H.; Era, M.; Tsutsui, T. *Applied Physics Letters*, **1998**, *72*, 2639-2641.

[170] Biscarini, F.; Samorí, P.; Greco, O.; Zamboni, R. *Physical Review Letters*, **1997**, *78*, 2389-2392.

[171] Lang, P.; Horowitz, G.; Valat, P.; Garnier, F.; Wittmann, J. C.; Lotz, B. *Journal of Physical Chemistry B*, **1997**, *101*, 8204-8211.

[172] Popova, N. A.; Yushko, É. G.; Krasovitskii, B. M.; Minkin, V. I.; Lyubarskaya, A. É.; Gol'dberg, M. L. *Chim. Geterotsikl. Soedin.*, **1983**, *1*, 22.

[173] Feygelman, V. M.; Walker, J. K.; Katritzky, A. R.; Dega-Szafran, Z. *Chimica Scripta*, **1989**, *29*, 241.

[174] Puschnig, P.; Ambrosch-Draxl, C. *Physical Review B*, **1999**, *60*, 7891-7898.

[175] Yang, S.-C.; Graupner, W.; Guha, S.; Puschnig, P.; Martin, C.; Chandrasekhar, H. R.; Chandrasekhar, M.; Leising, G.; Ambrosch-Draxl, C.; Scherf6, U. *Physical Review Letters*, **2000**, *85*, 2388-2391.

[176] Puschnig, P.; Ambrosch-Draxl, C.; Heimel, G.; Zojer, E.; Resel, R.; Leising, G.; Kriechbaum, M.; Graupner, W. *Synthetic Metals*, **2001**, *116*, 327-331.

[177] Birks, J. B. *Photophysics of Aromatic Molecules.*, John Wiley and Sons: New York **1970**.

[178] Guha, S.; Graupner, W.; Resel, R.; Chandrasekhar, M.; Chandrasekhar, H. R.; Glaser, R.; Leising, G. *Journal of Physical Chemistry A.*, **2001**, *105*, 6203-6211.

[179] Chandrasekhar, M.; Guha, S.; Graupner, W. *Advanced Materials*, **2001**, *13*, 613-618.

[180] Parra, M.; Belmar, J.; Zunza, H.; Zuniga, C.; Villouta, S.; Martinez, R. *Boletin de*

la Sociedad Chilena de Quimica, **1993**, *38*, 325.

[181] Parra, M.; Belmar, J.; Zunza, H.; Zuniga, C.; Villouta, S.; Martinez, R. *J. Prakt. Chem.*, **1995**, *337*, 325-327.

[182] Grekov, A. P.; Grigoreva, V. I. *The Journal of General Chemistry of the USSR*, **1961**, *31*, 3743-3745.

[183] Huisgen, R.; Sauer, J.; Sturm, H. J.; Markgraf, J. H. *Chemische Bericht Recueil*, **1960**, *93*, 2106-2124.

[184] Grekov, A. P.; Kulakowa, L. N.; Schwaika, O. P. *Zh. Obsh. Khim.*, **1959**, *29*, 3054.

Appendix

Synthetic procedures

1. Alkoxybenzoyl chloride and alkoxy benzoic acid hydrazide

4-Hexadecyloxybenzoic hydrazide (1a, *n*=15)

5g (0.13 mol) methyl 4-hexadecyloxybenzoate was dissolved in 50 ml 2-propanol and 10 ml hydrazine hydrate was added dropwise and the reaction was allowed to take place under reflux for 40 hours. After cooling down to room temperature the solid was filtered out and washed twice with 2-propanol.

Yield : 98 %, Melting point : 103-105°C

4-Nonyloxybenzoic hydrazide (1a, *n*=8)

10 g (0.036 mol) methyl 4-nonyloxybezoate was dissolved in 100 ml 2-propanol and 20 ml hydrazine hydrate was added dropwise and the reaction run at reflux for 17 hours. Then the mixture was cooled down to room temperature and the solid filtered out. Afterwards the solid was washed with 2-propanol and water.

Yield : 62 %, Melting point : 89-91°C (Lit.: 90-93°C [180, 181])

4-Decyloxybenzoyl chloride (1b, *n*=9)

3g (0.0108 mol) 4-decyloxybozoic acid was given in 36 ml $SOCl_2$ and the mixture was allowed to run at reflux for 14 hours. The surplus $SOCl_2$ was distilled in vacuum. The remaining liquid was used directly the next synthesis step.

4-Dodecyloxybenzoyl chloride (1b, *n*=11)

4.6 g (0.015 mol) 4-dodecyloxybenzoic acid was put in 50 ml $SOCl_2$ and the reaction ran at reflux for 16 hours. The surplus $SOCl_2$ was distilled in vacuum. The remaining liquid was cooled down to 4°C and the precipitated crystal was recrystallized with absolute ethanol.

Yield: 95 %, Melting point: 31°C

2. 1,2-Diaryl hydrazines

1c, 2c, 3c, 4c: 0.01 mol hydrazide was added to 35 ml absolute pyridine to form a suspension. 0.01 mol benzoyl chloride was dissolved in 15 ml absolute THF and added dropwise to the hydrazide suspension. The reaction ran 5 to 15 hours at room temperature until the result of thin film chromatography showed that all the raw materials were converted. At the end of the reaction the mixture was poured into 500 ml 5 % HCl. The precipitated white solid was filtered and washed with water several times until it is neutral.

The resulted hydrazine was then dried up and recrystallized.

2c (R = NH_2) : 0.07 mol 4-aminobenzoyl hydrazide was added to 500 ml 5% HCl and formed a suspension. 0.07 mol 4-nitrobenzoyl chloride was solved in toluene and dropwise added to the hydrazide suspension. Afterwards a saturated K_2CO_3 water solution was added to adjust the PH value of the mixture to 9. The mixture was stirred at room temperature for 1 hour and neutralized with thin HCl at the end of the reaction. The resulting solid was filtered, washed with water and dried.

1-(4-Cyanobenzoyl)-2-(4-hexadecyloxybenzoyl) hydrazine (1c, R = *p*-CN, *n* = 15)

Yield: 85% , Melting point: 239-245°C
IR (KBr, cm^{-1}): 2920, 2850, 2230, 1680, 1600, 1555, 1510, 1470, 1390, 1300, 1250, 1170, 1110, 860, 840, 750, 720, 695, 660, 625

1-(4-Cyanobenzoyl)-2-(4-dodecyloxybenzoyl) hydrazine (1c, R = *p*-CN, *n* = 11)

Yield: 95 %, Melting point : 213-218°C

1-(4-Cyanobenzoyl)-2-(4-decyloxybenzoyl) hydrazine (1c, R = *p*-CN, *n* = 9)

Yield: 97 %, Melting point: 196-206°C

1-(4-Cyanobenzoyl)-2-(4-pentyloxybenzoyl) hydrazine (1c, R = *p*-CN, *n* = 4)

Yield: 88 %, Melting point: 225-228°C

1-(4-Cyanobenzoyl)-2-(4-meyloxybenzoyl) hydrazine (1c, R = *p*-CN, *n* = 0)

Yield: 98 %, Melting point: 216-230°C

1-(3-Cyanobenzoyl)-2-(4-hexadecyloxybenzoyl) hydrazine (1c, R = *m*-CN, *n* = 15)
Yield: 29 %, Melting point: 178-182°C
IR (KBr, cm^{-1}): 3250, 2925, 2860, 2225, 1675, 1640, 1610, 1580, 1510, 1475, 1300, 1255, 1185, 1115, 1025, 845, 820, 805, 745, 722, 685

1-(4-Nitrobenzoyl)-2-(4-hexadecyloxybenzoyl) hydrazine (1c, R = NO_2, *n* = 15)
Yield: 47 %, Melting Point: 280-296°C

1-(4-Nitrobenzoyl)-2-(4-hexadecyloxybenzoyl) hydrazine (1c, R = NO_2, *n* = 11)
Yield: 76 % , Melting Point: 144-190°C (LC)

1-(4-Methoxycarbonylbenzoyl)-2-(4-hexadecyloxybenzoyl) hydrazine (1c, R = CH_3OOC, *n* = 15)
Yield: 57 %, Melting Point : 152-154°C (from Ethanol)

1-Benzoyl-2-(4-hexadecyloxybenzoyl) hydrazine (1c, R = H, *n*=15)
Yield: 99 %, Melting Point : 137-146°C

1-(4-Aminobenzoyl)-2-(4-nitrobenzoyl) hydrazine (2c, R = NH_2)
Yield: 38 %, Melting Point : 265°C
IR (KBr, cm^{-1}): 3450, 3380, 3150, 1680, 1640, 1600, 1520, 1510, 1410, 1350, 1240, 1130, 840

1-(4-Cyanobenzoyl)-2-(4-nitrobenzoyl) hydrazine (2c, R = CN)
Yield: 80 %, Melting Point: 295-298°C

1-Benzoyl-2-(4-nitrobenzoyl) hydrazine (2c, R = H)
Yield: 95 %, Melting Point: 244-246°C

1,2-Di(4-methoxycarbonylbenzoyl) hydrazine (4c)
Yield: 83 % , Melting Point: 300-302°C

3. 2,5-Diaryl-1,3,4-oxadiazoles

0.01 mol dibenzoylhydrazine was added to 35 ml $POCl_3$. The mixture was stirred at reflux for 2 to 20 hours. The resulting oxadiazoles are usually soluble in $POCl_3$, thus the mixture became a clear solution at the end of the reaction. The clear solution was further stirred at reflux for 1 hour. The clear solution was cooled down and added to water (1L) with crushed ice. The precipitated oxadiazole was filtered and washed with water, dried and purified by crystallization or by chromatography.

2-(4-Cyanophenyl)-5-(4-hexadecyloxyphenyl)-1,3,4-oxadiazole (*p*CEt16)
Yield: 83 %, Melting point: 123-127°C (from Ethanol)
IR (KBr, cm^{-1}): 2954, 2919, 2849, 2233, 1611, 1582, 1544, 1493, 1468, 1315, 1257, 1177, 1073, 1017, 963, 850, 840, 744, 721, 702, 661

2-(4-Cyanophenyl)-5-(4-dodecyloxyphenyl)-1,3,4-oxadiazole (*p*CEt12)
Yield: 97 %, Melting point: 122-126°C (from Ethanol)
IR (KBr, cm^{-1}): 2959, 2921, 2853, 2232, 1610, 1583, 1547, 1495, 1466, 1309, 1257, 1176, 1102, 1073, 1022, 848, 837, 745, 721, 701, 660, 552

2-(4-Cyanophenyl)-5-(4-decyloxyphenyl)-1,3,4-oxadiazole (*p*CEt10)
Yield: 97% , Melting point: 122-126°C (from Ethanol)
IR (KBr, cm^{-1}): 2954, 2921, 2851, 2232, 1610, 1583, 1547, 1495, 1467, 1390, 1308, 1257, 1178, 1103, 1073, 1022, 964, 851, 838, 745, 720, 702, 661, 633, 552, 525

2-(4-Cyanophenyl)-5-(4-pentyloxyphenyl)-1,3,4-oxadiazole (*p*CEt5)
Yield: 76 %, Melting point: 143-146°C
IR (KBr, cm^{-1}): 3095, 3064, 2955, 2938, 2888, 2864, 2853, 2230, 1607, 1586, 1496, 1491, 1479, 1425, 1413, 1395, 1316, 1301, 1257, 1179, 1127, 1106, 1070, 1012, 961, 854, 835, 809, 780, 741, 701, 663, 550, 523

2-(4-Cyanophenyl)-5-(4-meyloxyphenyl)-1,3,4-oxadiazole (*p*CEt1)
Yield: 85 %, Melting point: 191-195°C
IR (KBr, cm^{-1}): 3093, 3060, 3014, 2972, 2943, 2924, 2840, 2230, 1611, 1583, 1547, 1493, 1460, 1306, 1256, 1175, 1120, 1101, 1073, 1030, 963, 838, 747, 704, 625, 553, 525

2-(3-Cyanophenyl)-5-(4-hexadecyloxyphenyl)-1,3,4-oxadiazole (*m*CEt16)
Yield: 91 %, Melting point: 116-118°C
IR (KBr, cm^{-1}): 2955, 2920, 2850, 2234, 1612, 1543, 1493, 1468, 1309, 1259, 1173, 906, 838, 807, 742, 720, 683, 657, 587, 523, 471

2-(4-Nitrophenyl)-5-(4-hexadecyloxyphenyl)-1,3,4-oxadiazole (NIEt12)
Yield: 97 % , Melting point: 160-165°C
IR (KBr, cm^{-1}): 3107, 3073, 2954, 2921, 2850, 1612, 1585, 1556, 1540, 1496, 1482, 1466, 1364, 1351, 1309, 1252, 1176, 1163, 1110, 1102, 1077, 1070, 1008, 966, 865, 855, 841, 738, 721, 711, 660

2-(4-Methoxycarbonylphenyl)-5-(4-hexadecyloxyphenyl)-1,3,4-oxadiazole (MEEt16)
Yield: 44 %, Melting point: 137-140°C (from dioxane)
IR (KBr, cm^{-1}): 2956, 2919, 2849, 1723, 1617, 1587, 1549, 1498, 1473, 1439, 1309, 1283, 1258, 1193, 1178, 1111, 1101, 1019, 963, 868, 842, 824, 777, 739, 716, 662

2-Phenyl-5-(4-hexadecyloxyphenyl)-1,3,4-oxadiazole (HEt16)
Yield: 93 %, Melting point: 81- 84°C
IR (KBr, cm^{-1}): 3066, 2951, 1918, 2852, 1717, 1610, 1583, 1550, 1497, 1475, 1421, 1399, 1372, 1316, 1300, 1259, 1178, 1107, 1064, 1043, 1020, 992, 963, 836, 775, 738, 719, 704, 687, 654

2-(4-Aminophenyl)-5-(4-nitrophenyl)-1,3,4-oxadiazole (2d, R = NH_2)
Yield: 78%, Melting point: 265°C (Lit.: >300°C [182])
IR (KBr, cm^{-1}): 3460, 3360, 1605, 1555, 1520, 1495, 1340, 1310, 1180, 1110, 1070, 965, 855, 745

2-(4-Cyanophenyl)-5-(4-nitrophenyl)-1,3,4-oxadiazole (2e, R = CN)
Yield: 99%, Melting point: 277-279°C (Lit.:279-280°C [18])

2-Phenyl-5-(4-nitrophenyl)-1,3,4-oxadiazole (2d, R = H)
Yield: 90%, Melting point: 194°C (Lit.: 206-208°C [183])
IR (KBr, cm^{-1}): 1610, 1555, 1520, 1480, 1450, 1340, 1315, 1290, 1270, 1105, 1080, 1030, 995, 965, 930, 860, 785, 720, 695

2,5-Di(4-nitrophenyl)-1,3,4-oxadiazole (3d)
Yield: 78 %, Melting point: 310-312°C

2,5-Di(4-methoxycarbonylphenyl)-1,3,4-oxadiazole (4d)
Yield: 68 %, Melting point: 272°C (from DMF/Ethanol 9:1)
IR (KBr, cm^{-1}): 2970, 1730, 1550, 1495, 1440, 1430, 1280, 1195, 1180, 1120,1110, 1080, 1020, 965, 870, 835, 785, 730, 695

4. 2,5-Diphenyl-1,3,4-oxadiazoles with amide bridge unit

General procedure for reduction of nitro group to amide group

0.013 mol nitro compound and 4.1 g ammonium formate ($HCOONH_4$) was added to 65 ml methanol. 0.2 g Palladium/Carbon (Pd/C, 10 % Pd) as catalyst was poured into the mixture under nitrogen protection. Depending on the test results of thin film chromatography, the mixture was stirred at reflux for 2 to 20 hours. At the end of the reaction the mixture was warm filtered to eliminate the catalyst. The mixture was then cooled down or poured in water to let the product precipitate. Afterwards the solid was

filtered, recrystallized and dried.

2-(4-Cyanophenyl)-5-(4-aminophenyl)-1,3,4-oxadiazole (2e, R = CN)
Yield: 29 %, Melting point: 257-259°C (from Methanol)
IR (KBr, cm^{-1}): 3410, 3340, 3230, 2215, 1635, 1610, 1580, 1555, 1500, 1445, 1415, 1320, 1270, 1180, 1075, 1020, 965, 850, 840, 745

2-Phenyl-5-(4-aminophenyl)-1,3,4-oxadiazole (2e, R = H)
Yield: 73 %, Melting point: 194-196°C, (Lit.: 192°C [184])
IR (KBr, cm^{-1}): 3415, 3340, 3220, 1640, 1610, 1580, 1555, 1500, 1490, 1445, 1370, 1320, 1275, 1180, 1080, 970, 960, 830, 820, 775, 745, 715, 700, 690

General procedure for synthesis 2,5-diphenyl-1,3,4-oxadiazoles with amide unit.

0.01 mol alkyl acid chloride and 2 ml pyridine was dissolved in 60 ml DMF or DMAc. 0.01 mol amino substitute 2,5-diphenyl-1,3,4-oxadiazole was dissolved in 50 ml DMAc and dropped in under stirring. The reaction was allowed to run at room temperature for 2 hours and then poured into a mixture of crushed ice and water. The precipitate solid was filtered, recrystallized and dried.

2-(4-Dodecanoylaminophenyl)-5-(4-nitrophenyl)-1,3,4-oxadiazole (NIA11)
Yield: 79 %, Melting point: 214°C
IR(KBr, cm^{-1}): 3334, 3109,2956, 2923, 2853, 1677, 1602, 1552, 1525, 1496, 1467, 1421, 1412, 1341, 1316, 1256, 1184, 1108, 1072, 1013, 964, 854, 740, 711

2-(4-Dodecynoylaminophenyl)-5-(4-cyanophenyl)-1,3,4-oxadiazole (*p*CA11)
Yield:68 %, Melting point: 203-205°C
IR (KBr, cm^{-1}): 3361, 2956, 2921, 2851, 2233, 1692, 1612, 1600, 1579, 1560, 1525, 1492, 1470, 1412, 1312, 1253, 1183, 1160, 1103, 1074, 1016, 964, 850, 743, 721, 704, 550

2-(4-Dodecynoylaminophenyl)-5-phenyl-1,3,4-oxadiazole (HA11)
Yield: 50 %, Melting point: 178-183°C
IR (KBr, cm^{-1}): 3324, 3290, 2954, 2921, 2851, 1703, 1682, 1608, 1568, 1537, 1493, 1416, 1376, 1315, 1256, 1182, 1107, 1078, 1070, 1025, 964, 843, 777, 737, 706, 689

2,5-Di(4-stearaminophenyl)-1,3,4-oxadiazole (17AA17)
Yield: 77 %, Melting point: 261-265°C
IR (KBr, cm^{-1}): 3305, 2955, 2917, 2850, 1655, 1612, 1601, 1538, 1495, 1470, 1412, 1311, 1257, 1181, 1102, 1076, 963, 845, 738, 718, 705

2,5-Di(4-dodecanoylaminophenyl)-1,3,4-oxadiazole (11AA11)
Yield: 54 %, Melting point: 279°C (from Ethanol)
IR (KBr, cm^{-1}): 3300, 2960, 2920, 2850, 1715, 1670, 1600, 1530, 1490, 1410, 1315, 1255, 1160, 1075, 845, 745

2,5-Di(4-octanaminophenyl)-1,3,4-oxadiazole (7AA7)
Yield: 98 % , Melting point: 280-285°C (from Ethanol)
IR (KBr, cm^{-1}): 3332, 3301, 2956, 2855, 1713, 1677, 1600, 1530, 1491, 1412, 1317, 1255, 1169, 1100, 1079, 843, 744, 722, 707

5. 2,5-Diphenyl-1,3,4-oxadiazoles with ester bridge unit

General procedure

A tree-neck flask was firstly purged with dry nitrogen, then 0.0059 mol 4d and 0.0752 mol dodecanol were added in and heated to 100°C. Afterwards 0.3 ml tetraisopropylorthotitanat was injected in the mixture. The reaction was run at 130°C for 3 hours and a further 10 hours at 150°C. The mixture became a clear solution at the end of the reaction. After cooling down to room temperature, the precipitate solid was filtered and washed with ethyl ether several times and recrystallized to eliminate the surplus dodecanol.

2,5-Di(4-dodecyloxycarbonylphenyl)-1,3,4-oxadiazol (12EsEs12)
Yield: 70 %, Melting point: 145°C
IR (KBr, cm^{-1}): 2960, 2920, 2850, 1715, 1545, 1490, 1465, 1420, 1280, 1160, 1150,1100, 1010, 965, 940, 860, 780, 720

9 Acknowledgement

I would like to thank Prof. Dr. Ludwig Brehmer, my supervisor, for his kind hospitality and helpful discussions.

I would like to express my gratitude to Dr. habil. Burkhard Schulz for providing the possibility of chemical synthesis, for the numerous discussions and very helpful suggestions and, in particular, his unlimited patience in guiding me during the course of this work.

I would also like to thank Dr. Yvette Kaminorz for the discussion and suggestions.

Dr. Thomas Köpnick guided me at the beginning of chemical synthesis and I would never forget the two happy years working together with Ms. Edeltraut Loth and all other colleague of Institute of Thin Film Technology and Microsensorics, Teltow Seehof.

Special thanks go to Dr. Wolfgang Regenstein for his kind collaboration in the PL studies and for providing me the unlimited access to IR instrument.

Prof. Dr. U. Pietsch and Dr. T. Geue have provided the opportunity to carry out the X-ray experiments under heating. They did also give many helpful discussion and suggestions.

I would like to thank Mr. Minyou Kuo, National Sun Yisan University in Taiwan, for his very helpful discussions and help in experiments during his nine months of staying in Potsdam. The discussions went on even after he returned to Taiwan through emails and online video meeting.

I would like to acknowledge Dr. Jürgen Reiche, Mr. Minyou Kuo and, in particular, Mr. Wenfei Dong for the help in X-ray measurements. Mr. Burkhard Stiller, Ms. Dagmar Stabenow have helped greatly in AFM measurement, Ms. Monika Ehlert has carried out the DSC/TGA measurements, Dr. Xiaohui Yang has given many suggestions in experiments, here I would like to express my grateful thank to them.

I would like to thank Dr. Paul Quinn for correcting my English and giving me many helpful suggestions.

Our friends, Annika and Yogo Kusumi, have began to help us even when I was still in China. I wish to thank them for lots of happy times spent together.

In the past five years, my wife, Li Yi, has always provided me strong support, shared my stress, my worry and happiness. No words can express my thank to her.

I could never forget the love given by my and my wife's parents. In their eyes we are always children, we feel this from their countless call and from the packages full of my

favorite food.

At end I would like to thank the financial support provided by Deutscher Akademischer Austauschdienst (DAAD) under the project Nr. A/98/03492. This project provides me not only the opportunity to get a academic degree, but also to learn the language, the people and the culture of Germany.

Erklärung

Hiermit erkläre ich, dass die Arbeit von mir selbständig und ausschließlich mit den angegebenen Hilfsmitteln angefertigt wurde und bisher an keiner anderen Hochschule eingereicht worden ist.

Chenggang Xü

Potsdam, im März 2004